A SCREEN PRINTED CARBON NANOTUBE-BASED FIELD EMISSION DEVICE

A thesis submitted for the degree of Doctor of Philosophy

by

Edward Boughton

Department of Mechanical, Aerospace and Civil Engineering, Brunel University London

Abstract

Field emission devices have the potential to replace thermionic cathode electron sources in x-ray scanners and microwave devices. This study aims to exploit the high aspect ratio, small size and ballistic conductivity of carbon nanotubes (CNTs) to produce a field emission cathode with high current density and low turn-on field. A method of screen-printing CNT-containing inks has been developed and used to fabricate field emission cathodes on a variety of substrates. Increases in emission current density have been achieved by optimisation of CNT concentration and selection of CNT species. The device has the advantage over thermionic cathodes of requiring fewer connections, has no warm-up time and can be fabricated on several substrate materials. Additionally, a test setup has been developed to evaluate the performance of field emission devices capable of delivering high current densities in a diode configuration, featuring an adjustable anode-cathode gap, a current limiting resistor and the option of a phosphor-coated glass anode to assess emitter uniformity.

Contents

List of Figures

List of Tables

Glossary

batt refractory tile or slab supporting material during furnacing.

C-band radio frequency band with frequency range 4-8 GHz.

ImageJ open-source image processing software.

K_u-band radio frequency band with frequency range 12-18 GHz.

Kapton polyimide film with high dielectric strength and temperature resistance.

Macor proprietary machineable ceramic consisting of fluorphlogopite mica in borosilicate glass.

polymer gel a glycol-based gel thickened with hydroxypropyl cellulose forming the largest constituent of the nanostructured carbon-containing inks made here.

sp^2 atomic orbital hybridisation exhibited by carbon atoms with trigonal molecular geometry.

sp^3 atomic orbital hybridisation exhibited by carbon atoms with tetrahedral molecular geometry.

TMD Technologies Ltd microwave vacuum electronics company in Hayes, UK and sponsor of the present work.

X-band radio frequency band with frequency range 8-12 GHz.

Acronyms

APBN anisotropic pyrolytic boron nitride.

CAD computer-aided design.

CNT carbon nanotube.

CRT cathode-ray tube.

CT computed tomography.

CVD chemical vapour deposition.

DC direct current.

DLC diamond-like carbon.

DMF dimethylformamide.

DWNT double-walled nanotube.

EDS energy dispersive x-ray spectroscopy.

EPD electrophoretic deposition.

FE field emission.

FE-SEM field emission scanning electron microscope.

FED field emission display.

FEG field emission gun.

FEM field emission microscopy.

FTIR Fourier transform infrared spectroscopy.

HEG hydrogen exfoliated graphene.

HV high voltage.

IC integrated circuit.

IPA isopropyl alcohol.

ITO indium tin oxide.

LabVIEW Laboratory Virtual Instrument Engineering Workbench.

LCD liquid-crystal display.

LED light-emitting diode.

MIMIV metal-insulator-metal-insulator-vacuum.

MOCVD metalorganic chemical vapour deposition.

MOSFET metal-oxide-semiconductor field-effect transistor.

MPECVD microwave plasma-enhanced chemical vapour deposition.

MWNT multi-walled nanotube.

OFHC oxygen-free, high conductivity.

PECVD plasma-enhanced chemical vapour deposition.

PRF pulse repetition frequency.

PSU power supply unit.

PTFE polytetrafluoroethylene.

PVP polyvinylpyrrolidone.

RF radio frequency.

RIE reactive ion etching.

SAIT Samsung Advanced Institute of Technology.

SEM scanning electron microscope.

SWNT single-walled nanotube.

t-MWNT thin multi-walled nanotube.

TEM transmission electron microscope.

TEOS tetraethyl orthosilicate.

TGA thermogravimetric analysis.

TOF-MS time-of-flight mass spectrometer.

TWT travelling wave tube.

UHV ultra-high vacuum.

VI virtual instrument.

ZnO zinc oxide.

Symbols

E Electric field.

E_{TH} Threshold field.

E_{TO} Turn-on field.

J Emission current density.

J_{max} Maximum emission current density.

R_a Roughness average, measure of surface texture calculated as $\frac{1}{n}\sum_{i=1}^{n}|y_i|$.

β Geometric field enhancement factor.

ϕ Work function of a material.

h Planck's constant, $h = 6.63 \times 10^{-34}\ m^2 \cdot kg/s$.

k Boltzmann's constant, $k = 1.381 \times 10^{-23}\ J \cdot K^{-1}$.

mbar millibar, unit of pressure 1 mbar = 100 Pa.

Pa Pascal, SI unit of pressure.

Acknowledgement

This work was performed at TMD Technologies Ltd and Brunel University with funding from the UK Engineering and Physical Sciences Research Council.

The principal supervisor for the project was Professor Jack Silver. The second supervisor was Professor Paul Sermon. A profound thank you goes to my supervisors who rescued the project following the sudden departure of the original supervisors.

Thanks also to the following people at Brunel: Ashley Howkins, Terry Ireland, Lesley Hanna and Nico Nelson.

Some of the work was performed with two Master's students at Brunel University, James Kielty and Bernard Tashie-Lewis, as part of their final projects. Their involvement is acknowledged with thanks and is credited in the relevant sections.

I would like to thank TMD Technologies Ltd for funding the project. Vacuum electronics work is time consuming - and expensive - and I am grateful to have been able to rely on the support of the entire company throughout. My thanks to the owners, Peter Butcher and Howard Smith, the Managing Director, Dave Brown, and to the board, Tracey Ledwell, David Pike, Mike Clark, Martin Woolley and Jane McAlister.

Thanks to the following people at TMD: John Dunn, John Wilford, Jon Davis, Julie Pile, Phil Armstrong, Mike Waite, Roger Gates, Jonathan Warrens, Graham Adams and Chris Loftin. Tony Challis and Chris Gilmour may well be the world's most sympathetic and accommodating managers - thank you for your support.

Finally, thank you to Sophie Figgis and to my parents, Peter and Paula Boughton.

Chapter 1

Introduction to field emission devices

1.1 Introduction

A great many applications rely on electron sources, from the once ubiquitous but now obsolete cathode-ray tube (CRT) display to extremely specialised scientific analysis equipment. The overwhelming majority of these devices are based on thermionic electron emission. This technology has existed for over a century and is very well developed, but suffers from the inescapable necessity of heating the cathode to high temperature. For many applications a cold cathode electron source would offer distinct advantages allowing smaller, lighter and more efficient devices with no warm-up time. The work presented in this thesis addresses the question of whether a high-powered field emission (FE) electron source can be fabricated by screen printing nanostructured carbon materials, allowing simple and scalable manufacture at low cost. This chapter introduces the concept of field emission in contrast to the better-known thermionic emission mechanism before detailing some recent developments in field emitter fabrication technology. Finally, the current state of field emission sources in practical applications is discussed.

1.1.1 Aims & objectives

The aim of the work presented here is to develop a field emission device for application in a multi-cathode CT scanner of the type used in airport security baggage scanning. The requirement is for a cathode capable of generating an emission current density of 250-350 $mA{\cdot}cm^{-2}$ at a duty cycle of 0.012 %, corresponding to a pulse width of 85 μs with pulse repetition frequency (PRF) of 14.29 Hz. As the application demands a large number of electron sources for each scanner, the device must be made without exotic materials and

with inexpensive, scalable manufacturing techniques.

Further afield, higher emission current densities are required for vacuum electronics applications. Part of the work aims to identify variables affecting device performance, providing a path for future work to follow. In that context, deriving methods of testing device performance in a way consistent with current commercial vacuum electronics development was also mandated.

1.2 Thermionic electron emission

In thermionic emission, heat is applied to a material to give free electrons enough energy to escape into vacuum. Remarkably, the effect was discovered in 1873, prior to the discovery of the electron and remains the technology underlying the majority of electron sources today. The effect is described by the Richardson-Dushman equation [1]:

$$J = AT^2 \exp(\frac{-\phi}{kT}) \tag{1.1}$$

where J is the current density, A is Richardson's constant, T is the temperature of the material and k is Boltzmann's constant.

The quantity ϕ in equation 1.1, the work function, corresponds to the energy required for an electron in a solid to cross the potential barrier into vacuum. It can be seen that the emission current density increases with temperature. As a consequence, thermionic cathodes are made of refractory metals that can withstand operation at high temperature for long periods of time, most commonly tungsten. It is also evident that a low work function is desirable, and to this end the best performing modern cathodes undergo complex processes to lower the work function from the 4.55 eV of the unadulterated tungsten, to below 2 eV. A lower work function means that the cathode can either give higher current density at a given temperature, or the same current density at a lower temperature with longer lifetime. Work functions for some materials commonly used in thermionic electron sources are given in table 1.1.

1.2.1 Thermionic cathodes

For applications with modest current density demands filament electron sources are used in which a thin wire, usually of tungsten, is resistively heated to give electron emission. More demanding applications requiring pulsed operation use a solid cathode button of refractory metal, again usually tungsten, heated conductively from behind by an electrically

Table 1.1: Work functions of common materials used in thermionic electron sources [2] [3].

Material	ϕ **(eV)**
W	4.55
Mo	4.33
Re	4.72
Ru	4.7
Ba	2.52
Ca	2.87
Al	4.28
LaB_6	2.36

isolated heater wire. For high current densities, the work function of the material surface is reduced by introducing other materials into the cathode structure. Where a high brightness point source is required, lanthanum or cerium hexaboride single-crystal electron sources are used. These have the advantage of very small spot size and do not contaminate vacuum chambers with evaporated impregnant material, however they require higher operating temperature than impregnated dispenser cathodes and have shorter lifetime. Although the current density is high, these emitters have limited area. The performance of thermionic cathodes in applications for which nanostructured carbon-based field emitter arrays are considered attractive alternatives is discussed in more detail in section 1.7.

1.3 Field emission and Fowler-Nordheim theory

Field emission was first described by Fowler and Nordheim in 1928 [4]. The effect is described by the equation:

$$J = A\left(\frac{\beta^2 V^2}{\phi d^2}\right) \exp\left(\frac{-B\phi^{\frac{3}{2}} d}{\beta V}\right) \tag{1.2}$$

where A and B are the Fowler-Nordheim constants, β is the field enhancement factor, V is the applied electric potential and d is the separation between the anode and cathode. It can be seen that the Fowler-Nordheim formula describes an emission mechanism which is analogous to that of the Richardson-Dushman equation, but with the temperature dependance component replaced by a dependance on the applied electric field only. It follows that a field emission-based electron source can operate without requiring elevated temperature.

1.3.1 Field enhancement factor

The electric field gradient required for field emission to occur from a flat metallic surface is of the order of 1 GV·m^{-1}, which is considerably higher than those used in the applications discussed here. However, field emission occurs at lower applied fields from sharp tips. The quantity β in equation 1.2, the field enhancement factor, is a dimensionless quantity which measures the amplification of the electric field at the site of field emission:

$$\beta = \frac{E_l}{E_0} \tag{1.3}$$

where E_0 is the applied macroscopic electric field and E_l is the local electric field at the emission site. The origin of the field enhancement factor lies in the geometric properties of the emitter, with emitters having higher aspect ratio exhibiting higher field enhancement factors. It can be seen that a higher field enhancement factor is desirable, and therefore that best results come from taller, thinner emitters, with a long whisker with a rounded tip considered to be close to ideal [5]. It has been noted elsewhere however, that in the case of CNTs, the highest values of field enhancement factor come from sharp cone-shaped tips [6].

By using an array of tips with a sufficiently high field enhancement factor the required field to initiate field emission is reduced, allowing devices to operate with similar voltages to thermionic devices. Typical values for strongly performing carbon-based field emission devices are of the order of a few thousand, with the occasional published value in the tens of thousands [7] [8]. These figures are calculated from field emission test data and in the case of array devices represent an average across all the emitting tips.

For CNT-based devices there is typically a discrepancy between the β value calculated from experimental data and the theoretical maximum based on the tip geometry. This is a product of several factors, including CNT orientation, structure, purity and the influence of other materials present on the surface, but is most significantly attributed to the screening effect, whereby closely spaced emitting tips prevent each other from exhibiting their full geometric field enhancement effect. In its worst-case scenario, this effect causes very closely spaced emitting tips to behave similarly to a flat surface [9]. A resulting phenomenon in which macroscopic field emission devices are observed to have higher emission current density from the edges of the array is termed the edge effect [10].

Therefore, although it is desirable to have a large number of emitting tips when fabricating a field emission device, a compromise must be made in order to minimise the screening effect. Theoretical studies calculating the optimum arrangement of CNTs to balance these effects have reported that the best performance is achieved when CNTs are spaced at intervals of between 2 and 5 times CNT height [11] [12], with the most recently reported value

being 3 [13].

It has also been found experimentally that the field enhancement factor is affected by the distance between the emitter and the anode, with greater separations giving greater field enhancement factor for large area emitter arrays [14] as well as individual nanotubes [15].

1.4 Nanostructured carbon-based field emission devices

Work on developing practical field emission arrays began in the 1970s. Important work by Spindt et al. [16] developed arrays of metal cones. Although these devices were eventually capable of emission current densities of several amps per centimetre squared they suffered from field-induced sharpening which degraded performance. More recently nanostructured-carbon materials have been seen as strong candidates for field emission materials due to their versatility and small size allowing a theoretically very large number of emission sites in a given area. Carbon nanotubes are of interest due to their very high aspect ratio and were first used to fabricate a field emission device in 1995 [17]. Graphitic materials with sharp edges including those described as few-layer graphene have also been extensively researched as well as genuine single atomic layer graphene which can have an aspect ratio even higher than that of CNTs in cross-section.

A large number of nanostructured materials composed of carbon, carbon compounds, and inorganic materials have been investigated as candidates for field emission electron sources. A thorough review was conducted in 2005 in which the theory and application of a number of field emission devices were discussed, including Spindt tips, diamond-like carbon (DLC) and polycrystalline carbon [18]. There have also been a number of reviews covering field emission generally and specific areas of interest which are referenced in their appropriate sections. This chapter principally covers research performed more recently, except where the literature is of particular relevance to the experimental work presented. This section covers the principle methods of fabricating field emission devices based on nanostructured carbon along with research characterising the behaviour of the devices. A discussion of the properties and relative merits of the materials themselves is given in chapter 2.

Field emission from CNT-based devices fabricated by post-growth techniques suffers from low emission site density. Emission tends to be dominated by a small number of nanotubes which prevent others from turning on due to the screening effect. More uniform emitters can be produced by direct growth methods which allow better control of placement and orientation [19]. For vertically aligned CNTs it has been shown that an ideal array consists of emitters spaced at intervals of twice the CNT length. It has also been found that height anisotropies of over 5 % cause significant Joule heating leading to destruction of the nanotubes [11]. Theoretical studies indicate that optimum inter-nanotube spacing for

emission current density is highly dependent on the applied voltage, but only weakly dependent on nanotube thermal and electrical conductivity [9]. Calculations have also shown that, for nanoscale field emitters, space charge effects cause the behaviour to deviate from that predicted by the Fowler-Nordheim theory as emission current density rises [20].

Field emission behaviour is sensitive to the effects of residual gas species in the vacuum. A 2003 study using field emission microscopy (FEM) found that gas adsorbates sit preferentially on pentagonal sites on the tips of multi-walled nanotubes (MWNTs). Heating to 1300 K was found to remove adsorbates. In the case of hydrogen and nitrogen, the clean CNT surface was restored after heating. For oxygen species however, the tip structure was destroyed. Adsorbed molecules showed as bright spots on the phosphor screen, with the number seen to increase over time. The adsorbates were found to increase the overall electron emission of the CNT at a given field, with the level of current enhancement correlating with the size of the molecule [21]. The finding indicates that great care must be taken to minimise the partial pressure of oxygen for CNT-based field emitters in order to achieve a long operating life, but that unlike metal field emitter arrays they are not damaged by the presence of nitrogen.

Individual single-walled nanotubes (SWNTs) have been found to exhibit current saturation at 100 nA due to gas adsorbates. Higher currents remove them allowing a maximum of 2 μA per CNT [22].

1.4.1 In-situ growth

In-situ growth is achieved with chemical vapour deposition (CVD). A more detailed account of CVD growth methodology for carbon nanotubes is given in section 2.4.2. Plasma-enhanced chemical vapour deposition (PECVD) allows precise control of the location and orientation of CNTs on the substrate by controlling the patterning of the metallic catalyst. Consequently, this technique allows fabrication of the closest approximations to an ideal CNT emitter array achieved so far, giving high current densities and finding applications in commercially available products. It is also the most labour and cost-intensive of the techniques detailed here.

The most high-profile CVD field emission research is associated with Prof. W. I. Milne and Dr. K. B. K. Teo of Cambridge University, who have consistently achieved current densities upwards of 1 A·cm^{-2} using a PECVD technique with patterned nickel catalyst [23] [24] [25]. Thales S.A. have investigated carbon nanotube-based field emission cathodes grown using the Cambridge group's technique for use in a triode and travelling wave tube (TWT) [26], which are among the most demanding of the possible applications for field emission devices. A CNT array grown by the group is shown in figure 1.1.

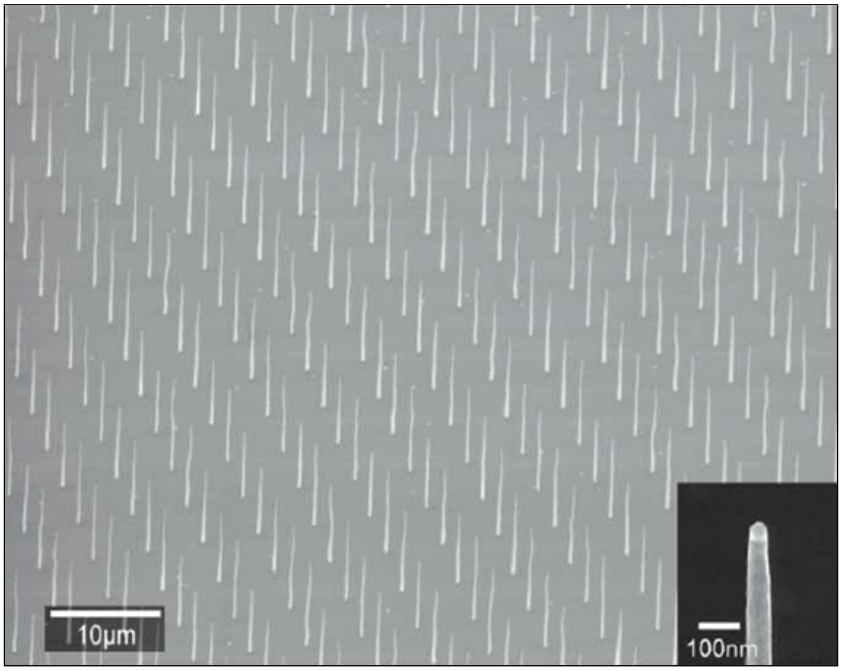

Figure 1.1: CVD-grown CNT array. *Reproduced from [23]*.

The group's growth technique has also been adapted to be be performed at temperatures as low as 450 °C making it compatible with display manufacture technologies [27].

A high field emission current density of 10 $A{\cdot}cm^{-2}$ has been drawn from a PECVD-grown array of nanostructured carbon described as nanocrystalline graphite, with protruding carbon nanowires and nanoribbons. Notably, the growth method requires no catalyst to be patterned on the silicon substrate, instead using a method of scratching the surface of the substrate with diamond powder to induce surface defects. The figure was achieved using a moveable anode with very small area, however [28] [29].

Field emission has been achieved from microwave plasma-enhanced chemical vapour deposition (MPECVD)-grown few-layer graphene. An electric field applied during deposition orients the graphene vertically. Performance suffers as a result of amorphous carbon deposits at the graphene-substrate boundary [30].

1.4.2 Printing

Screen printing is a wet deposition technique in which a thin layer of ink is deposited on a surface by using a squeegee to force the ink through a fine mesh. Although the fine control of emitter tip location and orientation that have been achieved with in-situ growth is impossible, the technique is attractive as it is low-cost, scalable and can easily be adapted to use different substrate or emitter materials.

Inks are made by dispersing carbon materials in liquid phase, often with additional components to optimise the rheological properties for screen printing. As a large number of emitter sites is desirable, so is a homogenous dispersion of the material in the ink. CNT and graphene dispersion has been an area of interest recently, applying equally to composite material, conductive polymer and flexible electronics as well as field emission research. CNTs do not disperse readily in a number of commonly used solvents, leading many researchers to use hazardous solvents such as dimethylformamide (DMF), functionalization of the CNTs or the addition of surfactants. Although a number of methods have been developed to make uniform CNT dispersions, it has recently been noted that it is difficult to measure the level of dispersion at the nanoscale [31].

Some of the most developed work in screen printed CNT-based field emitters has been performed at the Samsung Advanced Institute of Technology (SAIT), with an SWNT-based device giving 25 $mA{\cdot}cm^{-2}$ at an applied field of 2 $V{\cdot}\mu m^{-1}$. The formation of cracks in the deposited layer during the drying process results in a dense network of exposed CNTs [32]. Extensive optimisation work has been carried out, including assessment of the effects of both conductive and non-conductive ink additives [33].

For screen printed MWNT films incorporating glass frits as an ink component it has been found that there is an advantage to some exposure to air while heat treating. When compared to emitters heat treated in nitrogen alone those with a nitrogen-air mix had more exposed tips due to more ink components burning off from the surface. The effect is comparable to taping activation, but without the possibility of introducing contaminants [34].

Inkjet printing has also been used to fabricate CNT-based field emission devices. A method of printing SWNTs dispersed in DMF on indium tin oxide (ITO)-coated glass followed by annealing and adhesive tape treatment resulted in an emission current density of 250 $\mu A{\cdot}cm^{-2}$ [35].

Research into graphite-based screen printed field emission devices was conducted by Printed Field Emitters Ltd. from 1995-2005. The devices were made using nanoscale graphite flakes in a dielectric binder material [36] [37] [38]. Working prototypes of displays based on the devices were fabricated [39].

A number of studies of screen printing methods are notable for their application of post-deposition surface treatment techniques and are discussed in their relevant sections.

1.4.3 Electrophoretic deposition

Discovered in 1807, the phenomenon of electrophoresis concerns the movement of particles suspended in liquid under the influence of an applied electric field, and was considered for many years to be nothing more than a curiosity. However, it has more recently found a

number of applications including as a technique for controlling deposition of particles on surfaces. A more detailed discussion of the electrophoretic deposition (EPD) mechanism is given in section 2.5.5 along with the method used as part of the present work.

A review was conducted in 2006 of EPD-fabricated CNT arrays including their application as field emission devices, and similarly for EPD-fabricated CNT/ceramic composites in 2010 [40] [41]. A third review in 2013 covered EPD-fabricated graphene arrays, reflecting the recent trend in literature on applications of nanostructured carbon [42].

The research group of Prof. O. Zhou at the University of North Carolina have developed effective methods of producing field emission devices by EPD, including a method of depositing patterned CNTs using electrophoresis in conjunction with photolithography [43]. The method uses an $MgCl_2$ charger, vacuum anneal and taping activation step. The deposited CNTs align with the electric field applied during electrophoresis, which is beneficial for field emission applications.

Results from the group regularly report over an amp per centimetre squared from small-area cathodes, most recently 1.4 A·cm^{-2} from a 0.08 mm^2 cathode with a 15 μm-thick layer of deposited MWNTs, with emission current density decreasing as emitter area increases, attributed to the edge effect [44].

The associated company Xintek inc., is developing commercial multi-cathode x-ray machines based on the technology, with a micro-computed tomography (CT) scanner capable of high resolution imaging of small animals demonstrated in 2009 [45]. The group have also developed CNT synthesis techniques which are discussed in section 2.4.2.

1.4.4 Other wet deposition methods

Several authors have described a method of fabricating a field emission device by vacuum filtration of a CNT dispersion to create a densely-packed mat. In addition to their work with EPD deposition the University of North Carolina group experimented with vacuum filtration and spray deposition of SWNTs [46] [47].

A study in 2010 comparing emitters made by vacuum filtration and screen printing using the same commercially available Shenzhen Nanotech Port Co. MWNTs found that the vacuum filtration method produced superior results [48]. Turn-on field at 1 μA·cm^{-2} was found to be 0.93 V·μm^{-1} with field enhancement factor 9720 for the vacuum filtered cathode. The screen printed cathode had a turn-on field of 1.11 V·μm^{-1} and β of 6285. The highest emission currents reported were around 5 and 3 mA·cm^{-2} respectively. It was further found that the vacuum filtered device exhibited better CNT-substrate adhesion, and that emission performance was degraded as a result of annealing at temperatures above 400 °C which is a necessary step for screen printed field emitters.

Hydrogen exfoliated graphene (HEG) spin-coated on a steel substrate has exhibited field emission with turn-on field of 1.18 $V \cdot \mu m^{-1}$. Decoration with CuO nanoparticles reduced turn-on field to 1.1 $V \cdot \mu m^{-1}$ and RuO_2 nanoparticles to 0.91 $V \cdot \mu m^{-1}$ [49].

1.4.5 Single-point emitters

Single-point type emitters find application as high brightness, high coherence electron sources in scanning electron microscopes (SEMs) and transmission electron microscopes (TEMs). Studies report some of the highest field enhancement factors of any CNT-based field emission cathodes but require intensive fabrication methods which would be impossible to apply to large-area arrays [7] [50].

An unusual method of fabricating a high brightness FE source for use in the TEM by depositing a carbon cone on CNTs and mounting on a tungsten tip is reported to give extremely high field enhancement factor [51].

The electrophoresis method developed at the University of North Carolina (section 1.4.3) has also been adapted to fabricate a field emission cathode with a well-aligned single tip emitter [52].

An emission current of 10 mA has been achieved from a single emitter made of a CNT/tungsten composite material [53].

1.5 Enhancement

1.5.1 Surface coating of nanostructured carbon emitters

Various surface coating techniques have been applied to CNTs to improve field emission performance by lowering turn-on field, increasing emission current, reducing current fluctuation or increasing emitter lifetime. Compared to materials commonly used in thermionic cathodes, CNTs have a relatively high work function of 4.5–5 eV. Coating CNTs with a layer of a material with low work function is expected to lower turn-on field by reducing the potential barrier between the CNT and vacuum.

Coating with titanium carbide has been shown to improve CNT-based field emitters. TiC has a work function of 3.0 eV, high melting point and high electrical and thermal conductivity. A study investigating 1, 3 and 10 nm TiC coatings on MWNTs of less than 10 μm length and 10–20 nm diameter showed improvement in turn-on field was possible despite the increase in CNT diameter. Best results were demonstrated with the thinnest coating. Work function was estimated to be 2.8 eV, assuming a value of 4.5 eV for the untreated nanotubes [54].

A thin titanium film coating of PECVD-MWNTs produced Ti nanoclusters on the CNT edges. Raman spectroscopy found an improvement in the I_D/I_G ratio, implying the crys-

tallinity of the CNTs was improved. The authors attribute the effect to passivation of CNT defects [55].

Field emission performance of CNTs grown by PECVD then etched by N2 plasma was found to improve with deposition of a thin titanium layer of 5 nm, having lower turn-on field and higher emission current density [56].

For any possible application of field emission devices, a stable emission current is desirable. Fluctuations occur due to adsorption and desorption of molecules at the tips of CNTs, and to some extent to statistical fluctuations in the quantum tunnelling effect. There is therefore interest in coating CNTs with a material having a non-linear current-voltage behaviour, so that an increase in current causes a drop in the resistance of the coating. The electric field across the coating would then weaken, arresting the current increase. This effect would also work in reverse so that the overall effect of the coating would be similar to that of a varistor, inhibiting current fluctuation [57].

A seven-fold improvement in emission current density together with a three-fold reduction in turn-on field is reported in a study investigating the addition of caesium iodide to commercially obtained MWNTs deposited on a molybdenum substrate by electrophoresis [58]. A reduction in work function from 4.8 to 2.4 eV resulting from coating with metallic caesium, which has a work function of 1.93 eV [59], with separate field emission studies finding an improvement in performance as expected. Caesium is an impractical coating material however, due to its rapid oxidation in air [60].

A 2011 study investigated the effect of coating PECVD-grown CNTs with a thin layer of MoO_3 by metalorganic chemical vapour deposition (MOCVD). The MoO_3 is a wide bandgap semiconductor and was found to form Mo-C bonds at the CNT interface. The resulting Schottky barrier eased the transition of the electrons from the CNT into vacuum, reducing turn-on field from 2.34 to 1.33 $V{\cdot}\mu m^{-1}$. An increase in calculated field enhancement factor from 1800 to 7000 was also reported, although the effect did not have its origin in the emitter tip geometry. After coating emission was found to occur from the CNT sidewall and from MoO_3 whiskers formed on the CNT tip [61].

Thin multi-walled nanotubes (t-MWNTs) grown on a nickel substrate by PECVD were coated with a 20 nm layer of RuO_2 by radio frequency (RF) sputtering. An annealing step formed Ru nanoparticles, with several annealing temperatures used. Field emission performance was tested at each stage. It was found that the RuO_2 coating degraded FE performance, increasing turn-on field from 4.5 to 5.0 $V{\cdot}\mu m^{-1}$ and decreasing β from 1264 to 1032. The best result came after annealing at the highest temperature used of 1000 °C with turn-on reduced to 1.7 $V{\cdot}\mu m^{-1}$ and β increased to 4871. The highest emission current density reported was 1 $mA{\cdot}cm^{-2}$. [62]

Taking a slightly different approach to the other studies detailed here, a vapour-solid self-

catalysing process has been used to deposit zinc oxide (ZnO) nanostructures on screen printed MWNT films. Comparison of FE performance of the emitter with as-printed MWNTs and ZnO structures grown directly on a Si substrate showed a significant improvement in turn-on field, threshold field and field enhancement factor. In this case, the improvement is due to the combined aspect ratio of the ZnO structures and CNTs in an effect reminiscent of the multi-stage single-point emitters described in section 1.4.5 [63].

Improvements have also been demonstrated with non-metallic coatings. Coating CVD-grown MWNTs with a conducting polymer resulted in a reduction of turn-on field [64].

Table 1.2 summarises the effects of coating with different materials given in this section for relative comparison of the improvements achieved.

Table 1.2: Summary table of effects of surface coatings on FE performance: $E_{TO(0)}$ and β_0 are values of the emitters measured before coating; $E_{TO(c)}$ and β_c are for the coated emitter.

Coating	**Description**	$E_{TO(0)}$ ($V \cdot \mu m^{-1}$)	$E_{TO(c)}$ ($V \cdot \mu m^{-1}$)	β_0	β_c	**Reference**
Ti	Nanoclusters	0.95	0.8	8740	9386	[55]
Ti	5 nm layer	2.8	2.0	-	-	[56]
Cs	Evaporator coating	0.76	0.36	-	-	[60]
MoO_3	Nanoparticles	2.34	1.33	1800	7000	[61]
Ru	Nanoparticles	4.5	1.7	1264	4871	[62]
RuO_2	20 nm layer	4.5	5.0	1264	1032	[62]

1.5.2 Other enhancement methods

Mechanical

Significant improvements to field emission performance have been achieved by a simple method of applying adhesive tape to the surface of field emission devices. The technique is used for emitters fabricated by wet deposition methods and works by pulling emitter tips out of the surface, increasing their field enhancement factor, and by removing loose or excess material - both carbon and otherwise - which constitutes a barrier to emission.

Adhesive tape treatment has been shown to remove binder material from the surface of printed CNT-based emitters, significantly exposing nanotubes. In one study, 500 $mA \cdot cm^{-2}$ was achieved from a small cathode measuring 4 x 3 mm at an applied field of 12 $V \cdot \mu m^{-1}$ [65].

Similarly, beneficial effects can be had from removal of material covering CNTs by other means. A mechanical crushing method followed by blowing off removed material with high speed airflow improved field emission performance of screen printed emitters, reducing turn-on field from 2.5 to 1.7 $V{\cdot}\mu m^{-1}$ and increasing peak emission current eight-fold with significantly more uniform emission. The authors report that the method compared favourably to the taping method [66].

Ablative

There is also interest in post-treatment of emitters by exposure to reactive atmosphere. For emitters made by in-situ growth methods, this is intended to improve the structure of the CNTs, removing defects. For those made by wet deposition methods the motivation is normally to remove undesired material, exposing emitting tips.

As early as 1997, microwave oxygen plasma treatment was applied to CNT-based field emitters to improve performance, reducing turn-on field from 5.0 to 0.8 $V{\cdot}\mu m^{-1}$. A field enhancement factor of 8000 was reported [67].

Screen printed Shenzhen Nanotech Port Co. MWNTs were improved by 20 minute hydrogen plasma treatment in terms of emission current density at a given field and device emission uniformity. This is attributed to the cleaning of contaminants and the introduction of 30–50 nm features on the CNTs, primarily bent graphite layers and nano-onions, which increased the number of emission sites. The field required for an emission current density of 1 $mA{\cdot}cm^{-2}$ reduced from 9.12 to 6.53 $V{\cdot}\mu m^{-1}$ relative to the untreated CNTs, with turn-on field reducing from 2.42 to 0.98 $V{\cdot}\mu m^{-1}$ [68].

Treatment with argon plasma has been shown to improve CNT-based field emitter performance in several cases. Treatment of patterned thermal CVD-grown CNT-based field emitters with argon plasma resulted in improvements in field enhancement factor, turn-on field and emission current density. In the best case the current density increased almost two orders of magnitude from 2.35 to 48 $mA{\cdot}cm^{-2}$ at 5 $V{\cdot}\mu m^{-1}$. The reported β value increased from 1869 to 3463 with turn-on field reducing from 3.1 to 2.2 $V{\cdot}\mu m^{-1}$. Raman spectroscopy measurements found that the improvements correspond to a slight reduction in I_D/I_G ratio, with TEM showing that the CNT structure was altered by the treatment [69].

Likewise, argon plasma treatment of “graphene paper” has been shown to reduce turn-on field from 2.3 to 1.6 $V{\cdot}\mu m^{-1}$ with an increase in emission current density [70].

Argon ion irradiation has been shown to improve field emission performance on screen printed arc-discharge CNTs. The CNTs were observed to have straightened after the treatment [71].

Argon neutral beam treatment of screen printed CNT films at 100 eV for 10 seconds

significantly reduced turn-on field by exposing CNT tips without damaging them. Conversely, argon ion beam treatment had the opposite effects with CNTs showing damage. Turn-on field was reduced from 1.7 to 0.9 $V \cdot \mu m^{-1}$ while after ion beam treatment increased from 1.7 to 2.8 $V \cdot \mu m^{-1}$ [72].

Ten second treatment in a plasma of atmospheric pressure helium and neon reduced the turn-on field of screen-printed MWNT-based field emitters. Further improvements were had by applying a taping method before plasma treatment resulting in improved uniformity but slightly increased turn-on field [73].

Reactive ion etching (RIE) followed by hydrogen plasma treatment has been found to expose CNTs from under a silica binder layer in an MWNT-based screen printed field emitter. The untreated cathode initially had lower field for 1 $mA \cdot cm^{-2}$ due to local hotspots that were destroyed by RIE. Optimal performance followed 5 minutes of hydrogen plasma treatment. Although the produced device gave uniform emission, required fields were high, giving an emission current density of 1 $mA \cdot cm^{-2}$ at 6.45 $V \cdot \mu m^{-1}$ [74].

Electrical

For double-walled nanotubes (DWNTs) printed on ITO glass, an increase in maximum current to 19.2 $mA \cdot cm^{-2}$, an increase in field enhancement factor and a decrease in turn-on field to 1.15 $V \cdot \mu m^{-1}$ was reported following the application of a field of 3.05 $V \cdot \mu m^{-1}$. A change in surface morphology occurred at the same time, with CNTs becoming permanently vertically aligned [75].

In a study intended to test the effect of common processes used in the manufacture of displays on CNT field emitter arrays, printed MWNTs were found to lose performance in response to drying with medium heat, further with firing at 400 °C, and even further when the surface was polished. Plasma etching and chemical etching restored performance [76].

Applying an electrostatic field to screen printed SWNTs while drying improved field emission performance by aligning the CNTs with the field. The resulting device had maximum emission current density of 3.5 $mA \cdot cm^{-2}$ at an applied field of 3 $V \cdot \mu m^{-1}$ compared to 200 $\mu A \cdot cm^{-2}$ for the untreated emitter. The turn-on field was 1.22 $V \cdot \mu m^{-1}$ [77].

Summary

Table 1.3 summarises the various post-production techniques applied to field emission devices. All were found to give significant performance improvements, either in terms of reducing the applied field required for a given emission current density, increasing the emission current density at a given applied field, or both. Inherent differences in the materials, device parameters and test methods used in the studies make quantitative comparison difficult.

Table 1.3: Summary table of post-production enhancement methods.

Method	Untreated		Treated		Reference
	J ($mA \cdot cm^{-2}$)	E ($V \cdot \mu m^{-1}$)	J ($mA \cdot cm^{-2}$)	E ($V \cdot \mu m^{-1}$)	
Screen print, adhesive tape	1	12.5	8	4.5	[65]
Screen print, crushing	0.12	4.2	1	4.2	[66]
Screen print, hydrogen plasma	1	9.12	1	6.53	[68]
CVD, argon plasma	2.35	5	48	5	[69]
Screen print, electrostatic field	0.2	3	3.5	3	[77]

However, consideration of the practical requirements of applying each technique lead to the conclusion that adhesive tape treatment is most suitable for a low-cost, scalable manufacturing process.

1.5.3 Substrate materials

Choice of substrate material for a field emission device can have a significant impact on performance. A good substrate has high electrical and thermal conductivity and adheres well to the emitter material. Additionally, factors affecting choice of substrate can be application-specific, as practical field emission devices must be integrated into vacuum systems. They must therefore be suitable for the level of vacuum required and compatible with other materials and processes used. Given the maturity of research in conventional vacuum electronics, it is also desirable that field emission devices are as compatible as possible with existing designs.

Nanostructured carbon emitters have been fabricated on a wide variety of substrate materials, with the differences between emitter materials, fabrication methods and post-process treatments used rendering studies inherently incomparable except in rare cases where multiple substrates have been used with the same techniques.

For in-situ growth methods the choice of substrate material is limited by the requirements of the process, with silicon substrates commonly used [29] [55].

A CNT-based cathode on a molybdenum substrate has been tested using Pierce gun

geometry. Bakeout was found to improve field emission performance [78].

High thermal and electrical conductivity are desirable qualities. Resistance at the interface of the CNTs and substrate depends on Fermi energy levels aligning. For metallically conducting MWNTs metallic substrates are therefore expected to give the best performance [79]. Having the highest thermal and electrical conductivity of any element, silver has also been successfully used as a substrate for field emission devices [80].

CVD-grown MWNTs deposited on a stainless steel substrate by EPD had maximum emission current density of 3.5 $mA{\cdot}cm^{-2}$ at 2.4 $V{\cdot}\mu m^{-1}$ [81].

1.5.4 Binder materials

Binder materials work by one or more of three principal mechanisms. Conductive binder materials aim to reduce the barrier to emission by providing a continuous conductive path between the substrate and the emitter tips. Dielectric binders improve performance by reducing the screening effect between emitter tips, allowing increased field enhancement factor. The third effect, exhibited by both conductive and non-conductive binder materials, is to improve substrate-CNT adhesion, preventing removal of the emitter material under high electric field gradients.

In an experimental study using a dielectric silica binder, the observed performance enhancement has been attributed to a modification of the band structure, effectively lowering the CNT work function. Observations that CNTs fragmented with the coating, along with Fourier transform infrared spectroscopy (FTIR) results showing the presence of a Si-C peak suggest that the CNTs form sp^3 Si-C bonds at the coating interface [82].

A tetraethyl orthosilicate (TEOS) sol binder has also been found to improve emission from MWNTs by improving substrate adhesion and forming a protective matrix [83].

Silica films have been shown to suffer damage from residual gas ion impact. Oxygen was found to be very damaging deep into the film, while inert gases (helium, argon) caused only surface damage. Hydrogen caused minimal damage which was confined to the surface. Nitrogen caused no apparent damage to the film but diffused throughout [84].

In two related studies comparing glass frits, ITO powder and silver paste as binder materials in screen printing ink containing Iljin Nanotech MWNTs, glass frits were found to give the best performance, with a field enhancement factor of 17,000 reported at low currents [8] [33].

Simulation of binder materials with different dielectric constants concluded that the optimum binder material for CNT-based field emission cathodes has low dielectric constant and high sheet resistance [85].

An emitter made of SWNT bundles coated in a TiO_2 layer has been made by dipping a tungsten tip into a TiO_2 sol-gel containing dispersed nanotubes [86].

For graphite-based field emission devices, the metal-insulator-metal-insulator-vacuum (MIMIV) effect allows high field enhancement factors to be achieved with a dielectric coating [87].

1.6 Other types of field emission device

A brief mention is made here of some other important field emission technologies which are either the subject of current research or compete with nanostructured carbon.

1.6.1 Spindt tips

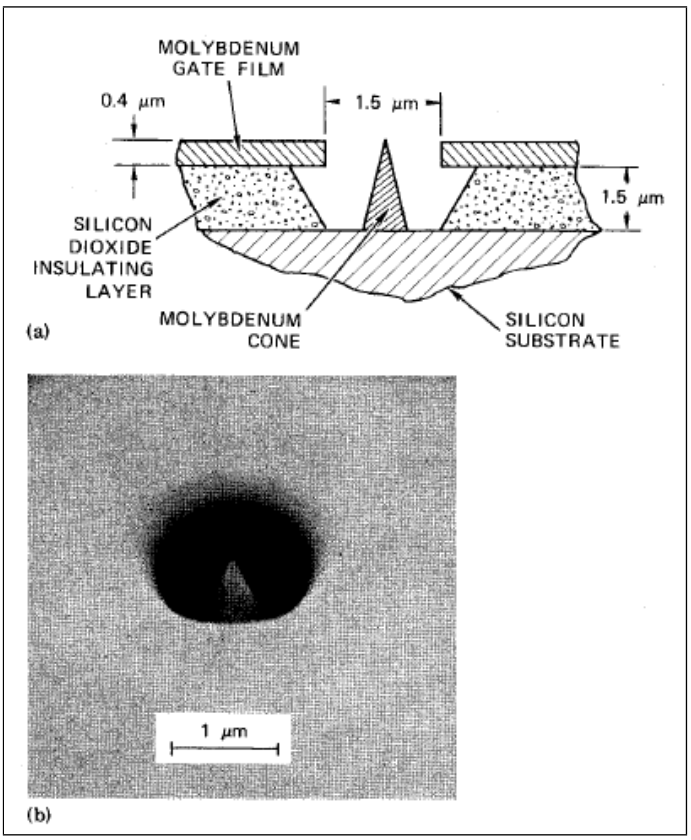

Figure 1.2: Spindt tip emitter. *Reprinted from C. A. Spindt, Journal of Applied Physics, 47, 5248, (1976), with the permission of AIP Publishing [16].*

Spindt tip technology was the first attempt to develop large-area field emitter arrays capable of high current densities. Modern Spindt tips are fabricated using electron beam lithography and consist of sharp molybdenum cones with an integrated gate electrode (figure 1.2). Although Spindt tip arrays are capable of current densities up to 10 $A \cdot cm^{-2}$, they are very

sensitive to residual gas, requiring high vacuum of around 10^{-7} Pa (10^{-9} mbar) for operation. The tip is typically of the order of 1.5 μm high with an aperture of similar width [16].

A number of investigations have fabricated working prototype microwave devices using Spindt tip emitter arrays (section 1.8.1).

1.6.2 ZnO-based field emitters

ZnO is a semiconductor from which a wide range of nanostructures can be synthesised. Despite its inferior electrical conductivity, the material is of interest to field emission devices as it can be made to form a variety of different nanostructures exhibiting high aspect ratio. ZnO tetrapods have been shown to have the highest experimentally derived field enhancement factor when used to fabricate a field emission device by spin-coating. The shape of the tetrapods is shown in figure 1.3. When placed on a flat surface, this shape always presents a sharp point aligned perpendicular to the surface. In field emission, this point will be aligned parallel to the applied field, maximising the field enhancement factor without the need for in-situ growth or post-process alignment methods. However, the shape will also have poor electrical and thermal contact with the substrate. A matrix of MWNTs has been shown to improve conductivity, with an emitter of combined MWNTs and ZnO tetrapods giving better field emission characteristics than either material separately. A very high field enhancement factor of 32,553 was published, with a turn-on field of 0.6 $V \cdot \mu m^{-1}$ and a maximum emission current density of 2 $mA \cdot cm^{-2}$ at 2.2 $V \cdot \mu m^{-1}$ [88]. A screen printing method was also tried in the same paper, but found that the process damaged the tetrapods. This field enhancement factor appears to be highest of any published study of a large-area emitter array.

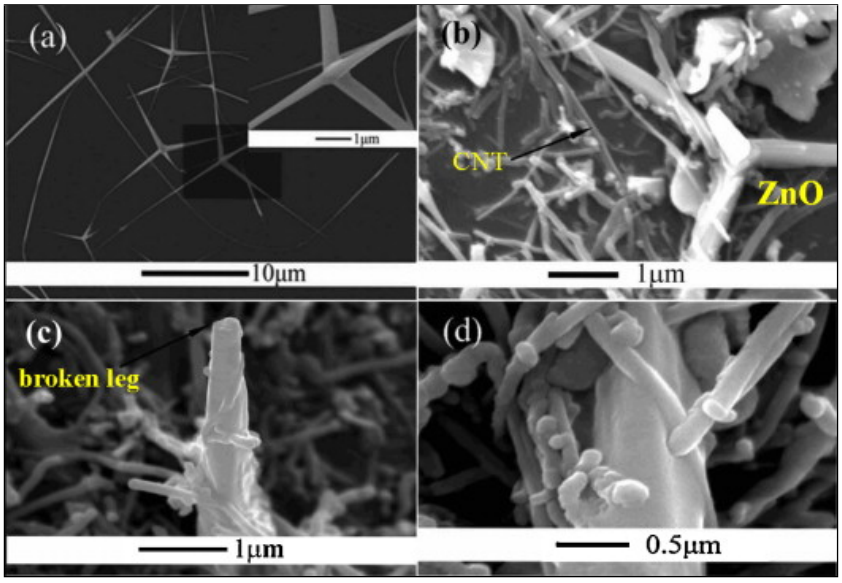

Figure 1.3: ZnO tetrapod. *Reproduced from [88].*

ZnO has also been investigated with the intention of producing flexible field emission devices. Current densities of the order of 1 $mA{\cdot}cm^{-2}$ have been achieved from flexible field emission devices composed of ZnO nanowires on a substrate of reduced graphene and polydimethylsiloxane [89]. Field emission from a number of morphologies of nanostructured ZnO has been tested. However, although the material can be used to make field emission devices with low turn-on field, the highest reported emission current density is 5 $mA{\cdot}cm^{-2}$ [90], meaning they are unlikely to be suitable for the applications of interest to the present work.

1.7 State of the art

High performance thermionic cathodes are most commonly made of tungsten with the inclusion of barium to reduce the work function. At operating temperature, a layer of barium oxide forms on the cathode surface is and gradually consumed and replaced by diffusion from the bulk. The barium oxide forms a dipole lowering the work function to lower than that of elemental barium. The effect is to lower the temperature required for a given level of emission, meaning the cathode will either give more emission at the same temperature or have a longer life. Modern vacuum electronics applications requiring high beam currents most commonly use the M-type dispenser cathode developed by Philips in the 1960s. The basis of these is a porous tungsten matrix into which barium calcium aluminate is impregnated by heating to 1350 °C. The ratio of the impregnant materials is adjusted to suit the application, with a trade-off between long life and high emission. The result of this process is known as a B-type cathode, and is suitable for applications requiring up to 4 $A{\cdot}cm^{-2}$. A final step of sputter-coating a thin film of osmium, rhenium or ruthenium renders the finished M-type cathode capable of upwards of 10 $A{\cdot}cm^{-2}$. The related CD50 dispenser cathode uses a mix of tungsten and osmium for the final sputter coating step, reducing the work function to 1.8 eV, and is capable of 17 $A{\cdot}cm^{-2}$ at 1050 °C with an operating life of up to 10,000 hours [91] [92]. Although these types of cathodes run at high temperature, “fast-warm” examples developed for defence applications requiring a rapid turn-on from cold are engineered to have a low thermal mass and efficient heaters which can reach operating temperature in a few seconds [93].

Scandate cathodes are capable of very high current densities, with the highest published value of 160 $A{\cdot}cm^{-2}$ at 1050 °C. Consequently they are under investigation for use in a 220 GHz TWT. Historically, scandate cathode technology has suffered from difficulty with emission uniformity and reproducibility. This cathode, made with a sintered scandia and tungsten mix rather than an impregnation method, is better than traditional porous tungsten impregnated with Sc_2O_3 and barium calcium aluminate. The cathode was successfully life

tested at 50 A·cm^{-2} for 10,680 hours [94].

Schottky emitters typically consist of a sharp tungsten tip coated with a thin layer of zirconium. Emission occurs due to both field and thermal effects. These sources are most commonly used in microscopy applications where high brightness and coherence are a priority. Consequently the technology is rarely comparable with CNT-based field emission arrays.

1.7.1 Requirement for field emission devices

Although modern thermionic electron sources perform well there are applications for which field emission devices would be advantageous. Field emission cathodes are considerably smaller, lighter and simpler than thermionic cathodes. Comparing the extreme case of a CVD-grown or printed carbon nanotube-based cathode with a typical thermionic cathode used in vacuum electronics it can be seen that the cathode can be made on a thinner substrate made of one of several comparatively ordinary materials. The emitter material itself consists only of a thin film of material. As it requires no heater the cathode has fewer electrical connections meaning a fault is less likely to develop, and maintenance or replacement is easier if it does. This is of particular advantage in applications requiring large numbers of cathodes. The low temperature of the cathode means the device is not subjected to thermal stress and does not have to be allowed to cool before being exposed to air, where exposing a thermionic cathode at working temperature to atmosphere will permanently damage it. It is also worth noting that, despite the cost of high quality CNT samples, the cathodes made as part of this work cost considerably less than a thermionic cathode, both in terms of material outlay and processing. It is therefore clear that if field emission cathodes can be made to compete with thermionic cathodes in terms of current density and lifetime they offer an attractive alternative.

Due to their chemical inertness, CNT-based field emission devices suffer less sputter erosion and contamination than their silicon or metal counterparts, and therefore experience less performance degradation. Consequently, they can operate under poorer vacuum conditions [95]. As CNTs are uniform diameter along their length, CNTs still present sharp tips even when damaged [96].

1.8 Applications of carbon-based field emission devices

This section discusses particular applications for which nanostructured carbon-based field emission devices are either already being used or are under investigation. It is shown that for some applications field emission cathodes offer an attractive alternative, despite having

yet to achieve the current densities available from high-performance thermionic sources.

1.8.1 Microwave devices

Microwave amplifiers are of use in communications and radar applications. Although the use of solid state technologies is increasing, vacuum electronics-based devices are still able to offer much higher power at higher frequencies. This, along with a very good reliability record and long lifetime, make them the preferred technology in the most demanding applications. Microwave devices use dispenser cathodes operating at some of the highest current densities of any application. Of particular interest here is the ability of the field emission cathode to be directly modulated at high frequency. Space applications are a significant growth area for vacuum electronics, in which weight, efficiency and waste heat are priority considerations. Spindt-types cathodes have previously been used to fabricate a number of prototype microwave devices including C-band [97], X-band [98] and K_u-band [99] TWTs.

Research is being carried out into internally-gated CNT-based electron guns but none have yet achieved both useful current densities and useful lifetimes in the same device [100].

Microwave devices operating at 1.5 GHz have been fabricated using the Cambridge University group's in-situ CNT growth technique described in section 1.4.1. Direct modulation of the electron beam was demonstrated with a device giving emission current density of 1 $A{\cdot}cm^{-2}$ [101].

NASA has also investigated CNT-FE cathodes for microwave devices, including CVD CNT cathodes for use in a THz frequency nanoklystron [102].

A thermal CVD-grown CNT-based field emission cathode capable of emission current density of 600 $mA{\cdot}cm^{-2}$ has been investigated for microwave amplifier applications. However, difficulties were experienced when the cathode was used with a grid electrode, with 350 $mA{\cdot}cm^{-2}$ from the cathode resulting in a beam current of only 45 $mA{\cdot}cm^{-2}$ [103].

1.8.2 X-ray machines

X-ray imaging is used for medical diagnosis, industrial inspection and for security scanning. 3D computed tomography scanning requires an x-ray image to be captured from a large number of different angles which presents technical difficulties. In the case of industrial inspection the object is commonly rotated with a fixed x-ray source and detector, requiring extremely precise control of the rotating stage and a long acquisition time. For medical imaging it is both impractical to rotate a patient and important to capture the data quickly as biological processes like breathing blur the image. Similarly for security scanning it is important to have high throughput. There are three methods of achieving these aims. An x-ray source and detector can be mounted on a gantry which is rotated around the patient/object.

This method is limited by the speed with which the apparatus can be moved. Some modern CT scanners use a magnetically-steered electron beam to rapidly capture multiple images. These systems are expensive and are limited by the extent to which a high energy electron beam can be steered. The third method is to use multiple x-ray sources and detectors, which means a large number of electrical connections. With thermionic cathode sources this means each cathode is supplied with both heater connections and drive voltage, and a lot of heat generated during operation. Field emission cathodes offer the possibility of fabricating a CT-scanner with a solid state cathode array, requiring fewer connections and generating minimal waste heat. As these scanners typically operate at low duty, a high proportion of the total energy use would be saved.

X-ray sources are the most developed of the possible applications for field emission cathodes. The most notable achievements in the field come from the group at the University of North Carolina using the EPD method described earlier (section1.4.3) using CNTs synthesised by the associated spin-out company Xintek Inc. The group's work has included using field emission electron sources to develop novel imaging techniques which would not otherwise be possible [104].

1.8.3 Space applications

In space missions, launch cost is directly related to the weight of the spacecraft, meaning new technologies that reduce the launch weight are always of interest. In the vacuum of space, waste heat is difficult to manage and power consumption very carefully minimised. In many spacecraft there are instruments which require cooling and others which require heating to work. As field emission devices are smaller and lighter than their thermionic counterparts, generate less heat and work at low temperature, they have the potential to find a number of applications in space.

Field emitter arrays find potential use in spacecraft as plasma contactors for electrodynamic space tethers. These conductive shielded cables are suspended from spacecraft orbiting in the Earth's magnetic field and are either used to generate power from the spacecraft's movement through the field, lowering the orbit in the process, or to raise the orbit by applying an electromotive force. Coulomb control is the proposed method of precisely aligning clusters of close flying satellites, in which electron beams transfer charge between satellites, the resulting electrostatic interactions causing the satellites to move relative to each other. For space applications field emission devices exhibit the advantages of low mass and efficiency. They have been found, however, to require inconvenient methods of protection from atmospheric contamination [105].

The high temperature and hence high power consumption of thermionic cathodes makes

them unsuitable for many low-power spacecraft instruments. Field emission electron sources have been used on the MODULUS-Ptolemy mass spectrometer and Rosina instrument on the Rosetta mission launched by ESA in 2004 [106] [107]. A CNT-based field emission device has been tested for use in a mass spectrometer intended for deployment in penetrator-type probes, with good results [108].

NASA have fabricated a time-of-flight mass spectrometer (TOF-MS) using a CNT-based field emission electron impact ionisation source [109].

An aligned MWNT cathode has been fabricated by vacuum filtration for application in spacecraft field emission electric propulsion beam neutralisers. The cathode is capable of 10 $mA{\cdot}cm^{-2}$.

1.8.4 Displays

Before the widespread adoption of liquid-crystal display (LCD) technology, the field emission display (FED) was considered a strong candidate for commercial flatscreens. FEDs consist of an array of addressable field emitter pixels, with the resulting electron beams exciting a phosphor screen. FEDs can therefore achieve the same brightness and contrast as CRT or plasma displays. Although LCD is expected to remain the dominant technology, FED research is still being performed, most commonly for specialist applications where LCD panels will not work but also in the possibility that the technology can be made competitive in the future. To be practically useful for display applications, a field emission device must be capable of giving an emission current density of 1 $\mu A{\cdot}cm^{-2}$ at an applied field of 2.2 $V{\cdot}\mu m^{-1}$ [77]. The uniformity and stability of emission is of more importance than the available maximum emission current density, as inhomogeneities will be directly visible as variations in brightness on the display. Consequently there is interest in improving uniformity of emitter arrays by post-treatment, with a number of techniques developed, including direct current (DC) electrolysis in NaCl solution of screen printed field emitter arrays, which gave significant improvement in the number of emitters. After treatment a smoother *I-V* curve was observed and maximum current increased from 115 $\mu A{\cdot}cm^{-2}$ to 2 $mA{\cdot}cm^{-2}$, with turn-on field reduced from 2.2 to 1.6 $V{\cdot}\mu m^{-1}$ [110].

1.8.5 Lighting

Over the past few years the traditional filament based light source has largely been replaced with energy-saving bulbs which work by gas discharge. These have the disadvantage of containing toxic elements and producing unpleasant light. Research into field emission light sources uses cathodoluminescent materials which produce light on electron impact, in the same manner as display applications. These have the advantage that the phosphors used

can be selected to give a wide variety of light spectra and have potentially very long lifetime. An important consideration in development of cathodes for commercial field emission light sources is that the applied field needed to give the required field is low enough for the device to be as efficient as competing lighting technologies. A recent result reported the fabrication of a field emission lamp cathode made by EPD of CVD-grown CNTs in a solution of caesium nitrate and calcium nitrate. The cathode gave an emission current density of 4 $mA{\cdot}cm^{-2}$ at an applied field of 1.8 $V{\cdot}\mu m^{-1}$ [111].

1.9 Description of the present work

The work presented here consists of the results of a series of experiments designed to develop a method of fabricating field emission devices by deposition of nanostructured carbon-based emitter materials in liquid-phase dispersion with a dielectric binder component. Low cost, scalable fabrication techniques were investigated with a focus on screen printing with inks containing CNTs to provide the required geometric field enhancement. Variations on emitter and substrate materials have been investigated, along with trials to establish optimal concentrations of emitter material and binder. The geometry of the emission device is also investigated. The work also includes an account of the development of a system to test the fabricated emitter devices, and their subsequent characterisation both in terms of field emission behaviour and through other experimental analysis techniques.

1.10 Conclusions

A number of technologies exist which use field emission-based devices as an electron source. Currently, these only find application in niche areas. Of the currently available methods of producing field emission devices from nanostructured carbon, the majority were developed with the objective of creating flat panel displays, which require low FE current density at low applied field. Technologies offering higher current densities usually involve intensive or proprietary processing techniques. Table 1.4 shows emission current densities available from different methods of fabricating field emission devices from the literature in cases where macroscopic emitters are fabricated and tested at applied fields comparable to those used in the present work. At the beginning of this work, no printed emitter gave an emission current density on the order of magnitude required by a multi-cathode CT baggage scanner. The large number of cathodes required by these devices and consequent advantages offered by field emission over thermionic electron sources made the requirement for an easily made large-area scalable emitter evident.

Table 1.4: Summary table of electron source technologies.

Material	**Technique**	J_{max} ($A \cdot cm^{-2}$)	**Reference**
CNT	In-situ growth	1	[25]
CNT	Wet deposition	1.9	[44]
Molybdenum	Spindt tip	12	[16]
Tungsten	Barium dispenser	17	[91]

Chapter 2

Materials & methods

2.1 Introduction

Carbon exhibits an unparalleled range of different properties in its many allotropes. At one extreme is diamond, the hardest naturally occurring substance with very low electrical conductivity. At the other extreme graphite is electrically conductive and soft enough that its layers separate under the shear forces applied when writing with a pencil. While the contrasting properties of these familiar materials have been well known for a long time, recent research has discovered new forms of carbon with even more exotic attributes. Nanostructured carbon - forms of carbon with a least one dimension in the range 1-100 nm - includes, amongst others, graphene and carbon nanotubes. Both of these new forms of carbon have demonstrated unusual electronic and mechanical properties, setting records for tensile strength and electrical conductivity as well as behaving as semiconductors in some cases. Presented in this chapter are details of the nanostructured carbon materials used in the experimental part of this project, along with the methods and other materials used to prepare them and fabricate working field emission devices.

2.2 Working safely with nanostructured carbon

Carbon nanotubes and other high aspect aspect ratio nanomaterials have been found to have the potential to cause serious adverse health effects [112]. The work presented here was carried out using appropriate precautions, handling dry nanomaterials only under fume extraction. Following the publication of the guidance document “Using nanomaterials at work” by the health and safety executive in 2013 [113], work was carried out in accordance with the requirements contained therein.

2.3 Graphite and graphene

2.3.1 Structure & properties

Graphite is a naturally occurring carbon allotrope in which carbon atoms are arranged in layers each with a hexagonal planar lattice. Graphene consists of an isolated single graphite layer. The structure of graphite, graphene and CNTs are illustrated in figure 2.1. The bonds between atoms in-plane are strong, giving graphene a tensile strength of 130 GPa [114]. The attractive forces between planes are very weak however, allowing layers of graphite to easily separate when subjected to shear forces.

Research into field emission from graphite began with Latham in the 1980s, who described the MIMIV model to explain the finding that field emission from graphite flakes in a dielectric matrix was higher than expected from the geometric properties of the material [87].

The superior field emission performance of graphite over diamond films has been explained by a negative electron affinity at the surface in combination with a metallically conducting bulk [115].

2.3.2 Synthesis

Graphite is found in its pure form as a naturally occurring mineral deposit. The synthetic graphite material used in this work is made by high temperature graphitisation of amorphous carbon. The method first used to fabricate graphene in 2004 used adhesive tape to remove progressively thinner layers from highly-ordered pyrolytic graphite, eventually producing a single atomic layer and winning its discoverers the 2010 Nobel prize in Physics [116]. Making useable quantities of single-layer graphene has proved difficult, however. Graphene for field emission applications is commonly synthesised by comparable CVD techniques to CNTs and by a microwave-enhanced adaptation of the Hummers acid-exfoliation method [117]. In theory this method can be used to produce single-sheet graphene, and many chemically exfoliated graphite products are sold as “graphene” or “few layer graphene”. In reality materials made this way contain flakes with a distribution of different thicknesses and, without subsequent treatment, exhibit a high degree of functionalisation meaning the properties of true graphene are not observed macroscopically.

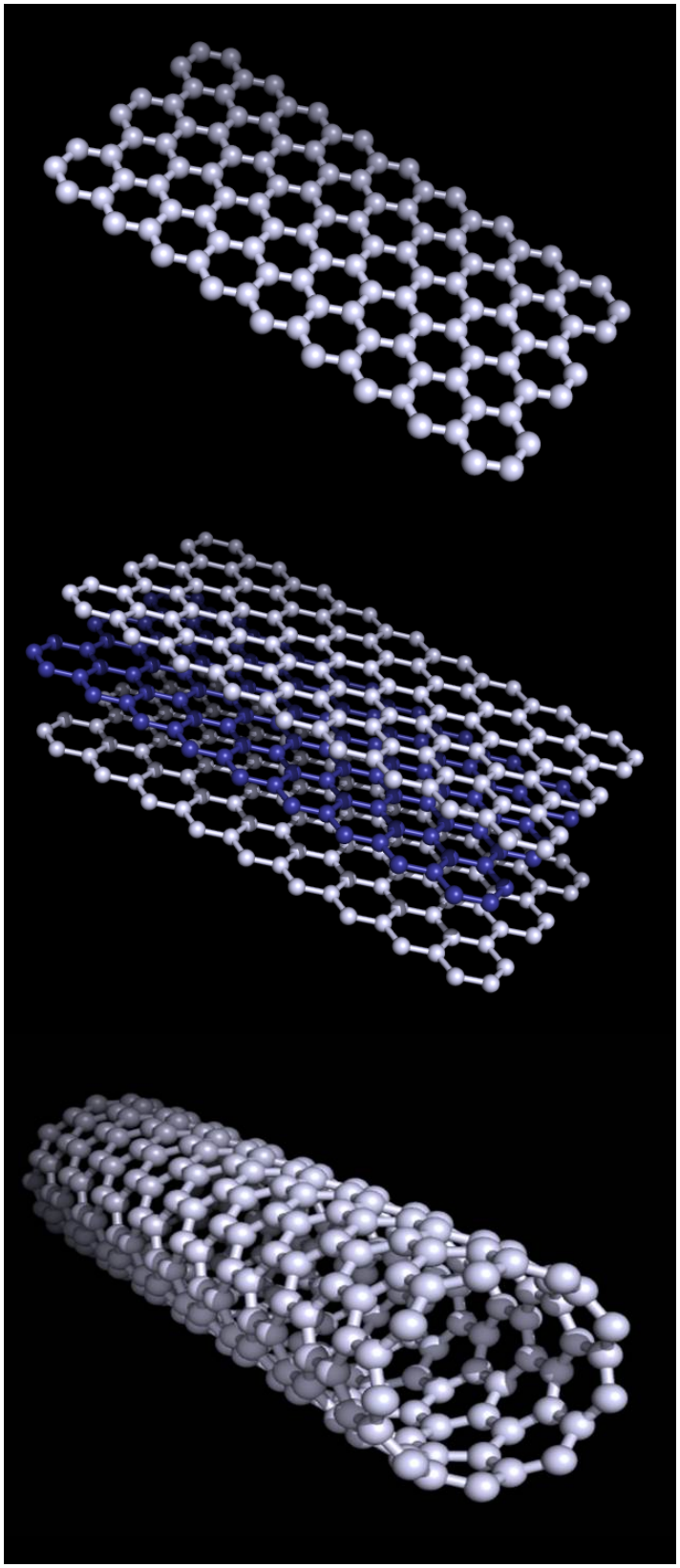

Figure 2.1: Graphene sheet, graphite and single-walled carbon nanotube.

2.3.3 Materials

The principal graphite used in this work was a synthetic flake product from TIMCAL labelled KS6, having an average flake size of 3.5 μm. Figure 2.2 shows an SEM image of the material.

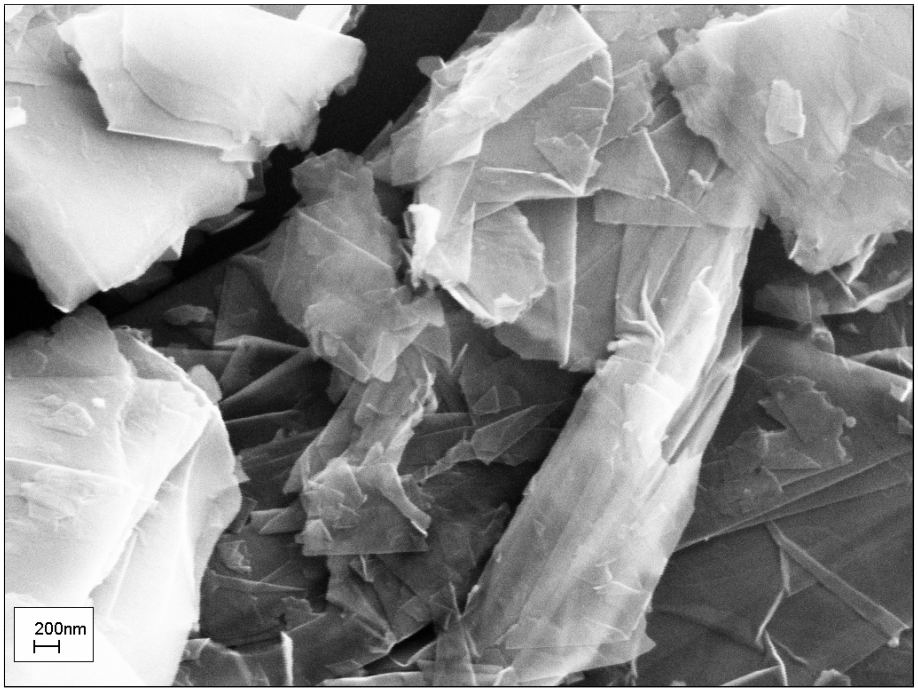

Figure 2.2: SEM of KS6 graphite flakes used to fabricate printed field emission devices.

Although experiments with commercially-obtained few-layer graphene materials were conducted as part of this study the so-fabricated emitters exhibited poor substrate adhesion, with the printed material easily removed from the substrate during the routine handling required to test the emitters. Under test the emitters were found to exhibit no consistent field emission at the level detectable with the experimental apparatus used. Consequently the results are omitted from this report.

2.4 Carbon nanotubes

First identified in 1991 by Iijima [118], carbon nanotubes (CNTs) are allotropes of carbon which can be thought of as rolled graphene sheets, forming nanoscale tubes (figure 2.1). A wide variety of species have been observed with a wide range of properties, including one of the highest known tensile strengths, high thermal conductivity and ballistic electron transport [119] [120]. These properties have led to a plethora of proposed applications from the everyday, such as strengthening concrete [121], to implantable blood glucose detec-

tors [122], to the exotic space elevator concept [123].

2.4.1 Structure & properties

The structure of a CNT is described by a chiral vector, which specifies a path between two points on the graphene lattice which would correspond to the circumference of the CNT when rolled (figure 2.3). The chiral vector is expressed in the form (n, m) in terms of the unit vectors $\vec{a}$ and $\vec{b}$. CNTs with $n = m$ are known as armchair, those with $m = 0$ as zigzag, and all others as chiral (figure 2.4). The vectors $\vec{a}$ and $\vec{b}$ are found to have length $\mid a \mid = \mid b \mid = 0.246$ nm [124]. CNTs formed by rolling graphene sheets would have open ends, but in practice CNTs are often found to be capped by curved graphene in which pentagonal rings of carbon atoms are substituted for the standard hexagonal rings (figure 2.5), or by particles of the catalyst materials commonly used in the synthesis process.

CNTs exhibit remarkable electronic properties due to their size and structural perfection. Armchair SWNTs and MWNTs conduct metallically, whereas zigzag and chiral SWNTs behave as semiconductors. An absence of the lattice defects present in other materials means metallic CNTs exhibit ballistic electron transport over distances of 1 μm as conduction electrons do not backscatter [119].

Individual MWNTs have been shown to be capable of up to 200 μA emission current [125], which indicates a high theoretical maximum emission current density from a macroscopic device. Using a CNT length of 10 μm similar to the best-performing material used in this work, and the optimal inter-CNT spacing of 3 times height calculated by Forbes [13] it can be calculated that an array with 1.1×10^5 CNTs/cm^2 would give emission current density of over 22 A·cm^{-2}, assuming a well-aligned array of CNTs with uniform height and structure. Shorter CNTs with the same aspect ratio would allow more densely-packed arrays giving even higher current densities. Using shorter CNTs also gives the advantage of a lower resistance along the CNT length [25]. In practice it has proved difficult to achieve such an arrangement, with even the most precisely arranged PECVD-grown arrays having a broad distribution of CNT heights.

The energy distribution of electrons emitted from MWNTs has been found to broaden with increasing voltage. Although theory previously predicted emission from MWNTs to preferentially occur from pentagonal tip-sites, it has been shown that the main peak in the energy distribution originates from hexagons while emission from pentagons formed a lower-energy sub-peak. It was also found that the energy distribution of gas adsorbates had no fine structure, and was similar to field emission from metals [126].

The work function of an individual nanotube depends strongly on its structure and surface condition, with the work functions of CNTs with amorphous carbon on the tip found to

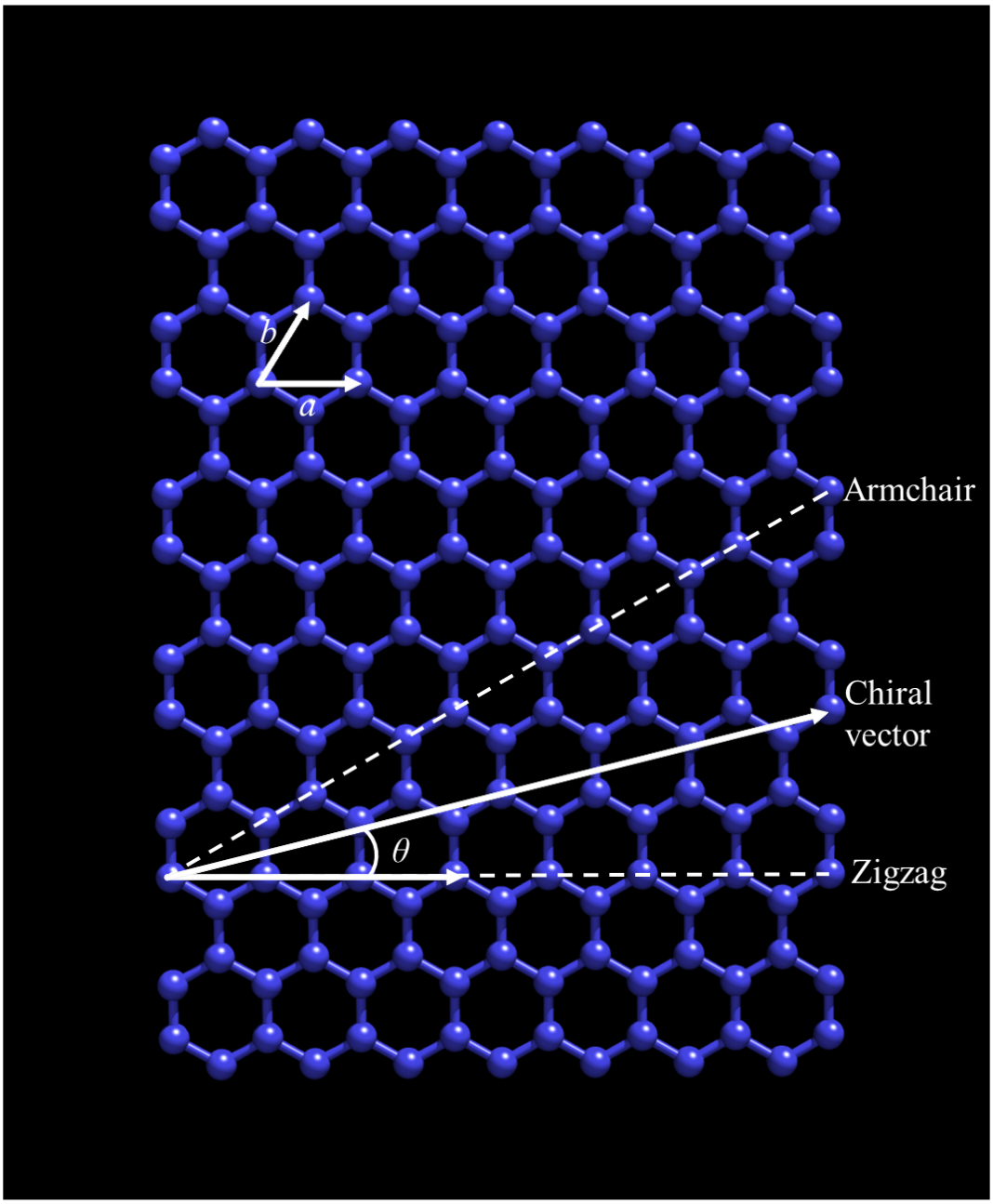

Figure 2.3: Illustration of CNT chiral vector.

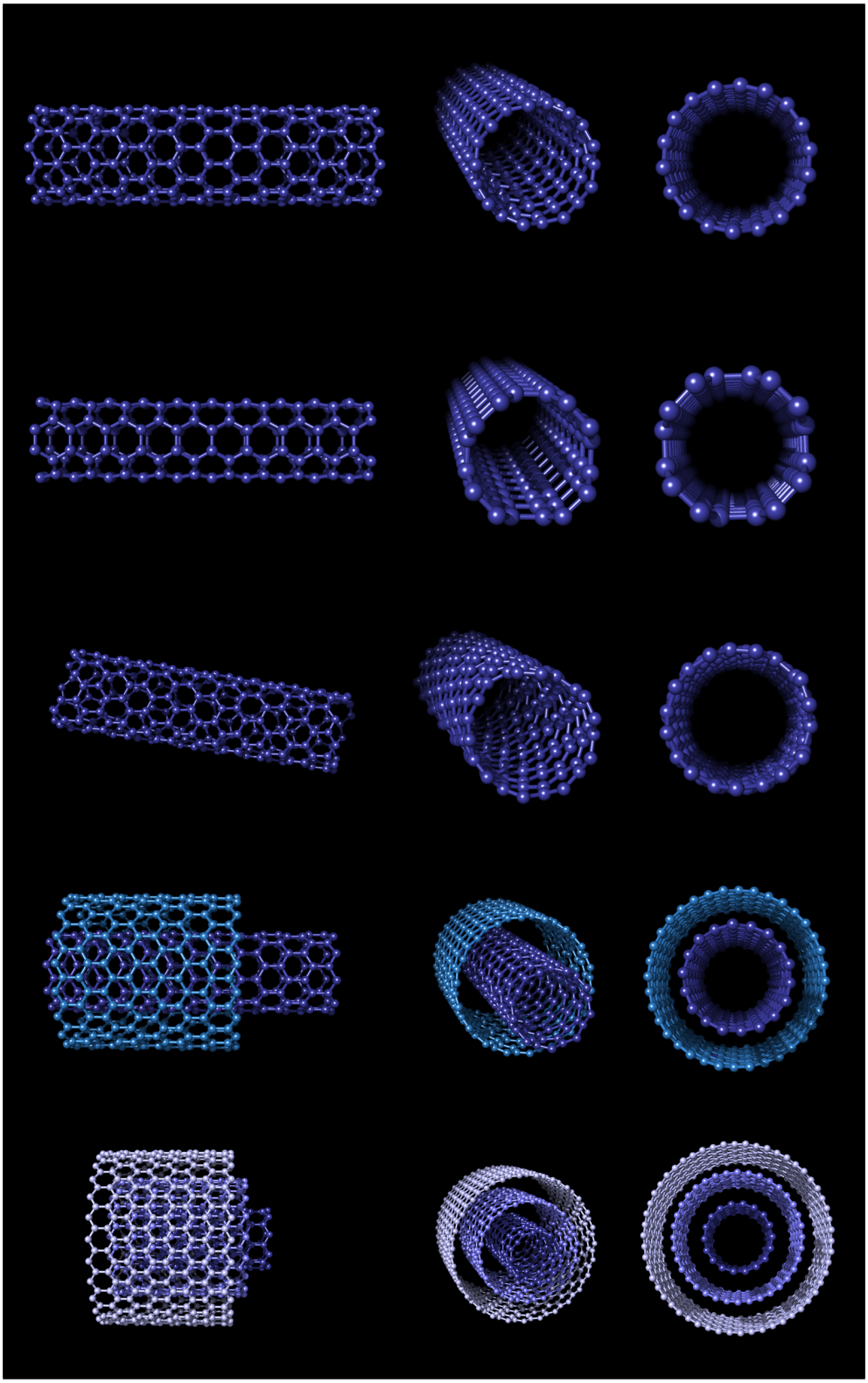

Figure 2.4: Top to bottom: zigzag, armchair and chiral SWNTs, DWNT and MWNT.

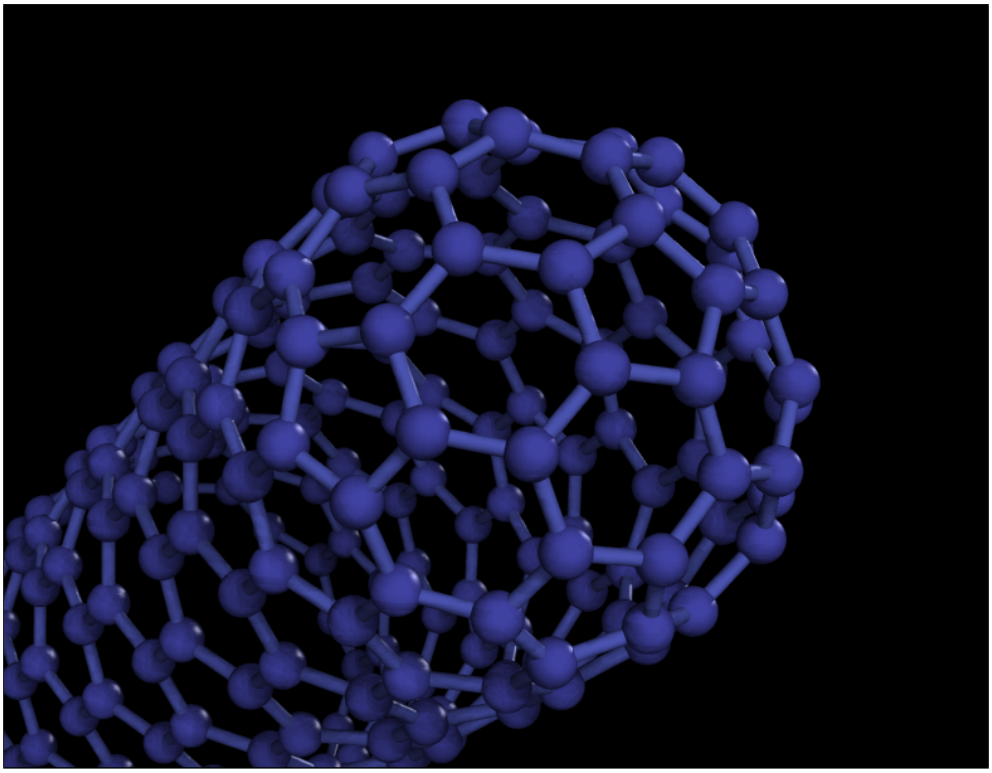

Figure 2.5: SWNT end cap showing pentagonal sites.

be lower than for pristine nanotubes. The same study found work functions of individual nanotubes between 4.51-4.78 eV depending on tip structure. Adsorbed atoms on the tip have also been found to decrease the turn-on field for an individual CNT [127].

CNTs can extend in an applied electric field, causing them to become emitters above a certain threshold field, and to shield other, shorter emitters [128].

Resistance of individual MWNTs has been shown to decrease with temperature, resulting in a negative feedback loop that stabilises temperature. MWNTs have been found to heat to 2000 K by Joule heating during field emission, which is thought to clean and improve the structure [129].

Nanotube tips have been shown to open when heated by laser to close to their sublimation temperature of around 3000 °C. The same effect was also observed at 1000-1500 °C in an atmosphere of oxygen with pressure of approximately 1 Pa. One dimensional atomic wires of carbon were then found to unravel from the open ends of nanotubes undergoing field emission [130]. Heating MWNTs above 500 °C in air results in their decomposition into CO_2, however [131].

A study of individual thermal-CVD MWNTs using a combined SEM and TEM apparatus found that for currents above 10 μA for an individual CNT, the Fowler-Nordheim plot becomes nonlinear due to thermal enhancement of emission [132]. Simulation of the process

shows that the CNTs are significantly cooled by the Nottingham effect. This effect is due to the preferential emission of electrons with higher than average energy and becomes more important at high emission current density [133].

2.4.2 Synthesis of carbon nanotubes

CNTs were discovered only recently, and consequently much about their formation remains unknown. Although it was initially assumed that they were rare, it turned out that nanotubes would form under a wide range of conditions. Descriptions of the two current most commonly used ways of synthesising MWNTs for FE devices follows. In each case, the guiding principle is the same: controlling the potential energy available to carbon atoms to allow them to form CNT structures in an inert atmosphere. With few exceptions, common methods of CNT synthesis result in a yield with a distribution of attributes, rather than uniform size, shape and species.

Arc discharge

In the arc discharge method, an electrical arc is maintained between two graphite rod electrodes under controlled atmosphere. The electrodes are consumed and CNTs or fullerenes are formed, which can then be recovered from the chamber. The anode is consumed preferentially by the process, and the gap between the two electrodes is adjusted to ensure it remains consistent. A DC arc in an atmosphere of helium is most common, though RF arcs and atmospheres of hydrogen or air have also been used successfully. A DC discharge in an argon atmosphere was used in Iijima's discovery of CNTs, for example [118]. The process produces MWNTs by default, though the inclusion of metal or metal oxide catalysts in the electrodes allows SWNTs to be produced. Typical catalysts include Fe-Ni, Co-Ni, Y-Ni, Rh-Pt [124]. A recent review includes a summary of arc discharge processes developed for the manufacture of CNTs [134].

CVD

Most commonly used in the semiconductor industry, CVD is a process where a substrate such as a silicon wafer is exposed to a volatile precursor which decomposes on the surface to deposit material. The result is dependent on the conditions under which the reaction occurs, most notably the temperature and atmosphere. To grow CNTs by this method a carbon-containing precursor such as methane, acetylene or carbon monoxide is used and the substrate is patterned with nanoparticles of catalyst materials such as iron, nickel or cobalt. Of the methods of synthesising CNTs, CVD gives the most control over the structure

and morphology of the product. As a method of fabricating field emission devices, the technique has the advantage that a finished field emission cathode can be grown, requiring no further processing steps [135].

In thermal CVD, resistive, inductive or infra-red heating is used to control the substrate temperature and provide the necessary energy for the reaction to take place. Typically, temperatures of 650-900 °C are employed. Resulting CNTs are closely packed and vertically-oriented with catalyst particles at either the tip or root where the CNT meets the substrate.

PECVD was developed by the semiconductor industry to allow the technique to be used on components which cannot withstand the high temperatures of thermal CVD. Energy comes from a RF discharge between two electrodes, producing a plasma. Although PECVD can work at room temperature, CNT growth processes are performed at temperatures between 400 °C [136] and 900 °C [128]. CNTs produced this way have more defects than those produced by thermal CVD or arc discharge, as they suffer ion bombardment during the growth process [124].

Recent developments in the synthesis of SWNTs by CVD are described in [137], in which the authors note that significant challenges remain before fine control of CNT properties can be achieved.

Metallic catalyst material remains in the growth product and removal methods are damaging to the nanotubes. There has therefore been recent interest in developing CVD-growth methods which do not use a metallic catalyst [138].

It was reported in 2010 that in the case of an iron catalyst, the growth mode could be switched from tip to base by plasma treating the patterned catalyst prior to growth. The authors proposed that the growth mode is dependent on the oxidation state of the catalyst. Base grown CNTs were found to have a smaller diameter than tip grown [139].

A review in 2010 covering the preceding decade's developments in synthesis concluded that CVD provided the best fabrication method [140].

2.4.3 Materials

The CNT materials used in this work along with the manufacturer's quoted geometric properties are given in table 2.1. SEM images of the materials are shown in figure 2.6. All were obtained commercially and used without further purification.

Table 2.1: Emitter materials and their properties.

Supplier/batch	Species	Length	Diameter	Purity
Rosseter H008	MWNT	200-300 nm	8.4 nm	40 %
Brunel-grown	MWNT	300 μm	100 nm	90 %
Xintek XNA-SP-36150	t-MWNT	10 μm	7 nm	88 %

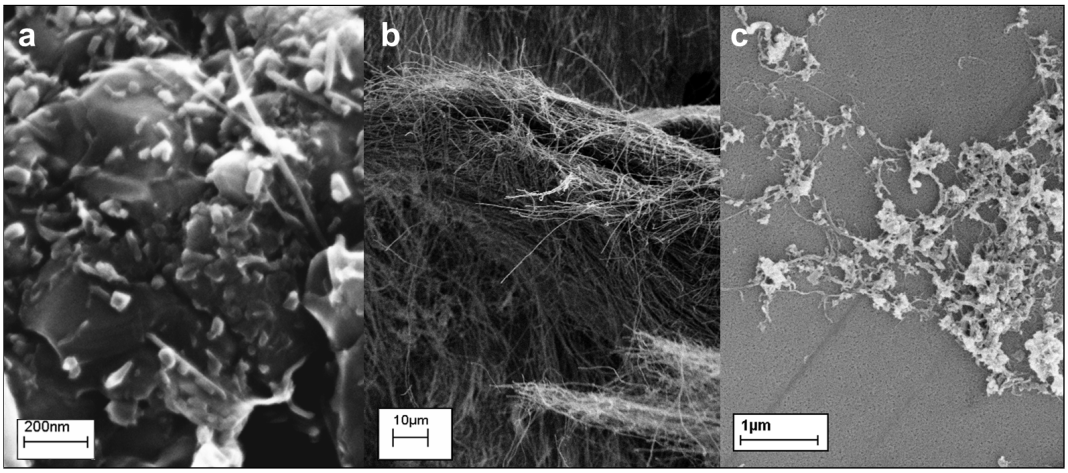

Figure 2.6: CNT materials used in this work: Rosseter (a), Brunel-grown MWNTs (b) and Xintek (c).

2.5 Emitter fabrication

The main body of work presented concerns the preparation and test of field emission cathodes screen printed using a series of carbon-containing inks on a conductive metal substrate. Except where stated, all work preparing inks and their component materials, fabrication of field emission devices and subsequent characterisation and test was performed by the author. Fabrication of the printed samples and field emission testing was carried out at TMD Technologies Ltd. Experimental work was principally to characterise the field emission behaviour of the fabricated cathodes and assess the effect of changing the composition of the inks and the material they were printed on.

2.5.1 Preparation of inks

The inks produced for this project consist of a nanostructured carbon emitter material as described in section 2.4.3, a dispersant, an inorganic binder, a polymer gel to provide viscosity, and several solvents. Sonication is used initially to disperse the carbon and dispersant in the binder before the butoxyethanol is added. The mixture is then sonicated further. The polymer gel is added and the mixture is stirred vigorously, at which point the mixture becomes homogenous. Octanol is added to modify the rheological properties and the mixture is again stirred vigorously. A final mixing is performed using a SpeedMixer DAC 150 FVZ centrifugal mixer at 3000 rpm for 3 minutes. The result is a thick ink with colour varying from dark grey for the graphite-based ink to deep black for inks made with even low concentrations of the Xintek CNTs (figure 2.7).

The ink formulation shown in table 2.2 is for a mid-range CNT concentration ink made for the final data set and can be considered typical. Full formulations of the inks used are given in Appendix B.

Table 2.2: Example formulation of ink used in section 6.3.

Component	**Weight (g)**	**Mass fraction**
CNT	0.0529	0.0074
polyvinylpyrrolidone (PVP)	0.0104	0.0015
Silica binder	0.4880	0.0697
Polymer gel	4.300	0.6143
Butoxyethanol	1.792	0.2560
Octanol	0.3582	0.0512
Total	7	1

Figure 2.7: CNT-based ink.

2.5.2 Silica binder

The inorganic binder material forms a small proportion of the ink recipe, but a large proportion of the final product after firing, where only silicon dioxide remains as a glassy polymer matrix. The function of this material is two-fold, both mechanical and electrical. Firstly, the binder fixes the emitter material to the substrate, preventing it from migrating under the influence of the applied field. Secondly, it insulates the individual emitters, increasing field enhancement factor by reducing the screening effect.

The binder used was made using a sol-gel process with the following reagents:

TEOS	46.8 g	
isopropyl alcohol (IPA)	108.97 g	
Dilute HNO_3	12.51 g	69 % diluted 1:25 (2.65 %)

All reagents were cooled to approximately 5 °C. TEOS and IPA were mixed in a 250 ml beaker, before the acid was added. As the reaction is exothermic, an ice-water bath was used to maintain temperature. The mixture was stirred for 2 hours using a magnetic stirrer until the TEOS is fully hydrolised by the following reaction [141]:

$$Si(OC_2H_5)_4 + 2H_2O \longrightarrow SiO_2 + 4C_2H_5OH \tag{2.1}$$

The sol-gel process yields a fully hydrolysed well-ordered SiO_2 network which is stable at temperatures of 576 °C [142].

2.5.3 Polymer gel

The polymer gel referred to in table 2.2 was made in the lab for use as a common vehicle for all the inks, comprising approximately 60% of the ink by weight. The function of the gel was only to provide a consistency which allowed the ink to be printed and to disperse the emitter material effectively. There follows a list of reagents and a description of the method used:

Hydroxypropyl Cellulose	30 g
Ethanol	54 ml
Propylene Glycol	180 ml
Water	126 ml

The ethanol, propylene glycol and water were mixed in a round-bottomed Quickfit reaction flask and vigorously stirred using a mechanical stirrer while the hydroxypropyl cellulose was slowly added. The temperature was then raised to 70 °C using a heating mantle until bubbles of ethanol vapour began appearing. A water cooled Graham condenser was used to cool and return ethanol vapour to the mixture, keeping volume constant. As heating continued the mixture increased in viscosity resulting in a clear homogeneous gel. The mixture was then allowed to cool naturally before transferring to a storage receptacle.

2.5.4 Screen Printing

A DEK 240 manual screen printer (fig. 2.8) was used to apply a thin, uniform layer of ink to the substrate in the desired pattern. Heat treatment at 450 °C followed to polymerise the silica. Where a copper, molybdenum or stainless steel substrate was used, a hydrogen atmosphere was used in the final heat treatment step and the samples were sealed in nitrogen after cooling to prevent oxidation of the substrate.

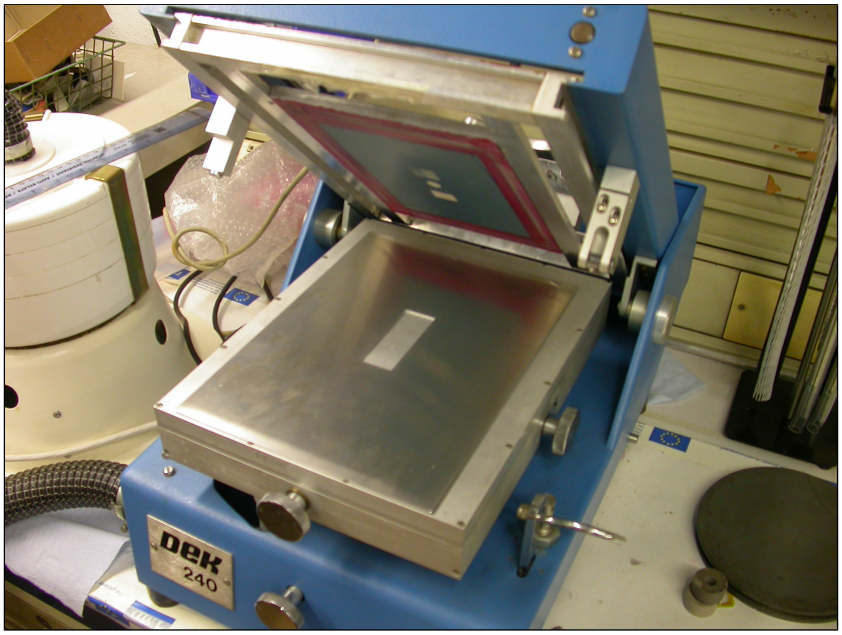

Figure 2.8: Dek 240 screen printer.

2.5.5 Electrophoretic Deposition

EPD is method of depositing suspended particulate matter on a substrate using an electric field applied between two electrodes in a liquid dispersion. The effect is illustrated in figure 2.9. Application of the field results in movement of the suspended particles towards one of the electrodes, allowing controlled deposition. Patterning of the deposited material can be achieved using masking techniques and the deposition rate is controlled by varying the applied voltage and deposition time. Examples from the literature of field emission devices fabricated using EPD techniques to deposit nanostructured carbon are given in section 1.4.3. EPD was performed at Brunel University, with processing and field emission testing performed at TMD Technologies Ltd.

For the EPD experiments performed here a jig was designed and fabricated which enabled the chosen substrate to be held parallel to a steel plate while a potential difference was applied between the two. A computer-aided design (CAD) model of the jig is seen in figure 2.10. Constant-voltage or constant-current modes were available. The direction of migration of the CNTs was found to vary with the species of nanotube used and the presence of binder. Patterning of the substrate was achieved by covering the substrate with a positive photoresist and exposing it to UV light with a stencil in place. The developed substrate then allowed deposition of CNTs in only the desired areas. Following deposition, the same heat treatments were applied as for the screen printed devices.

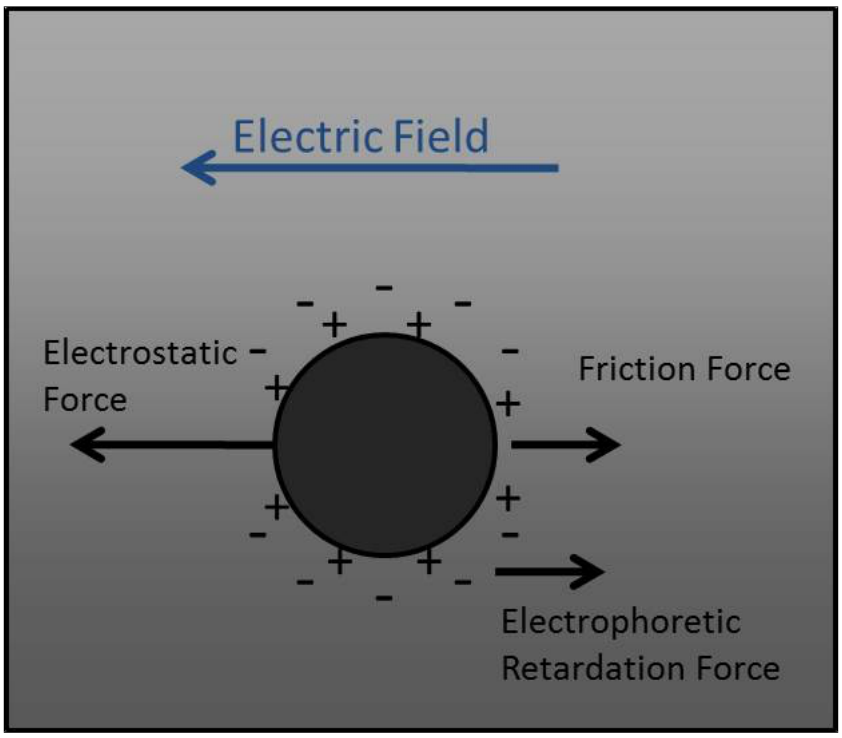

Figure 2.9: Diagram of the electrophoretic effect.

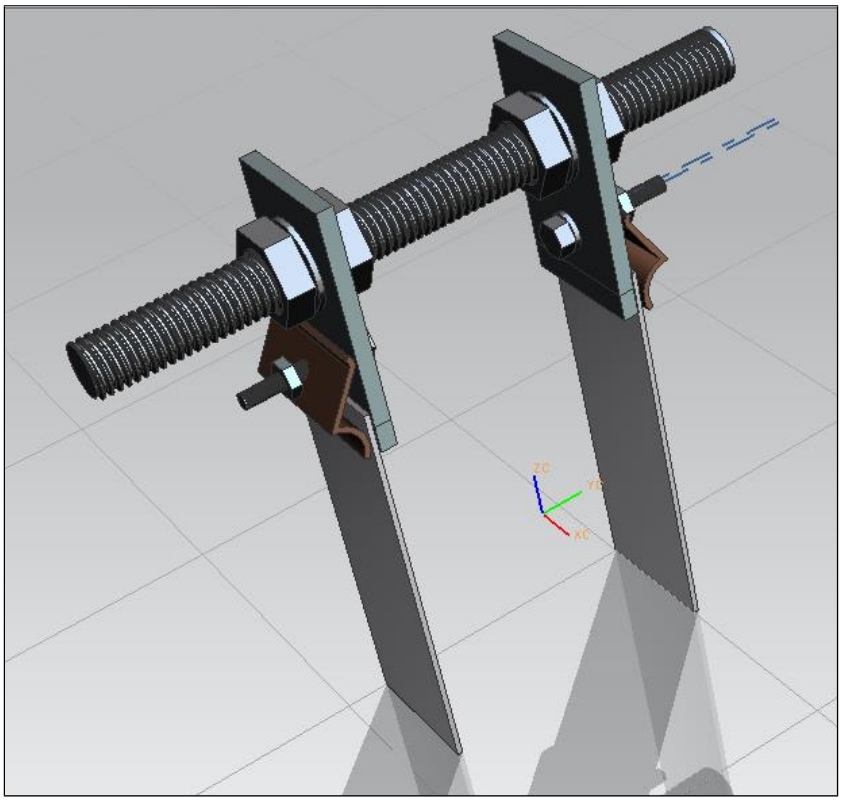

Figure 2.10: CAD model of EPD jig. *Reproduced from [143]*.

2.5.6 Heat treatment

In order to drive off unwanted ink components and polymerise the silica binder a heat treatment process was performed on the field emission devices after deposition, first on a hot plate at 60 °C and 150 °C for 15 minutes each, and subsequently in a furnace at 450 °C. The atmosphere in the furnace was varied according to the requirements of the substrate material, with details given in section 2.5.7 below. Heat treatment in air was performed using a K&F muffle furnace. Heat treatment in hydrogen was performed using a Camco J class furnace (figure 2.11). Table 2.3 lists all the ink components with the temperatures at which they either entirely vapourise or burn off, along with typical values for the proportion of the ink they each constitute. It can be seen that the hot plate treatment removes water, isopropyl alcohol, nitric acid and ethanol, and that after furnacing only the CNTs and silica should remain.

Figure 2.11: Camco J class furnace with maximum temperature of 1150 °C in 100 % wet or dry hydrogen at atmospheric pressure or high vacuum.

Table 2.3: Vapourisation/burnoff temperatures of ink components.

Component	Temperature (°C)	Ink proportion by weight (%)
CNT	550-800	0.25-2
PVP	330	$<$0.5
Butoxyethanol	171	26
TEOS	166-169	1-4
Octanol	195	5
IPA	82.6	2.5-8.5
Water	100	19.5
Nitric acid (HNO_3)	121	$<$1
Hydroxypropyl cellulose	450	5
Ethanol	78.37	8.5
Propylene glycol	188.2	28
Silica (SiO_2)	2230	$<$1.2

2.5.7 Substrate preparation

Field emission devices were fabricated on several substrates as part of this project. This section describes the methods used to prepare the different types of substrate prior to deposition of the carbon emitter materials and any post-deposition processing. Photographs of emitters printed on each substrate type are included in section 6.4. Substrate materials were chosen based on desirable characteristics including thermal and electrical conductivity, and price. Table 2.4 lists the thermal and electrical conductivities of the substrate materials used in the work presented here.

Table 2.4: Thermal conductivities and electrical resistivities of substrate materials at 273.2 K [144] [145].

Material	Thermal conductivity, λ ($W{\cdot}m^{-1}{\cdot}K^{-1}$)	Electrical resistivity, ρ ($10^{-8}\Omega{\cdot}m$)
Gold	319	2.05
Copper	403	1.54
Stainless steel	14.5	55.0
Molybdenum	139	4.85

Gold/NiCr/Glass

In the early part of the project gold-coated glass microscope slides were used as substrates. Gold is a logical candidate as a printed field emitter substrate as it is highly electrically and thermally conductive and is chemically inert, making it easier to maintain a pristine surface and therefore good contact between the substrate and emitter material. Its high price limited the use of gold to a thin layer rather than a solid piece. The slides were 76 x 26 x 1 mm and were evaporator-coated with a 100 nm layer of gold, with a nichrome adhesion layer between the gold and glass. The slides were prepared for printing by ultrasonication in solvent. After printing the samples were heated to 60 °C and 150 °C for 15 minutes each on a hotplate to drive off the solvent components of the ink before heat treatment at 450 °C for two hours in air.

Copper

Copper has the highest thermal conductivity of any metal apart from silver and is relatively inexpensive. Although it forms a resistive oxide layer in air copper was considered to be a good candidate as a substrate as it can be easily cleaned, the oxide layer is easily removed with standard processes and it is readily available. To fabricate field emission devices 99.9% pure copper sheet with a mirror finish was supplied in 26 x 76 x 0.5 mm sheets by Metal Sheets, Liverpool. To eliminate any curvature induced by the machining process, the sheets were heated to 850 °C in a hydrogen atmosphere, de-stressing the copper and allowing it to take the shape of the flat ceramic batt on which it was placed. Copper substrates prepared in this way were sealed in nitrogen until immediately before they were printed on, at which point a hot alkali clean was performed to remove any residual grease. After a thorough rinse, the substrate was etched in a dilute nitric acid bath for at least 10 minutes until the surface was free of oxidation. Printing was performed immediately after drying to minimise formation of an oxide layer between the metal and the emitter material, heated to 60 °C and 150 °C for 15 minutes each on a hotplate to drive off the solvent components of the ink and sealed in nitrogen immediately thereafter. The emitters were then heat treated in atmospheric pressure dry hydrogen at 450 °C for two hours before being sealed in nitrogen again to protect them until field emission testing was performed.

Stainless steel

Stainless steel was investigated due to its ready availability and ubiquity in modern manufacturing. Mirror finish 304 grade stainless steel 26 x 76 x 2 mm sheets were supplied by Metal Sheets, Liverpool. An initial heat treatment to flatten the substrate was not required,

however burrs and sharp edges were removed in the TMD Technologies Ltd machine shop before the same cleaning, printing and subsequent heat treatment processes given above for the copper substrates was implemented.

Molybdenum

As a refractory metal molybdenum is commonly found close to thermionic emitters in application. If a field emission cathode was incorporated into an existing design for a thermionic device molybdenum is a plausible substrate as it would minimise issues with expansion matching. Although molybdenum is an uncommon material it was tested here as TMD Technologies Ltd expressed an interest and had suitable material in stock. 50 μm-thick molybdenum sheet was cut to a similar size to the other emitters, printed on using the same screen printing technique and underwent heat treatment in hydrogen atmosphere at 450 °C for 2 hours in the same procedure as the copper emitters. As the molybdenum substrate was comparatively thin, it was mounted on a flattened copper sheet using conductive silver paste which was allowed to dry thoroughly prior to testing.

2.6 Characterisation techniques

2.6.1 Scanning electron microscopy

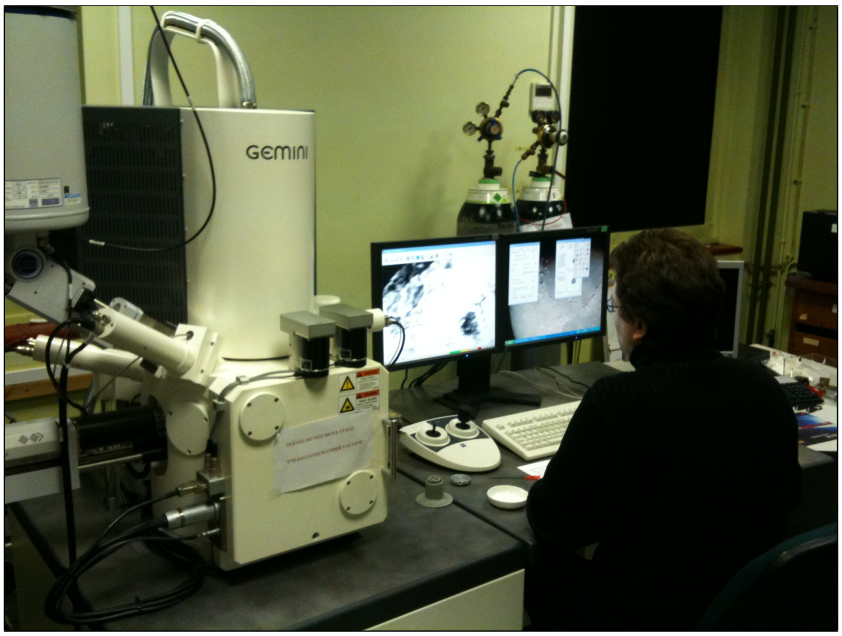

Figure 2.12: Ziess Supra 35 VP field emission scanning electron microscope.

The Abbe theory places a fundamental limit on the resolution of a light microscope, relating it to the wavelength of the incident light:

$$d = \frac{\lambda_l}{2n \sin \theta} \tag{2.2}$$

where d is the resolution, λ_l is the wavelength of the incident light, n is the refractive index of the lens material and θ is the half-angle of the cone of light between the edge of the lens and the object being imaged. Taking example values of $\lambda_l = 500$ nm corresponding to green light in the approximate centre of the visible spectrum and $n = 1.498$, the refractive index of the most commonly used optical polymer and a half-angle θ of 60°, it can be calculated from equation 2.2 that the smallest object that can be resolved is 193 nm.

The de Broglie wavelength, λ_e, of an electron is described by the equation:

$$\lambda_e = \frac{h}{m_e v} \tag{2.3}$$

where h is Planck's constant, m_e is the electron mass and v is the velocity of the electron. More energetic electrons have smaller wavelength and can therefore be used to image smaller objects.

In SEM, an electron beam is accelerated by high voltage, typically 20 kV, giving individual electrons a wavelength of 9 pm. A significantly higher resolution can therefore be achieved than with a light microscope. The electron beam can also give other information about a sample such as electrical conductivity and elemental composition through x-ray generation, electron backscattering, secondary and Auger electron emission and cathodoluminescence.

Of the three types of electron source typically used in SEMs: tungsten filaments, lanthanum hexaboride crystals and field emission gun (FEG)s; only FEGs can provide the resolution necessary to observe nanostructured carbon-based field emitters in detail. Modern field emission scanning electron microscopes (FE-SEMs) use a Schottky emitter, in which a combination of heat and electric field enhancement cause electrons to leave the material by both providing energy and lowering the potential barrier. A tungsten tip with radius 0.1 μm provides a highly concentrated electron beam with a brightness over a thousand times greater than that achieved with a filament. The Zeiss FE-SEM at Brunel University (figure 2.12) has a resolution of 5 nm allowing powerful imaging of the field emission devices presented in this work. The SEM was used extensively to study the emitters before and after field emission testing, typically with low beam voltage (3-6 kV) and current to avoid damaging the emitters. The in-lens detector was primarily used with a short working distance of a few mm, achieving up to 250,000 times magnification despite the difficulties of imaging conductive CNTs in an insulating silica matrix.

2.6.2 Raman spectroscopy

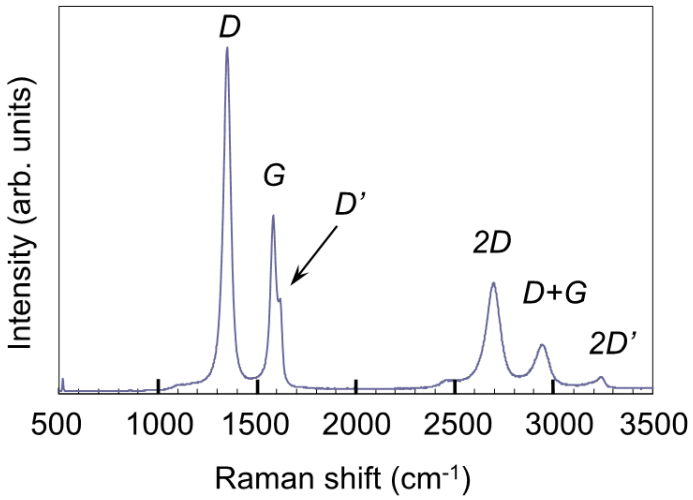

Figure 2.13: Raman spectrum of graphene. *Reproduced from [146]*.

In Raman scattering, incident photons are scattered inelastically by molecules, resulting in emission of photons of a different frequency. Raman spectroscopy takes advantage of this effect by measuring the frequency shift of scattered photons of laser light incident on a sample. The obtained spectrum of frequency shifts shows characteristic peaks, the locations of which give information about the bonding configurations of molecules in the sample. The technique is especially well suited to nanostructured carbon samples, which show two characteristic peaks corresponding to different types of covalent bonds between carbon atoms. An example of a Raman spectrum is shown in figure 2.13, in this case from a sample of PECVD-grown graphene nanowalls. The G peak, at 1580 cm^{-1}, corresponds to sp^2 orbital hybridisation in the material and is associated with the presence of graphitic bonding. The D peak at 1350 cm^{-1} is associated with sp^3 orbital hybridisation, indicating the presence of amorphous carbon. With MWNT samples, the most common method of analyzing Raman data is to divide the intensity of the D peak by that of the G peak, known as the I_D/I_G ratio, which gives information about the purity of the CNTs. Samples with a low I_D/I_G ratio have fewer structural defects. The D' peak commonly manifests as a shoulder on the upper side of the G peak and is characteristic of defects in graphitic structure, and is smaller in better quality MWNTs [147]. The instrument used in this work was a Horiba Jobin Yvon LabRAM HR800 Raman spectrometer at Brunel University using a green laser of wavelength 532 nm.

2.6.3 Thermogravimetric analysis

Thermogravimetric analysis (TGA) is a technique which uses a sensitive balance to record changes in weight as increasing temperature is applied to a sample. TGA is commonly

performed in air or an inert atmosphere and gives information about the temperature at which physical or chemical changes occur, for example vapourisation (seen as a reduction in weight) or oxidation (seen as a gain in weight). The instrument used in this project was a TA Instruments Q500 Thermogravimetric Analyser at Brunel University. TGA was performed in air using a temperature ramp rate of 10 °C per minute up to 1000 °C. Ink samples were heated to 150 °C on a laboratory hotplate before TGA.

2.7 Conclusions

A number of methods of producing CNT-containing materials are used, with commercially available examples of all types. A method of screen printing several materials using a common vehicle with a polymer gel base and silica binder has been selected for principal study here, with 4 different metallic substrates used. EPD has also been studied and a technique for fabricating emitters developed. Analysis techniques included SEM, Raman spectroscopy and TGA.

Chapter 3

Instrumentation and testing

3.1 Introduction

A significant part of the work was to develop and assemble custom experimental equipment to test field emission devices. As the aims of the project differed from those typically detailed in the literature, specifically to achieve maximum current, and used a larger-area cathode, a different equipment profile was required. This section presents the technical specifications of the test instrumentation along with a description of the developed test processes.

3.2 Working safely with high voltage

The circuit described in this section operated with sufficiently high voltage and stored energy to pose significant danger. Consequently the high voltage section was housed in a grounded aluminium case which was installed inside the vacuum chamber housing. The circuit was designed to discharge in the absence of an input signal, and could be manually discharged without physical access. Access to the components required the case to be removed from the vacuum chamber housing and disassembled. Individual components were insulated from the case using Kapton and from each other using silicone potting material, with polytetrafluoroethylene (PTFE) sheet added where the electric field gradient was high. A single shielded high voltage cable was connected between the switching circuit in the vacuum chamber housing and the Glassman power supply unit (PSU) in an adjacent equipment rack. Interlocks were installed allowing high voltage only to be generated when the vacuum chamber housing was closed and when the vacuum gauge registered a chamber pressure below 5×10^{-4} Pa. Opening the vacuum chamber housing required a key which was kept elsewhere except when working on the equipment and the entire test setup was behind a safety barrier with warning signs. Appropriate high voltage training was given and all work

carried out in accordance with the document Electricity at work: Safe working practices published by the Health and Safety Executive [148].

3.3 Test rig

Two test rigs were designed and built as part of the project. The first functioned as a proof-of-concept exercise, evolving iteratively as emitters were tested. It was abandoned as the emitters improved, eventually exceeding the capabilities of the rig and resulting in its destruction. Its replacement was a more considered design of more ambitious specification, intended to test emitters thoroughly and rigorously from the outset, and was used to collect all data presented here. A full description of the second rig follows. In both cases, the function of the rig was to allow a negative high voltage to be applied to the field emission device and varied, with a parallel anode plate at ground potential a known distance away, so that the I-V characteristics of the cathode could be recorded.

3.3.1 Design

A schematic of the final test rig is shown in figure 3.1 and the full technical drawing included in appendix C. Materials were chosen which were capable of withstanding high temperatures and the rig was larger and heavier than previous designs, giving it a much greater thermal mass to prevent overheating. Ultra-high vacuum (UHV)-compatible materials were chosen to minimise outgassing. Machinable Macor ceramics were used to separate the anode and cathode plates (figure C.6, figure C.8: item 6). Macor was chosen because it can withstand temperatures of up to 1000 $^{\circ}$C, is high vacuum-compatible and can be precisely machined unlike other ceramic materials. It was intended that the legs (figure C.5, figure C.8: item 5) should also be Macor, but a shortage of the material and consequent extremely high price at the time led to PTFE being used instead. Three Mitutoyo micrometer screws were incorporated to allow adjustment of the anode-cathode gap with an accuracy of ± 5 μm. Roger Gates and Jonathan Warrens at TMD Technologies Ltd assisted with materials selection and created the technical drawing. Leemark Engineering, Hayes fabricated the metal and ceramic parts. Final assembly and testing was performed by the author. A photograph of the finished rig is seen in figure 3.2.

The anode-cathode gap was set by an electrical contact method using a digital ohmmeter connected to the anode and cathode plates of the test rig. The rig was initially set with the micrometer screws retracted so that the upper portion of the test rig was supported by three spacers placed between the anode and cathode. Each spacer was made from two sections of anisotropic pyrolytic boron nitride (APBN) rod with a rectangular cross-section

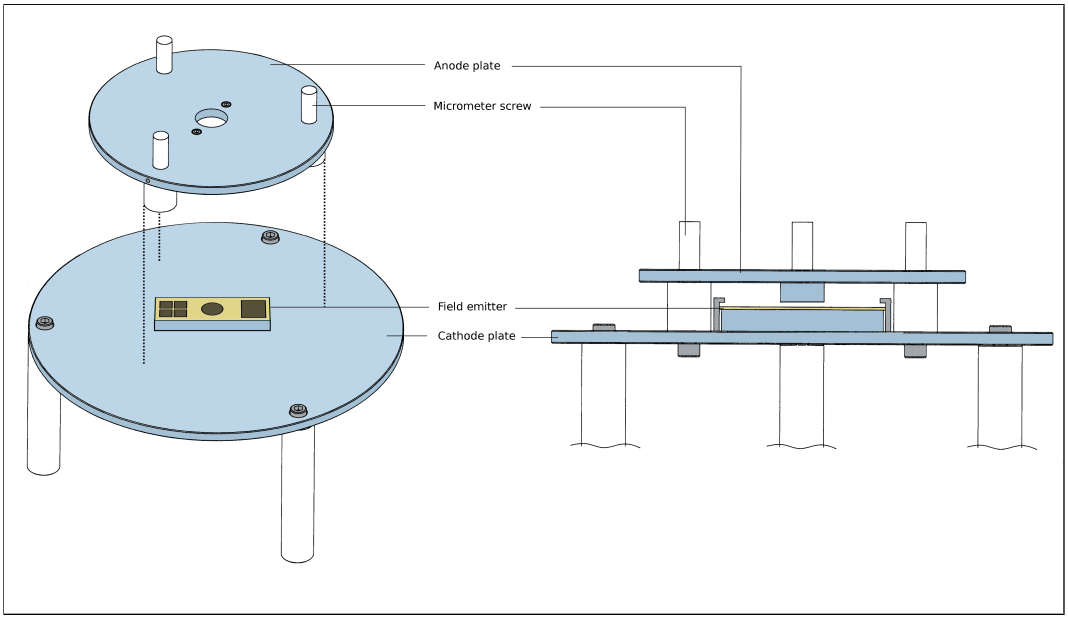

Figure 3.1: Schematic of second-generation test rig.

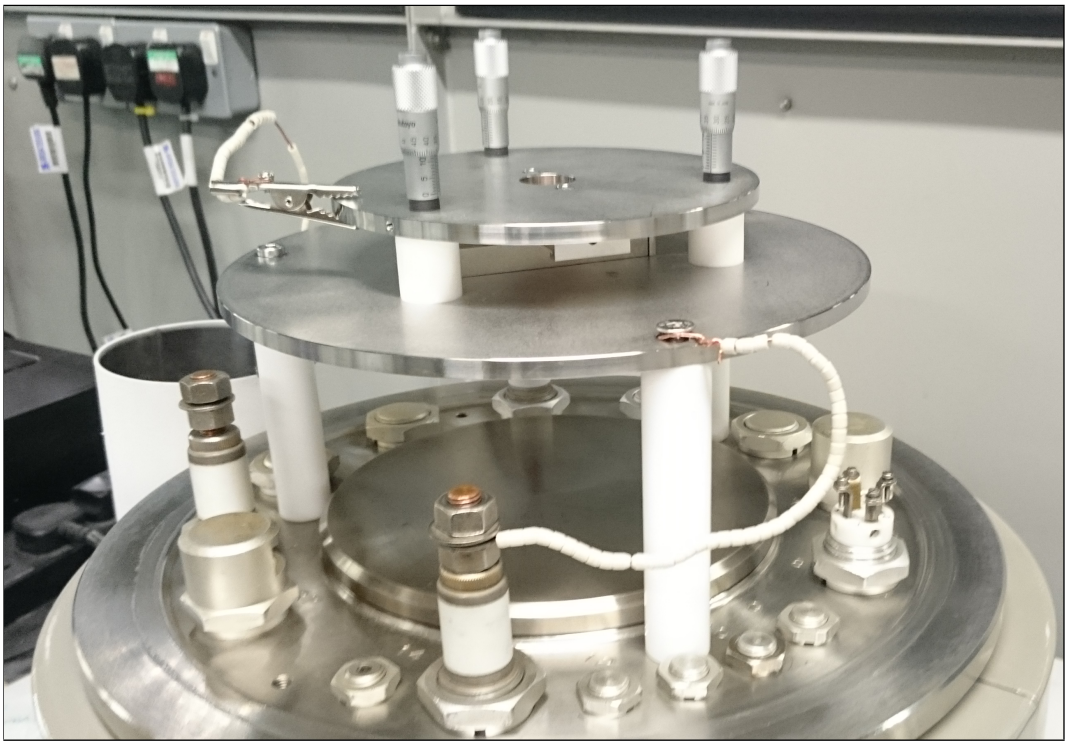

Figure 3.2: Field emission test rig shown on base of test chamber.

and a height of 400 μm. The inner section of each spacer was coated with a thin layer of carbon allowing electrical conductivity between the upper and lower surfaces with resistance around 6 kΩ, while the outer section was electrically insulating. Observation of a resistance between the anode and cathode of 2 kΩ indicated good contact between both electrodes and the conducting spacers. The micrometer screws were adjusted incrementally. Observation of a sharp transition between maximum conductivity and an open-circuit reading from the ohmmeter indicated uniform separation of 400 μm and that the plates were parallel. At this point the micrometer positions were recorded and the spacers removed. Any required adjustment to the anode-cathode gap could then be made using the micrometer screws.

3.4 Hardware

3.4.1 Vacuum chamber

The test chamber used was a modified Edwards sputter coater chamber with an oil diffusion high vacuum pump and rotary vane backing pump. Pressure was measured by a Pfeiffer Vacuum PKR 251 Compact FullRange gauge. The chamber had base pressure of 1.0×10^{-5} Pa (1.0×10^{-7} mbar). FE testing began when the pressure fell to 5×10^{-5} Pa, which was typically achieved in approximately an hour and a half.

3.4.2 High voltage supply

PSU: Glassman EK08N75

A negative-type Glassman HV EK series PSU was used, supplying up to 75 mA at 8 kV. The PSU had voltage regulation better than 0.005 %, ripple voltage of less than 0.02 % and arc sensing circuitry to detect arcing and cut output to prevent damage. Constant voltage operation was used exclusively in this application. Parameters were controlled via the front panel of the PSU, via input pins on the rear accepting voltages of 0–5 V corresponding to 0–100 % of the rated voltage or current, or via an optional Laboratory Virtual Instrument Engineering Workbench (LabVIEW) interface module. Although the PSU came with a simple LabVIEW control program, new code was written to add test capability, including on-screen graphing of the test variables and high resolution data logging. Preliminary DC tests were performed with the PSU connected directly to the vacuum chamber feedthroughs, but the results presented here were collected by using additional hardware to pulse the high voltage (HV) to simulate the requirements of a commercial x-ray baggage scanner.

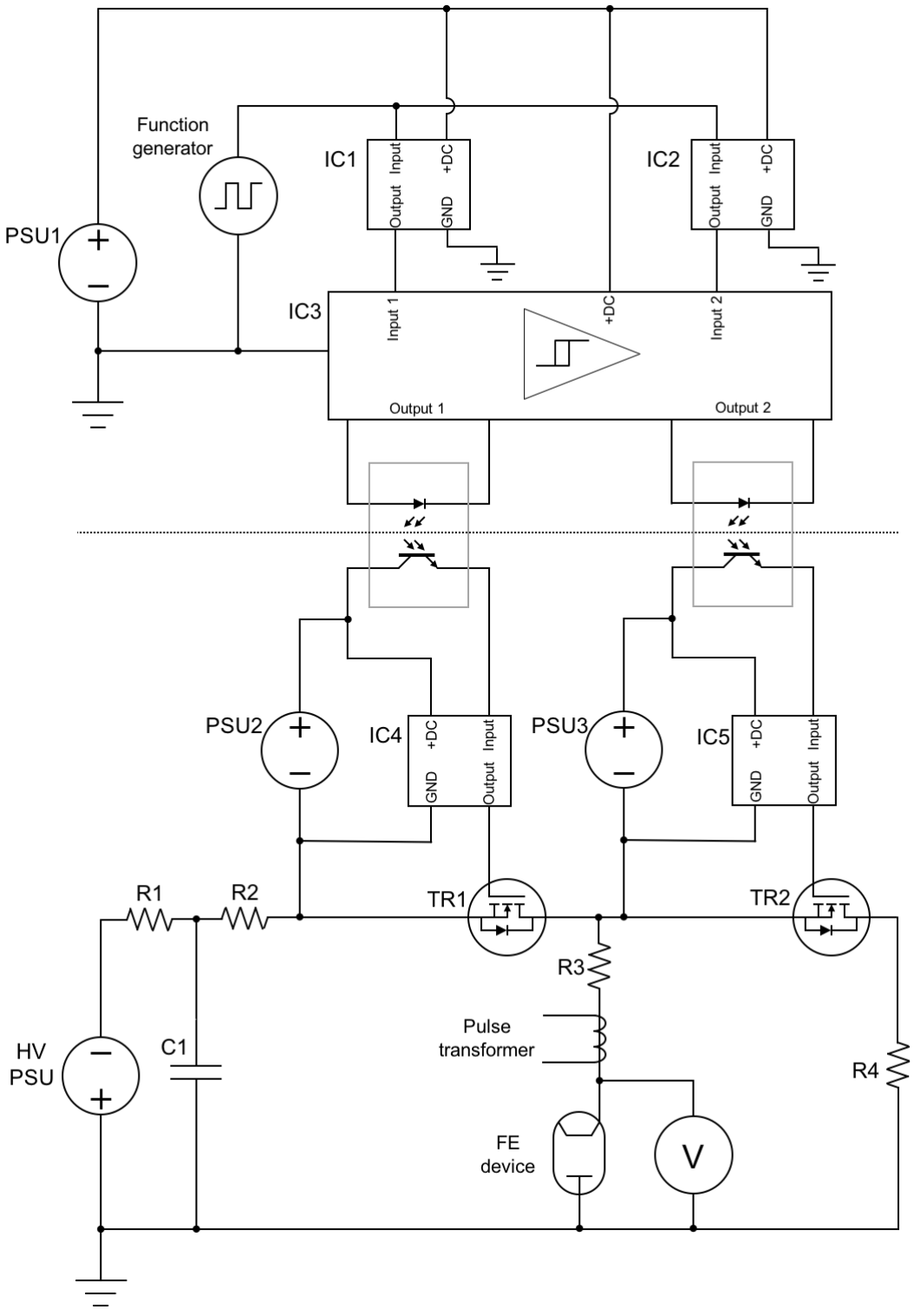

Figure 3.3: Pulsed field emission test circuit diagram.

Switching circuit

Figure 3.3 is a schematic circuit diagram of the setup used to pulse the high voltage supply. Two high-voltage enhancement-mode metal-oxide-semiconductor field-effect transistors (MOSFETs) were used, arranged in a push-pull configuration. R1, R2 and C1 in figure 3.3 form a filter to prevent the arc-sensing circuitry of the PSU output reacting to rapid switching behaviour. Each MOSFET (TR1 and TR2) was driven by an independent circuit with a floating DC power supply. Two optocouplers with 1 m optical fibre were used to safely couple the switching signals to the floating high-voltage sections. On the low-voltage side, an Agilent 33210A function generator was used to generate rectangular pulses with amplitude of 1 V. A two-channel Schmitt trigger integrated circuit (IC) was used to generate two nested square pulses which were then amplified by MOSFET driver ICs and used to drive the light-emitting diode (LED) section of the optocouplers. The pulse widths were adjusted so that a short delay occurred between the two MOSFETs changing state, ensuring there was no overlap where the high voltage PSU was shorted to ground. R3 in figure 3.3 is the series resistor discussed below.

Series resistor

Breakdown events are a common part of the initial testing of an electron source, as material outgassed by the cathode and anode form conducting paths. Damage caused to the emitter surface by breakdown events is shown in figure 3.4.

A ballast resistor was added to the circuit in series with the field emission device (figure 3.3, R10). Having a resistance of 5 kΩ, the function of the resistor was primarily to limit the maximum current in the circuit to prevent damage to both the test hardware and the emitter during breakdown events.

Ohm's law states that the current in a conductor is related to the potential difference across it by the equation:

$$V = IR \tag{3.1}$$

where V is the potential difference, I is the current and R is the resistance of the conductor. In the case of the field emission device and resistor in series, the equation becomes:

$$V_{FE} + V_B = I(R_{FE} + R_B) \tag{3.2}$$

where V_{FE} and V_B are the potential differences across the field emitter and ballast resistor respectively, and R_{FE} and R_B are the resistances of the field emitter and ballast resistor respectively. The resistance of the field emitters tested varies throughout the test from upwards of 1 MΩ at low applied field to around 30 kΩ at high fields and currents. From the above equation it can be seen that in a typical test with a maximum potential difference of 4.4 kV, even if the resistance between the anode and cathode drops to zero, the maximum current in the circuit will be 880 mA.

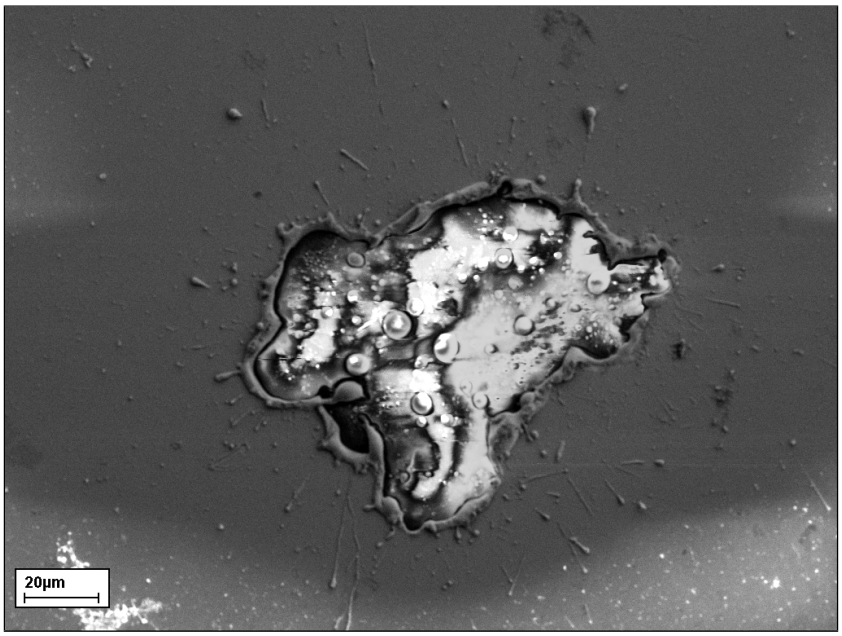

Figure 3.4: Emitter surface showing damage caused by breakdown event.

Tektronix DPO3034

For pulsed testing a Pearson current transformer and Tektronix P6015A 1000:1 voltage probe were used in conjunction with a Tektronix DPO3034 digital oscilloscope. The current transformer measured current in the cathode high voltage wire, and voltage was measured at the emitter substrate surface. The oscilloscope displayed the voltage and current pulses throughout the tests along with the signal from the function generator which drove the switch. The shape and timing of the pulses on these three channels provided information about the behaviour of the circuit as well as the performance of the emitters.

3.5 Software

National Instruments LabVIEW is a software package allowing programs, known as virtual instruments (VIs) to be written in a graphical programming language named “G”. The framework allows relatively quick creation of control software for any instrument with a compatible driver. In this case, LabVIEW was used to integrate the Glassman EK series power supply, the Agilent function generator controlling the switching circuit, and the Tektronix oscilloscope. Control of the voltage, duty cycle and period were therefore achieved programmatically, and large amounts of data recorded automatically. This made performing experiments easier, and most importantly ensured that each test within a data set was performed consistently with the same time intervals between measurements. Figure 3.5 shows a screenshot of the front panel of the VI used to record the final data set taken in the project, where the user-controlled parameters are entered. In this case, the user defines the anode-cathode gap, the oscilloscope channels from which to record data, the file path to record data to, and the location of the input file containing the voltage and duty profile of the test. A graph of current vs. time is also displayed during the test as well as information about the number of breakdown events detected. Figure 3.6 illustrates the function of the main control loop of the program.

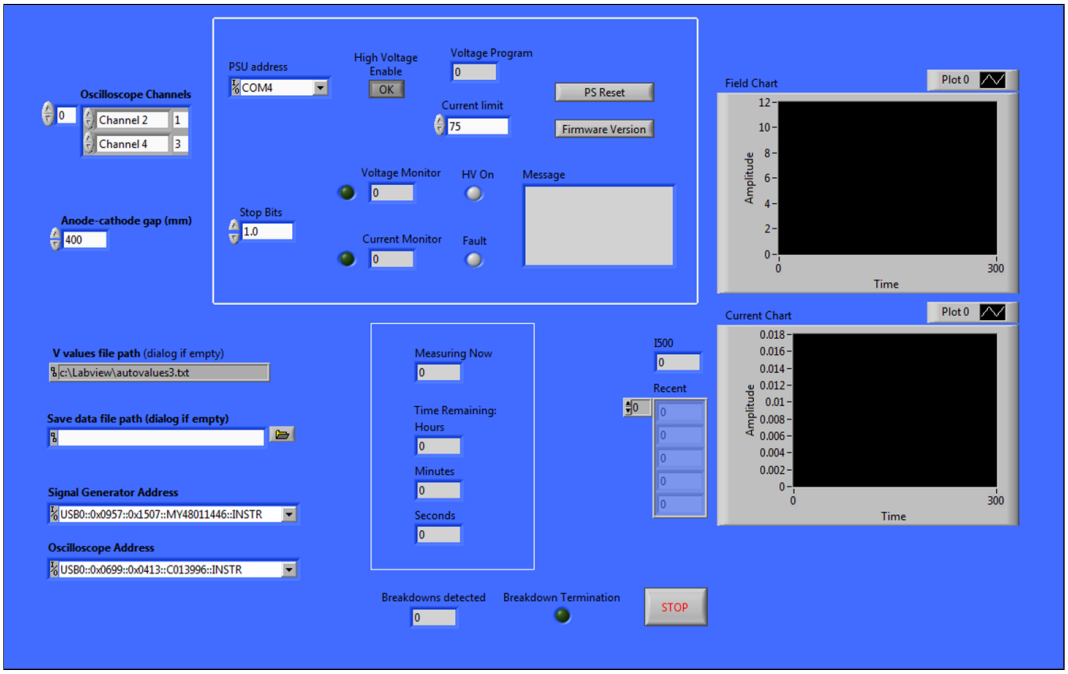

Figure 3.5: Control software front panel in LabVIEW.

The purpose of the LabVIEW VI was to integrate control of the Glassman PSU and Agilent function generator controlling a solid-state switch with data collection from the Tektronix

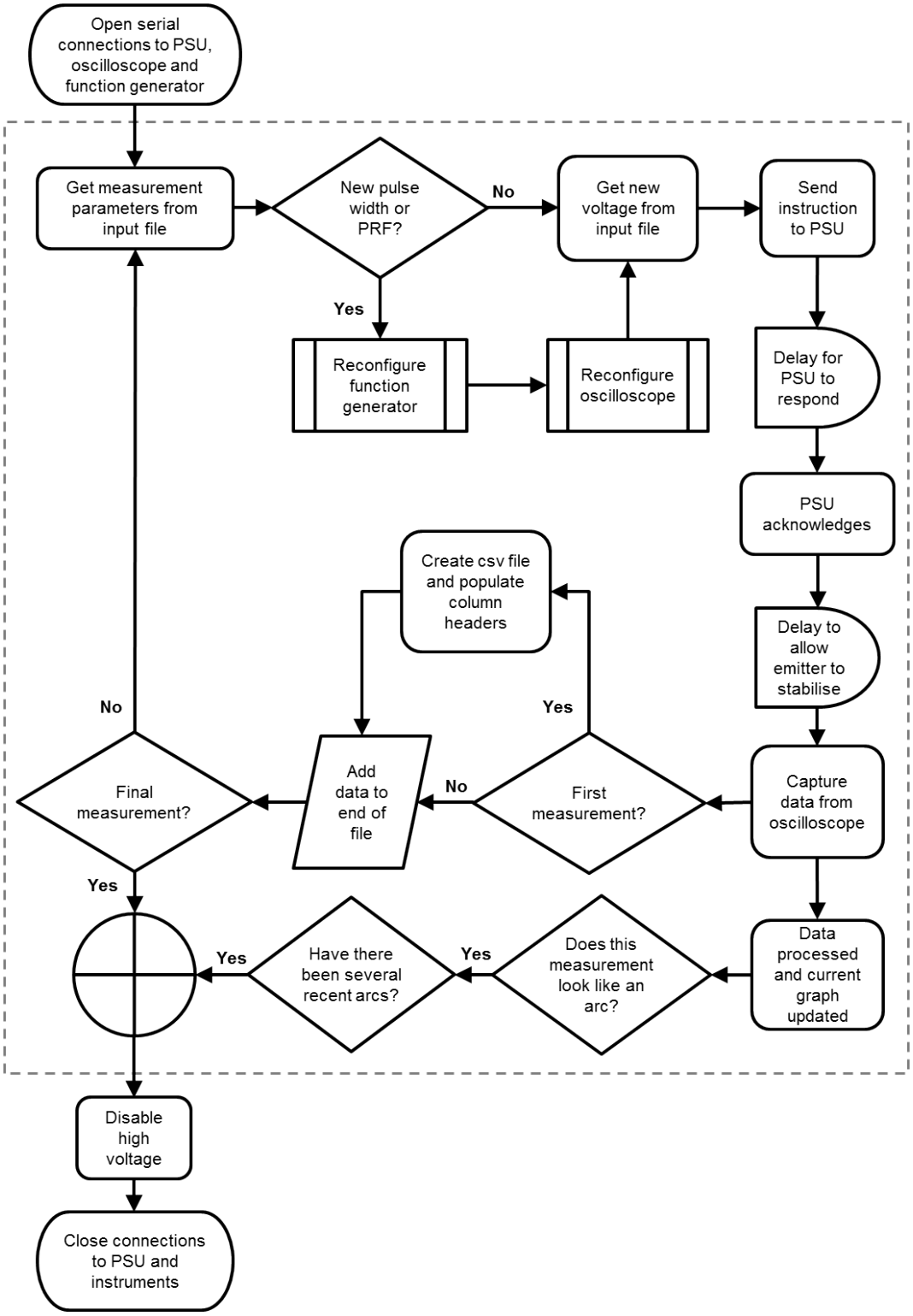

Figure 3.6: Flowchart illustrating function of main software loop.

oscilloscope. The central feature of the program is a loop which sets the duty profile by sending an instruction to the function generator, sets the output voltage by sending an instruction to the PSU and captures the resulting voltage and current pulse data from the oscilloscope, in that order. The loop is designed so that oscilloscope data is only captured after receiving an acknowledgement from the PSU, and incorporates a delay to ensure the data is only gathered once the circuit had stabilised. The pulsed emission circuit inhibited rapid changes in peak voltage by design, and it was found in testing that a delay of around 1.5 seconds was sufficient. The software took as input a tab-delimited file of voltage, pulse width and period values which was loaded at the start and queried at each cycle of the main loop. The output was a second tab-delimited file of the voltage and current waveforms together with a timestamp which was saved at each cycle, meaning that data was still saved if the program did not reach the end of the intended test. As well as saving the full data, the midpoint of the voltage and current waveforms were extracted from each cycle of the loop and plotted against time on screen to show the progression of the test. Following the observation that breakdown events often corresponded to recorded current values with the wrong polarity, a breakdown detection feature was added which continuously examined the midpoint of the current waveform and logged the number of events. Detection of two breakdown events in a row or in three out of any five consecutive measurements terminated the test. The test could also be terminated manually using the on screen stop button, and terminated automatically on reaching the end of the input data. On termination, an instruction was sent to the PSU to set output voltage to 0 V, followed by instructions to both the PSU and function generator to disable output, rendering the entire circuit inactive. Finally, connections to all instruments were closed.

3.6 Testing

Testing a field emission device involved applying a voltage between the device and a parallel plate with a known separation in vacuum. A negative potential was applied to the field emission cathode and the anode plate held at ground. The voltage was varied and the resulting emission current recorded. When considering the behaviour of the device the applied electric field, E, is calculated:

$$E = \frac{V}{d} \tag{3.3}$$

where V is the applied voltage and d is the cathode-anode separation. Emission current density, J, is calculated:

$$J = \frac{I}{A} \tag{3.4}$$

where I is the measured emission current and A is the area of the printed field emission device. Except where otherwise stated, the field emission test results in the work presented here were collected from a device with an area of 1 cm^2, and consequently the emission current and emission current density had the same numerical value.

Pulsed input

Under the pulsed voltage test regime 1000 data points were recorded for voltage and current at each measurement. Values used for analysis were obtained by taking a mean of points 400 to 600 to give a value for the pulse amplitude compensating for noise. A mean of points 100 to 200 was also taken and subtracted from the amplitude to compensate for any offset.

Figure 3.7(a) shows the recorded voltage for a single measurement under pulsed operation. In this case the pulse width was 70 μs. Although the switching circuit was slowed down (section 3.4.2) the pulse still has a rapid rise time. Figure 3.7(b) shows the corresponding current measurement. The sharp peak at the leading edge of the pulse is charging current due to the capacitance of the test rig.

Pulsed field emission testing was carried out using a duty profile which represented a likely requirement of a commercial airport CT baggage scanner, with the following parameters:

Pulse width	85 μs
Period	70 ms
PRF	14.29 Hz
Duty	0.12 %

Anode

The early tests performed in this project used an aluminium anode for DC testing at low currents up to 5 $mA{\cdot}cm^{-2}$. This anode was in a fixed position and was regularly abrasively polished to remove material damaged during testing. With the introduction of the revised test rig design a replaceable anode was used, removing the need for polishing and the consequent risk of altering the surface finish or deforming the material. Anodes made from the same 75 x 25 x 1 mm polished copper sheet as the emitter device substrates described in sections 2.5.7 and 6.4.2 were used. Copper has the advantage of both a higher melting point and thermal conductivity than aluminium. Stainless steel anodes were also used, again

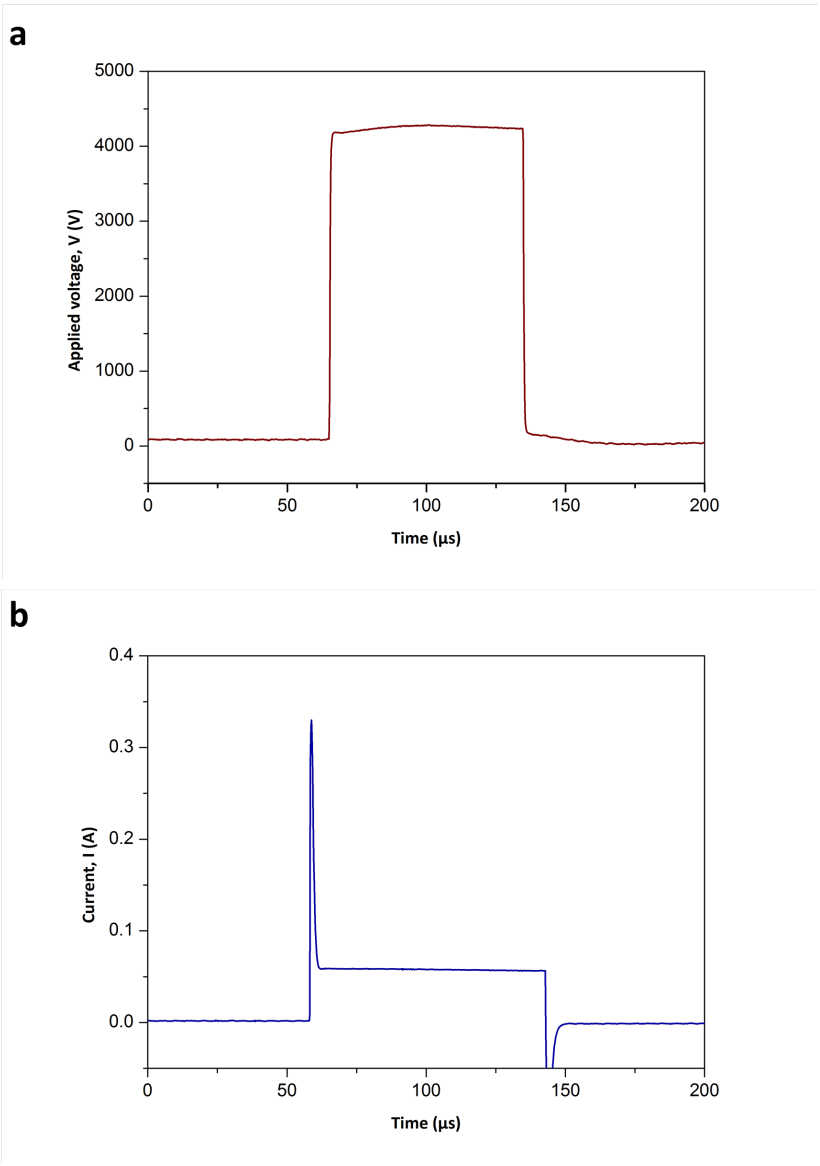

Figure 3.7: (a) Voltage pulse at 0.12 % duty. (b) Corresponding current pulse.

made from the same material as the equivalent emitter devices described in sections 2.5.7 and 6.4.3. It was observed visually that the copper suffered cumulative damage more quickly during testing and was therefore replaced more frequently than the stainless steel. However, no performance changes were ever observed which related to either the anode lifetime or a difference between the materials. The anode is discussed further in section 4.4.

A phosphor-coated transparent anode was also used to allow emission uniformity to be observed. The anode was made by coating ITO/glass slides with a ZnO phosphor using a settling method in IPA. The anode was found to be suitable for use only with low emission current densities to avoid removal of the deposited phosphor layer. Figure 3.8 shows an emitter under test with the transparent phosphor-coated anode in place. Field emission electrons impacting the phosphor result in emission of blue-green light.

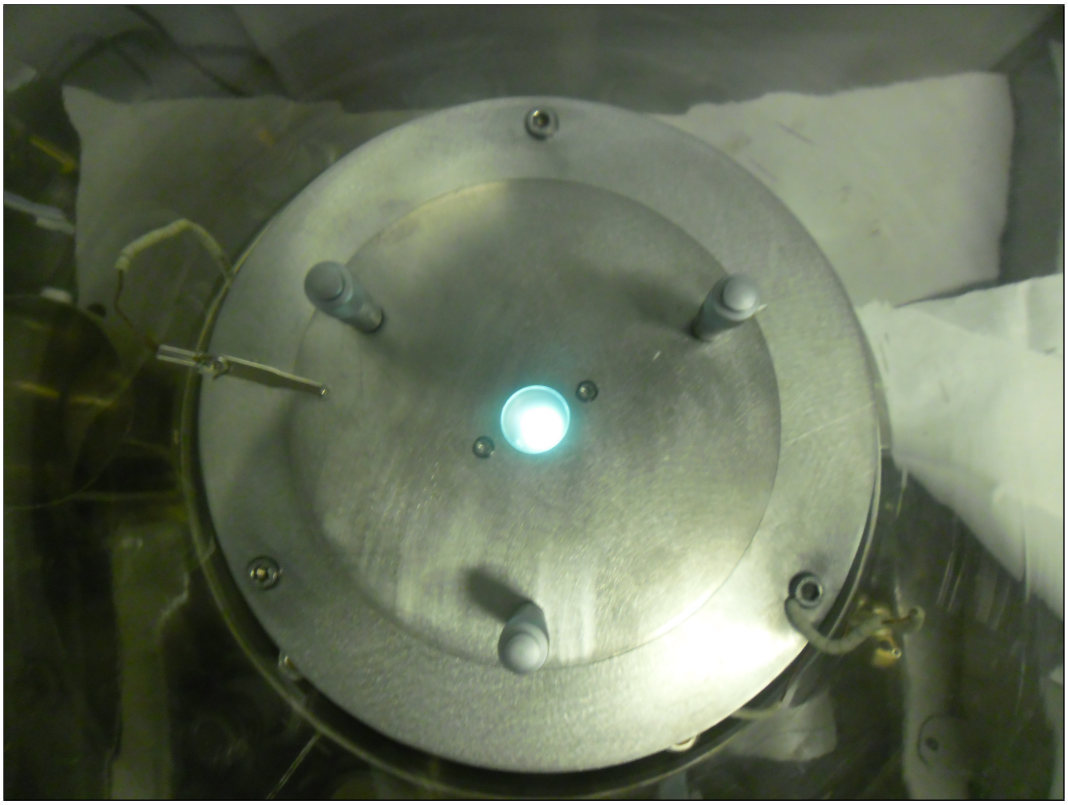

Figure 3.8: Phosphor screen anode during emission test at 6 $V{\cdot}\mu m^{-1}$.

3.6.1 Test procedure

Standard field emission test

Figure 3.9 shows the recorded data from a standard automatic field emission test. The green plot is the voltage applied by the PSU. The peak voltage was increased incrementally

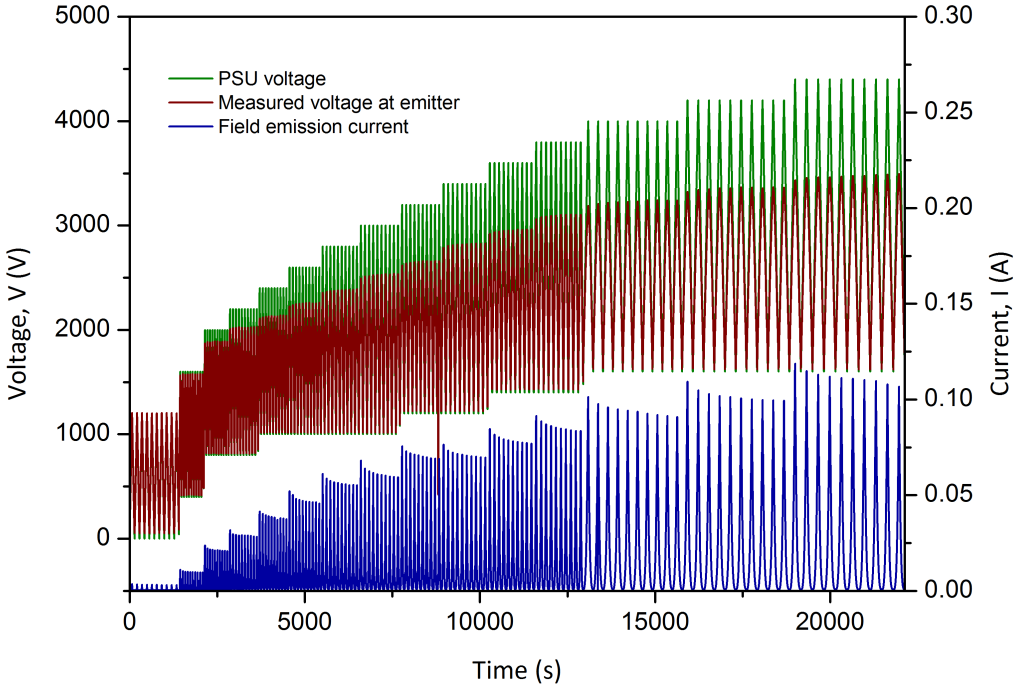

Figure 3.9: Applied voltage, voltage measured at the emitter substrate surface and resulting field emission current during typical test.

as the test progressed. The red plot is the measured potential difference applied between the anode and cathode. Finally, the blue plot shows the measured emission current.

Lifetime test

For the lifetime test the voltage was set manually using the power supply front panel controls and only data recording was performed by software. The same data was recorded as for the fully automatic pulsed emission tests.

3.7 Treatment of data

3.7.1 Turn-on field

Turn-on field, E_{TO}, is defined in the literature as the lowest field at which field emission is observed. This is therefore necessarily variable depending on the current resolution of the equipment used. Common definitions in the literature use a measured current from 0.1 to 100 μA [61] [63] [77] [117] [149]. The equipment used in this project was intended to deal with relatively high currents, with the tradeoff of a current resolution of 100 μA. Turn-on field is defined here as the field required for an emission current density of 200 $\mu A \cdot cm^{-2}$.

3.7.2 Threshold field

Threshold field, E_{TH}, denotes the applied field required for a field emission device to give a specified emission current density. As with turn-on field, numerical definitions vary between studies according to practical considerations, with commonly-used values defined as the field required to give an emission current density of between 1 and 10 $mA \cdot cm^{-2}$ [68] [77]. Measurement of the threshold field has less dependance on the sensitivity of the equipment, and is useful in comparing field emission devices which have exhibited different maximum emission current densities with different applied electric fields. In the work presented here, use of a resistor in series with the device under test results in a reduction in the field applied to the device with increasing emission current (section 3.4.2). Threshold field analysis allows comparison between different samples independently of this variation. Unless otherwise stated, threshold field is defined in the work presented here as the applied field at which the current density reaches 10 $mA \cdot cm^{-2}$.

3.7.3 Fowler-Nordheim analysis

Equation 1.2 introduced the field enhancement factor, β, which is a measure of the ratio of the macroscopic applied electric field to the local field at the emission site. It is common

practice in the literature to calculate a β value for a fabricated field emitter as it provides a common metric by which different field emission technologies can be compared. The following method is used to calculate field enhancement factor from the experimental data in the work presented here.

Recalling equation 1.2:

$$J = A(\frac{\beta^2 V^2}{\phi d^2}) \exp(\frac{-B\phi^{\frac{3}{2}} d}{\beta V}) \tag{3.5}$$

Substituting $E = V/d$,

$$\implies J = A(\frac{\beta^2 E^2}{\phi}) \exp(\frac{-B\phi^{\frac{3}{2}}}{\beta E}) \tag{3.6}$$

$$\frac{J}{E^2} = A(\frac{\beta^2}{\phi}) \exp(\frac{-B\phi^{\frac{3}{2}}}{\beta E}) \tag{3.7}$$

$$\ln(\frac{J}{E^2}) = \ln(A\frac{\beta^2}{\phi}) + (\frac{-B\phi^{\frac{3}{2}}}{\beta E}) \tag{3.8}$$

Comparing terms with the equation of a straight line in cartesian coordinates, $y = mx + c$, it is found that a plot of $\ln(\frac{J}{E^2})$ vs. $\frac{1}{E}$ will be a straight line of gradient m,

$$m = \frac{-B\phi^{\frac{3}{2}}}{\beta} \tag{3.9}$$

$$\implies \beta = \frac{-B\phi^{\frac{3}{2}}}{m} \tag{3.10}$$

Values were taken to be $B = 6.83\times10^9$ $\text{eV}^{3/2}$ $\text{V}\cdot\text{m}^{-1}$ [150] and the work function of graphite, $\phi = 5$ eV.

Despite its widespread use to characterise nanostructured carbon field emission devices with arrays of sharp emitting tips, the Fowler-Nordheim equation was not intended to describe emission from large-area arrays. The equation in its most commonly used forms, including that used to calculate field enhancement factors for devices presented here, neglects the effects of temperature and the image charge of emitted electrons on the potential barrier between emitter and vacuum [151]. The equation is used in this work only to allow relative comparison of the data presented herein.

3.8 Conclusions

In this chapter, the development of a test gear for field emission devices has been documented, beginning with a fixed-gap test jig with manually adjusted DC applied voltage and

culminating with a programmable, pulsed set up with adjustable anode-cathode gap, detailed automatic recording of experimental data and breakdown protection for the test gear and FE device.

Chapter 4

Description of field emitter characteristics

4.1 Introduction

This section describes the behaviour of printed field emitters during testing. The results presented here are taken from work performed in parallel with those presented in the subsequent chapters, and are all from samples printed using inks based on the Xintek CNT material on copper substrates.

4.2 Testing

Figure 4.1 shows a typical plot of the data gathered in a field emission test. In this case, the plot is of the final *J-E* cycle of an automatic test, in which the highest voltage is applied to the emitter. The emitter was subjected to several cycles at this peak applied field as described in section 3.6.1. Also shown is a Fowler-Nordheim plot, which can be used to calculate field enhancement factor as described in section 3.7. Further results are included in Appendix D.1.

4.3 Behaviour of emitters under test

4.3.1 Fowler-Nordheim plot

In macroscopic arrays of large numbers of CNTs, variations in CNT height, diameter and tip structure mean there is a broad distribution of geometric field enhancement factors present. Longer CNTs with fewer neighbouring CNTs dominate observed emission current at low applied fields due to the nonlinear relationship between the local field and emission current.

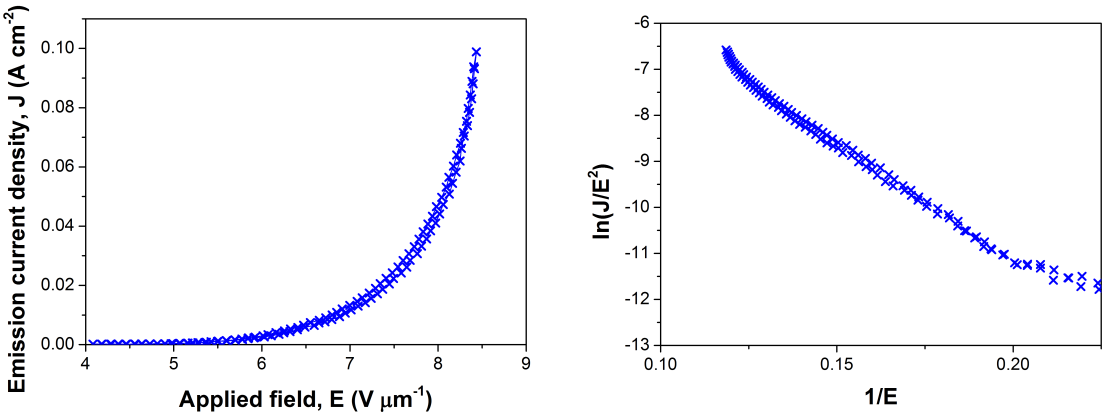

Figure 4.1: *J-E* plot of emission test with corresponding Fowler-Nordheim plot.

As the applied field rises, more nanotubes turn on. The result is a curved Fowler-Nordheim plot at lower applied fields (higher values of $1/E$). If the CNTs are not aligned, as is the case in the present work, variations in orientation also manifest as deviations from the straight line of the Fowler-Nordheim plot. Protruding CNTs have also been shown to straighten under the influence of an applied field, becoming more aligned with the macroscopic field vector and increasing individual geometric field enhancement factor. This effect is stronger at higher applied fields, and is more pronounced in longer CNTs [152].

At higher emission currents joule heating causes the temperature of the emitting CNTs to rise, resulting in a thermionic contribution to the observed emission current, which is easily seen on the Fowler-Nordheim plot. At lower values of $1/E$, $\ln(J/E^2)$ attains higher values than would be expected from field emission alone. Adsorbates have been shown to increase field emission current, and desorb at elevated temperature, resulting in unstable emission and damage to CNT tips [132] [21]. Protruding CNTs will, in general, have increasing temperature along their length, due to the longer conduction path. At high temperatures carbon sublimes from the nanotubes, reducing their length and therefore field enhancement factor [125]. With the screening effect of the longer CNTs removed, a larger number of shorter CNTs then turn-on [11] [19].

Contact resistance between CNTs and the substrates has an effect on the maximum emission current density available from an emitter. In cases where contact resistance is a limiting factor, a deviation is seen from Fowler-Nordheim behaviour where emission current saturates at high fields [153].

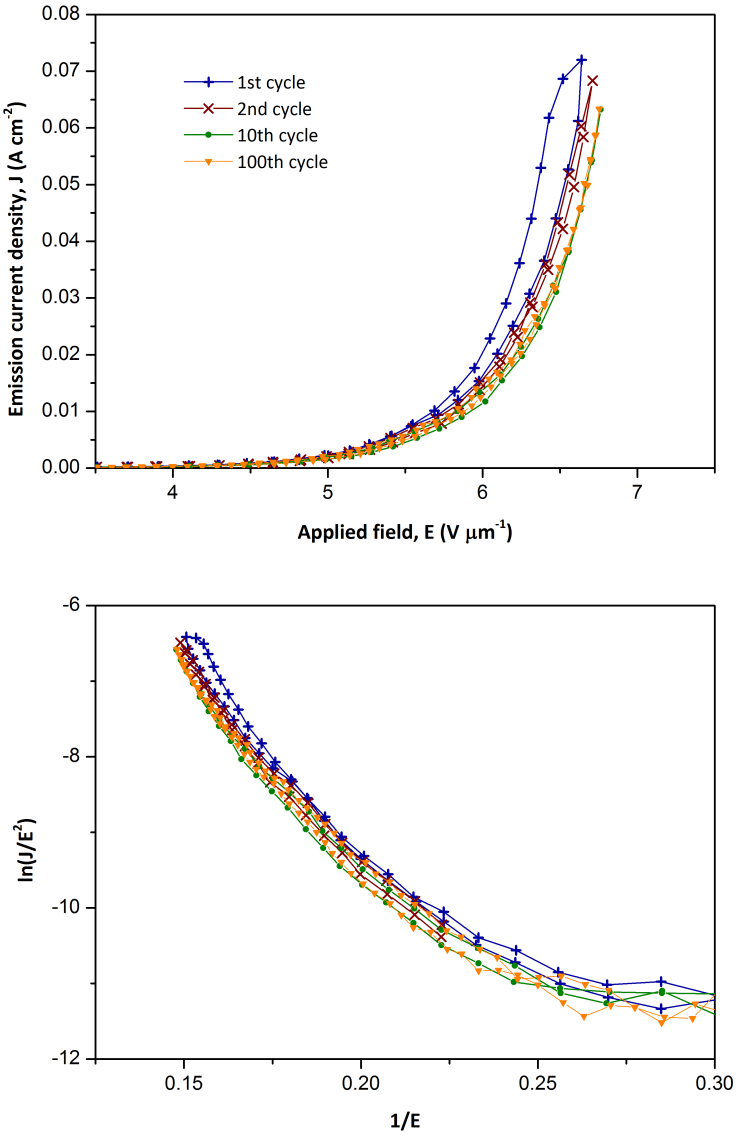

Figure 4.2: *J-E* plots of repeated cycles showing conditioning behaviour, with corresponding Fowler-Nordheim plot.

4.3.2 Conditioning

Initial application of voltage to a printed field emission device does not produce stable, repeatable emission current. In the case of the emitters described here, a voltage cycle with a peak field exceeding that previously applied to the emitter commonly resulted in a *J-E* curve in which greater emission current was produced at a given applied field with rising voltage than with falling voltage. The ramp up curve does not follow the characteristic pattern of a field emission curve, and does not correspond to a linear Fowler-Nordheim plot. Once peak voltage has been reached, the down sweep has a more familiar shape, and in many cases repeated cycling to the same peak voltage yields *J-E* curves which resemble the initial down sweep closely.

Figure 4.2 shows the first, second, tenth and hundredth *J-E* curves taken from a sample printed using the Mk-5 ink used in section 6.3 with a peak applied voltage of 3.2 kV. During the first cycle emission current is higher when *E* is increasing than decreasing. The Fowler-Nordheim plot shows significant deviation from linearity at higher applied fields. Subsequent cycles indicate a reduction in field enhancement factor and more closely approximate a linear Fowler-Nordheim plot. Comparison of the 10th and 100th cycles shows little variation. Except where otherwise stated, *J-E* data used in calculations for this study were the tenth cycle at that applied field.

4.3.3 Changing field enhancement factor

Figure 4.3 shows the *J-E* and Fowler-Nordheim plots for the successive voltage cycles of a standard automatic test (see also figure 3.9). In each case the displayed plot is from the tenth cycle for a given maximum applied field. The peak applied field of each cycle is increased as the test progresses. It is observed that as the device is subjected to higher applied fields and therefore emits with higher current density, the Fowler-Nordheim plots become steeper, indicating a reduction in average field enhancement factor, and a reduction in curvature. This is consistent with the presence of a broad distribution of of field enhancement factors in the sample initially, with an increase in emission at higher fields due to thermal effects. As observed previously, application of a higher applied field results in a change to the Fowler-Nordheim plot consistent with thermal damage, with the subsequent plots showing a reduced field enhancement factor. This in combination with the increasing linearity of the plot as the test progresses suggest that damage occurs preferentially to longer CNTs with higher field enhancement factor, resulting in a narrower distribution of lower average values. In figure 4.4, SEM images of the emitter surface show disordered nanotubes of various lengths before testing. After testing, only short nanotubes can be seen protruding with longer nanotubes lying flat on the surface.

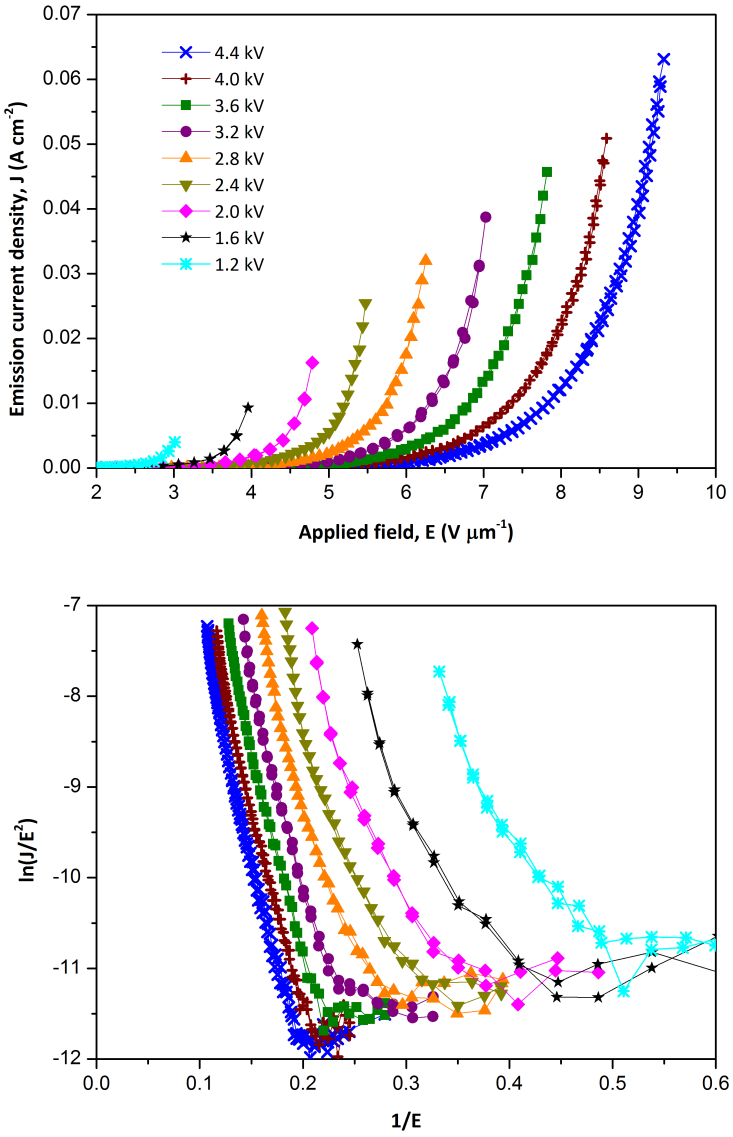

Figure 4.3: Fowler-Nordheim plots of *J-E* cycles with increasing applied field showing change in field emission behaviour during test.

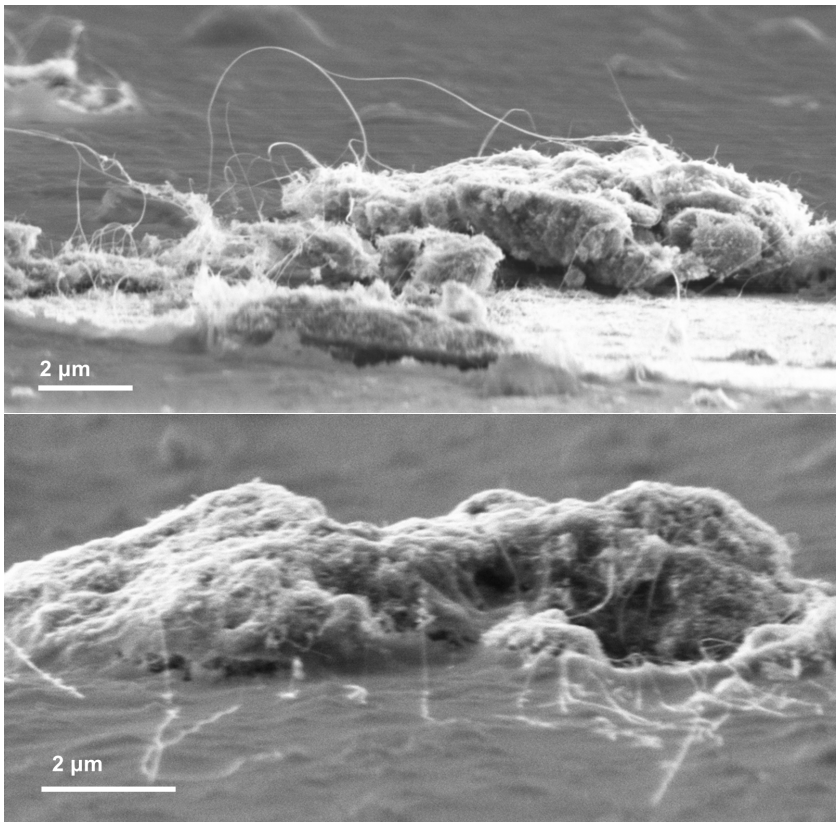

Figure 4.4: Low-angle SEM images of emitter surface. Top: pristine emitter. Bottom: surface following standard emission test.

4.4 Anode

Figure 4.5 shows a steel anode which has suffered visual damage after several high-current tests. A more detailed image of a copper anode in figure 4.6 shows the discoloured area to have patches of the same colour as the anode material. Examination of the anode surface under SEM found deposited material (figure 4.7) in the areas showing visual damage, which were found to have an energy dispersive x-ray spectroscopy (EDS) signal indicating the presence of a low level of carbon. Raman spectroscopy of the damaged anode area shows that this carbon is highly disordered (figure 4.8), and likely to indicate deposition of amorphous carbon either from destroyed nanotubes or residual ink components, rather than simply migration of the nanotubes themselves [154].

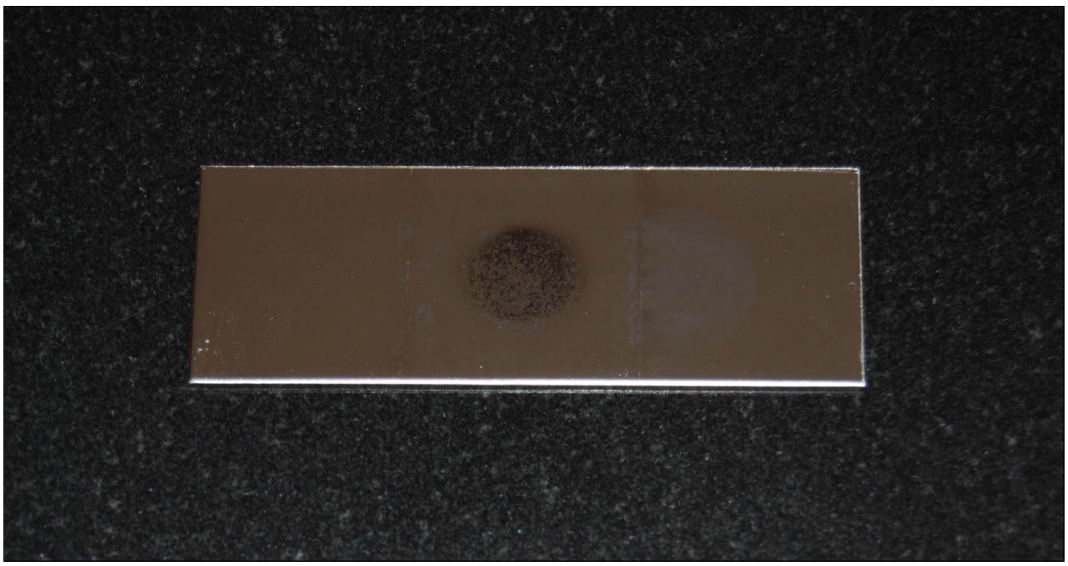

Figure 4.5: Steel anode exhibiting damage after FE testing.

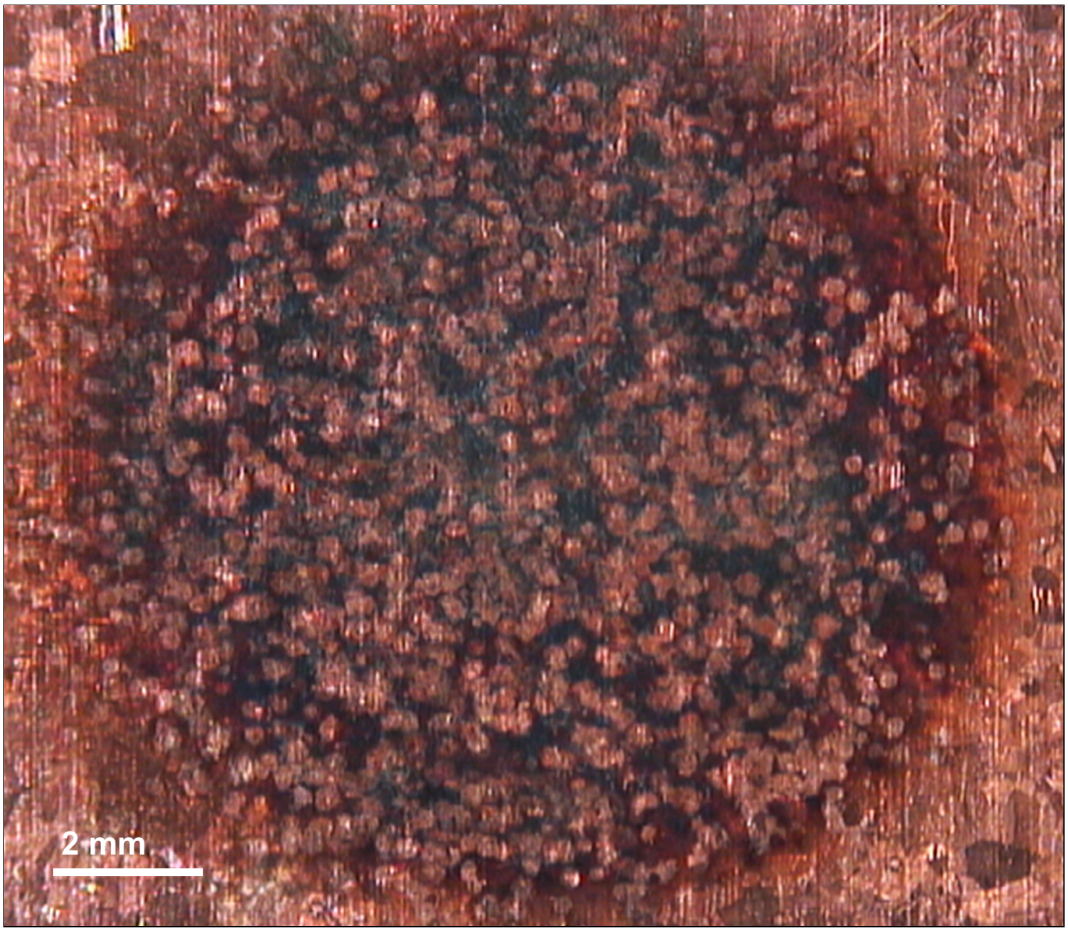

Figure 4.6: Copper anode exhibiting damage after FE testing.

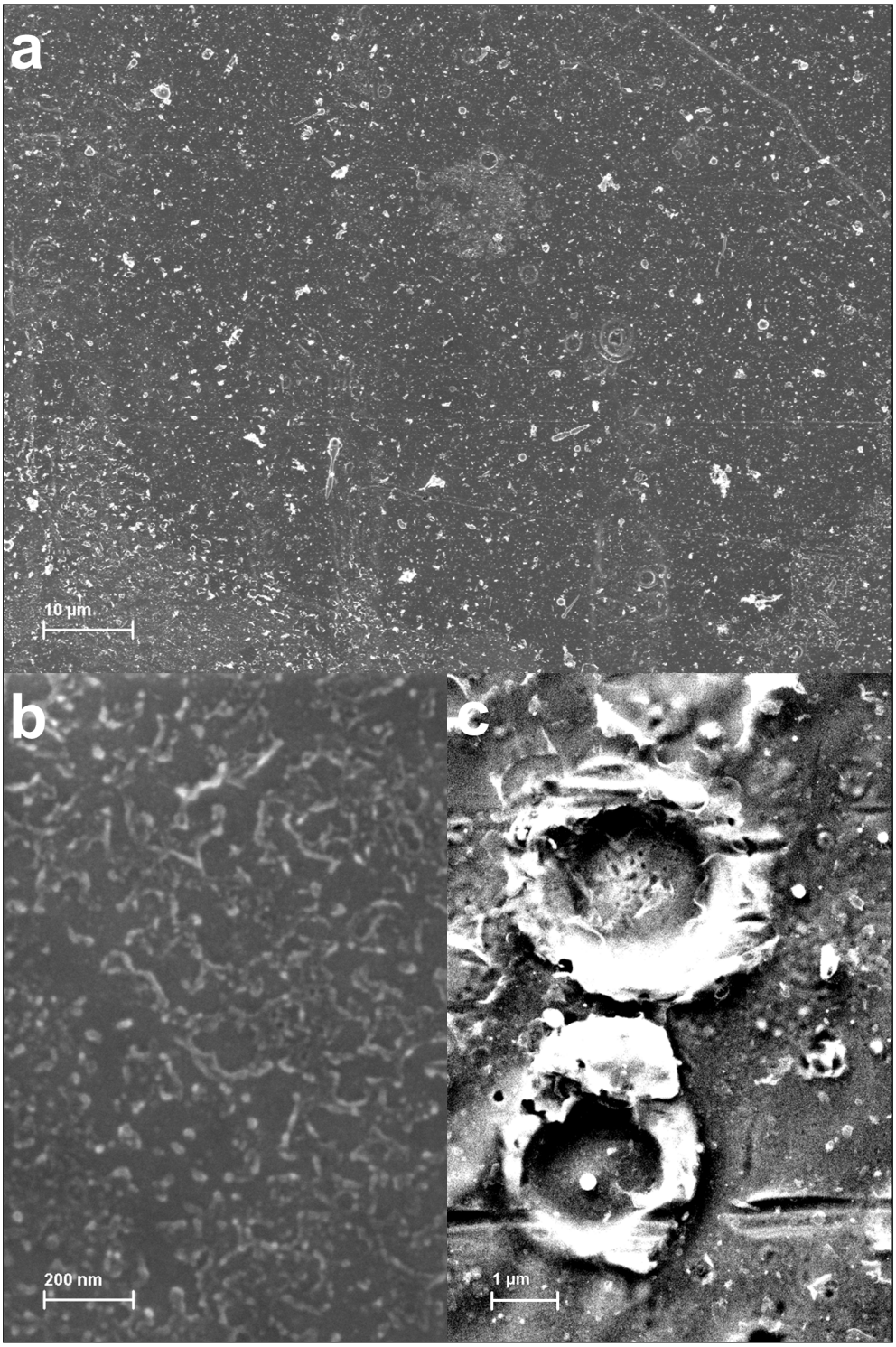

Figure 4.7: SEM of discoloured area of copper anode showing deposited material (a,b) and arc damage (c).

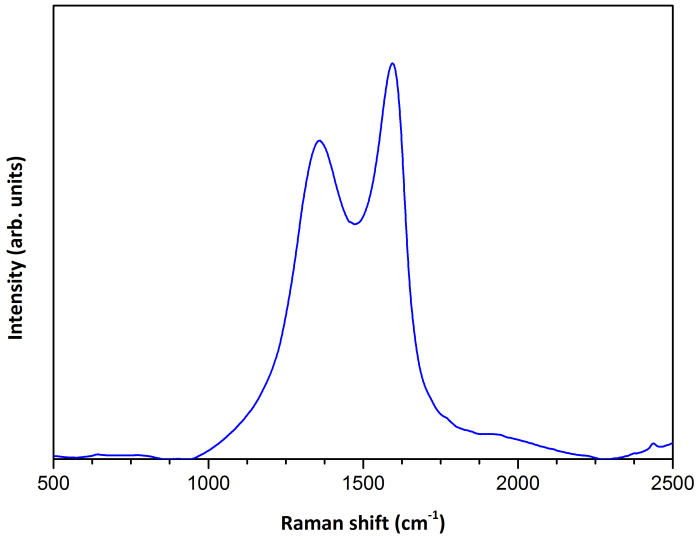

Figure 4.8: Raman spectrum of copper anode surface.

4.5 Conclusions

The fabricated emitters have been shown to exhibit Fowler-Nordheim behaviour, with deviation observed under certain conditions. This behaviour indicates thermal effects occur at high applied fields, and that a broad distribution of individual field enhancement factors is present in the array initially, becoming narrower as testing progresses. Emitters exhibit non-reversible damage during field emission testing at newly applied fields, which is consistent with destruction of the CNTs through Joule heating, and is supported by SEM images of the surface showing damaged nanotubes lying flat on the substrate surface following field emission testing, with only shorter tubes protruding. Amorphous carbon material has also been found to be deposited on the anode as a result of field emission testing.

Chapter 5

Comparison of emitter materials

5.1 Introduction

Although the possibility of synthesising CNTs by CVD techniques as part of this work was considered, previous studies suggested significant difficulty in developing a method giving a product with good field emission characteristics. Furthermore, it was found that there were many commercial suppliers offering a wide variety of nanostructured carbon materials, with many already having demonstrated field emission performance. It was therefore concluded that any study into CNT growth undertaken as part of this work would be unlikely to result in an improved emitter material, and that the shortest development path to a low cost, scalable field emission device would make use of commercially available products. This chapter describes an investigation into the performance of field emission devices fabricated by screen printing using inks containing four different nanostructured carbon materials. In each case, the morphology and crystalline structure of the material were considered and the same fabrication and test methods applied.

5.2 Experimental

Table 5.1: Properties of carbon emitter materials.

Manufacturer/material	Length	Diameter	Purity	Figure
TIMCAL KS6	3.5 μm		99 %	5.1
Rosseter Holdings H008	200-300 nm	8.4 nm	40-60 %	5.3
Brunel University MW3007	300 μm	100 nm	90 %	5.5
Xintek XNA-SP-36150	10 μm	7 nm	88 %	5.7

Gold-coated glass microscope slides were the substrate for all experiments. Substrate preparation was carried out as described in section 2.5.7, and screen printing as described in section 2.5.4. A list of the nanostructured carbon materials investigated is given in table 5.1, along with their properties according to the manufacturers specification.

Figure 5.1(a) shows KS6 graphite flakes suspended in ethanol by sonication and allowed to dry on the surface of a silicon wafer. Figure 5.1(b) shows the surface of an emission device fabricated by screen printing an ink containing the flakes by the method described in section 2.5. It was observed that the material was easily dispersed by the ink components giving a homogeneous ink and a consequent uniform distribution on the surface of the device. Figure 5.2 shows an EDS spectrum confirming the presence of deposited carbon and silicon along with gold, nickel and chromium from the substrate.

Figure 5.3 shows the Rosseter H008 CNT material. CNTs can be seen with length consistent with the manufacturer's specification. A large amount of other material is also present, appearing to consist of other forms of graphitic carbon. EDS shows the presence of gold, nickel and chromium from the substrate, as well as carbon and silicon (figure 5.4).

The Brunel-grown multi-walled nanotubes are shown in figure 5.5. The CNTs are long and closely packed forming a brush-like structure with each visible fibre consisting of many nanotubes when viewed under higher magnification. The CNTs dispersed well and were uniformly distributed on the emitter surface forming a network of randomly oriented tubes lying flat in the plane of the substrate. Figure 5.6 again shows only carbon, silicon, and the substrate elements detected on the surface by EDS.

Figure 5.7(a) shows an SEM image of the Xintek material in which it can be seen that the CNTs are disordered and a small amount of particulate matter is present. When incorporated into an ink the CNTs were found to be difficult to disperse. In the image of the surface of the printed emitter device in figure 5.7(b) it is seen that the material has formed clusters of varying size, with the image taken at higher magnification in figure 5.7(c) showing that the clusters consist of densely packed randomly oriented nanotubes on the emitter device surface. The EDS spectrum in figure 5.8 confirms carbon and silicon have been deposited on the substrate surface.

Raman spectroscopy of the raw powder form of the emitter materials was performed. The resulting spectra of the four materials are shown in figure 5.9, and were used to calculate the I_D/I_G ratios included in table 5.2. The graphite material gave the lowest I_D/I_G ratio, indicating that it contained the lowest proportion of disordered carbon. The Rosseter and Xintek CNTs had similar ratios around 0.2, with the Brunel-grown CNTs having a higher ratio indicative of a lower proportion of graphitic carbon suggesting that the material is a poorer candidate for use in field emission devices.

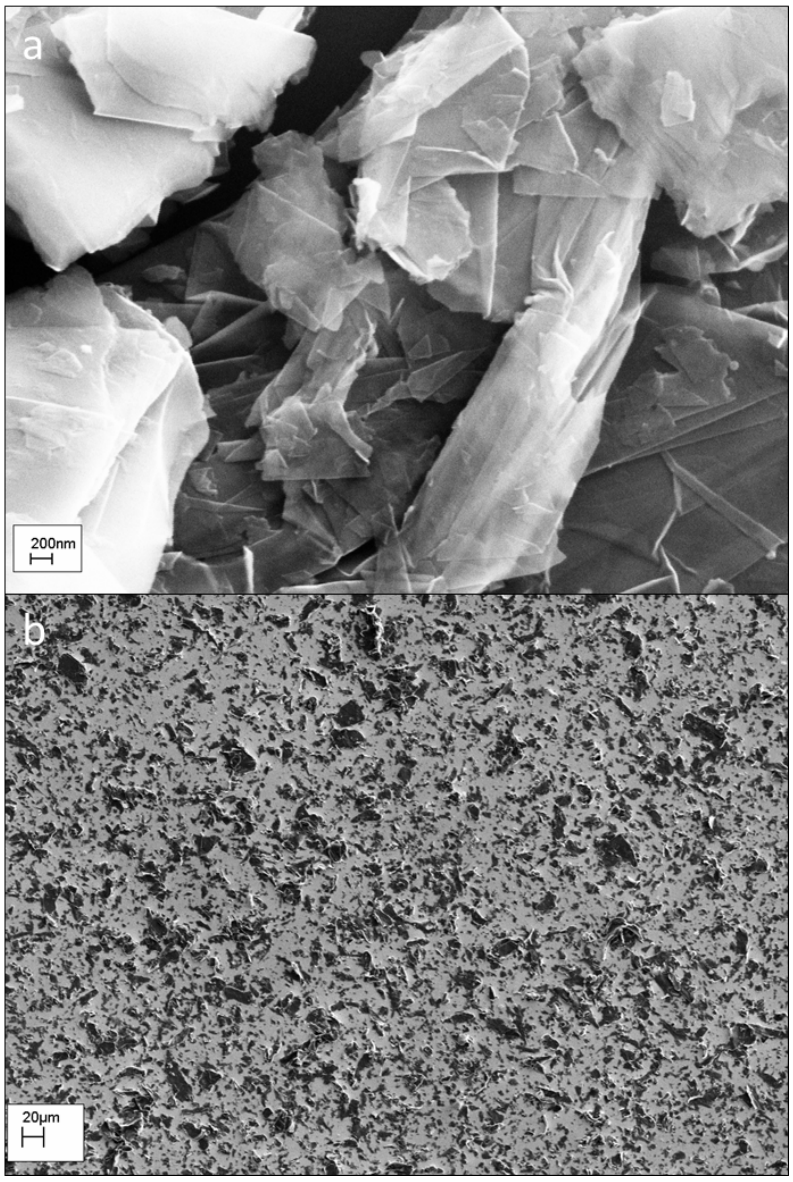

Figure 5.1: SEM of KS6 graphite flakes (a) and surface of field emission device made using them (b).

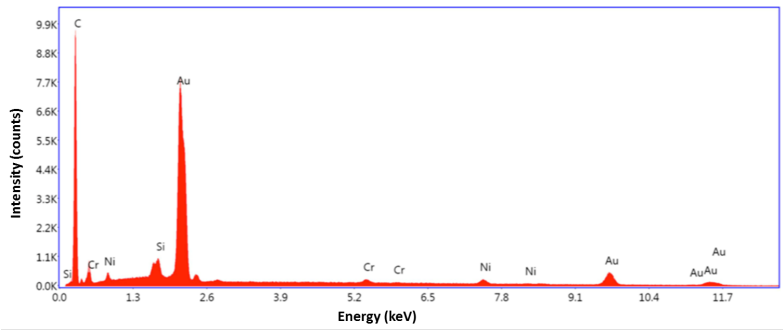

Figure 5.2: EDS spectrum of emitter device printed with KS6 graphite material.

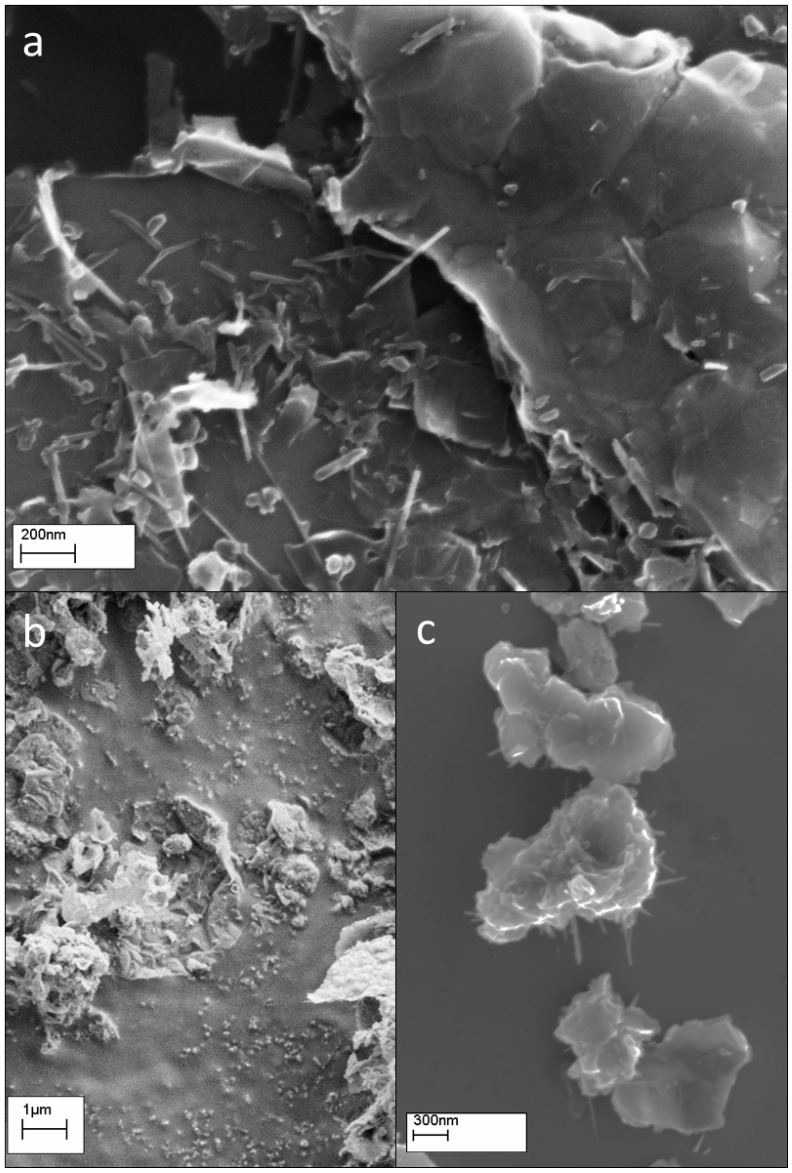

Figure 5.3: SEM of Rosseter CNTs (a) and surface of field emission device made using them (b, c).

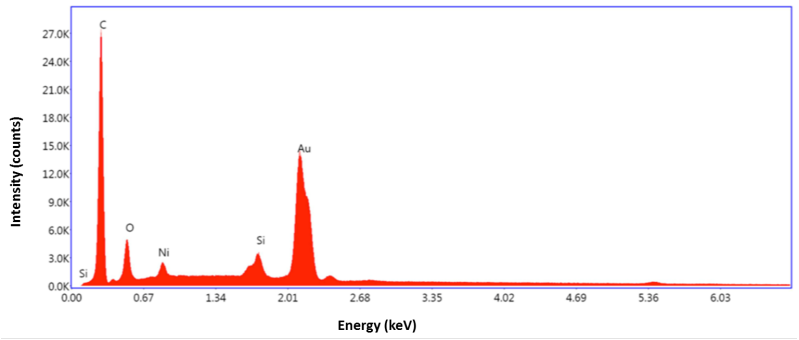

Figure 5.4: EDS spectrum of emitter device printed with H008 CNT material.

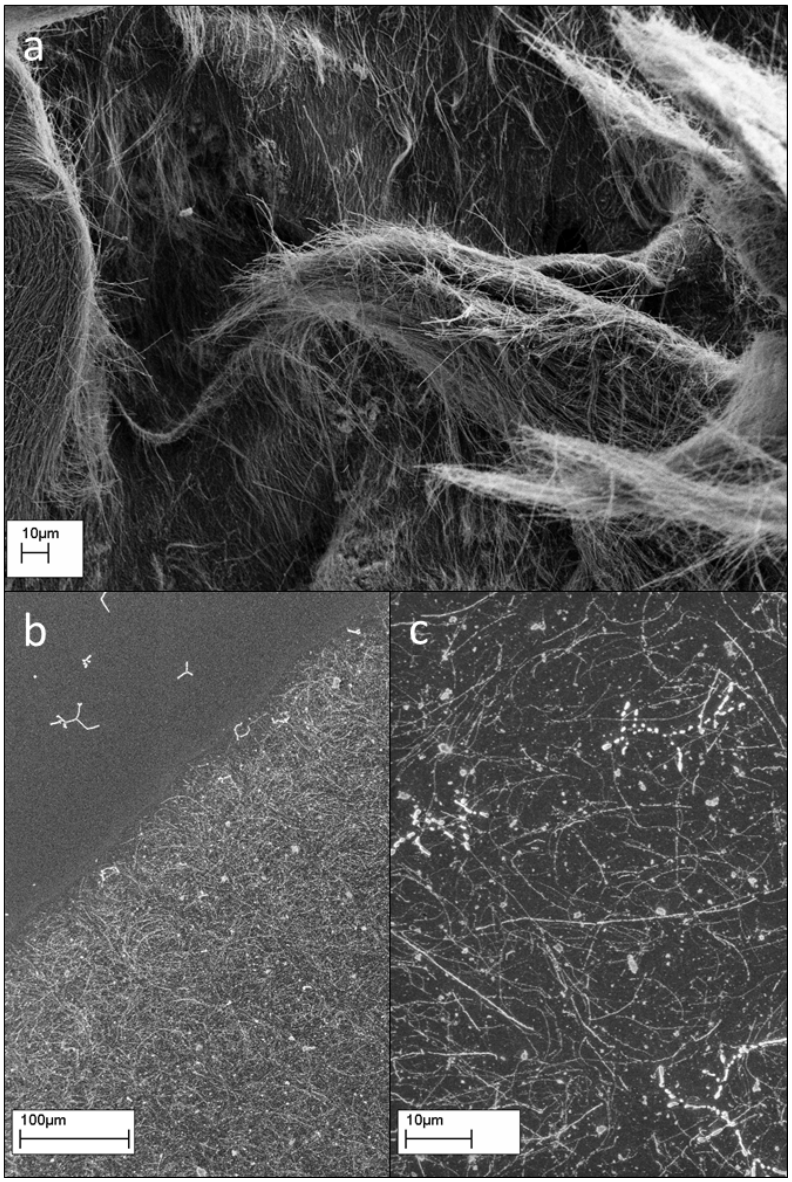

Figure 5.5: SEM of CVD CNTs grown at Brunel University (a) and surface of field emission device made using them (b, c).

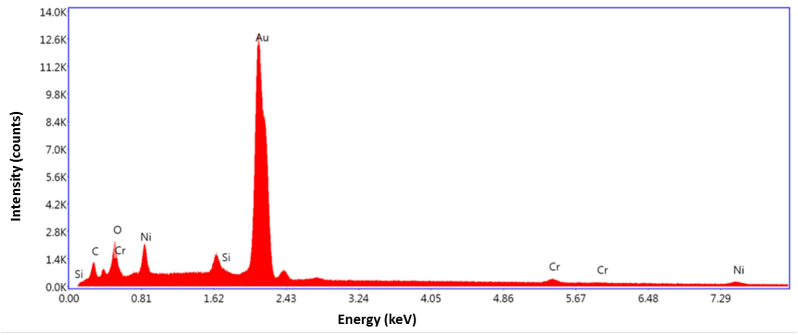

Figure 5.6: EDS spectrum of emitter device printed with Brunel-grown MWNT material.

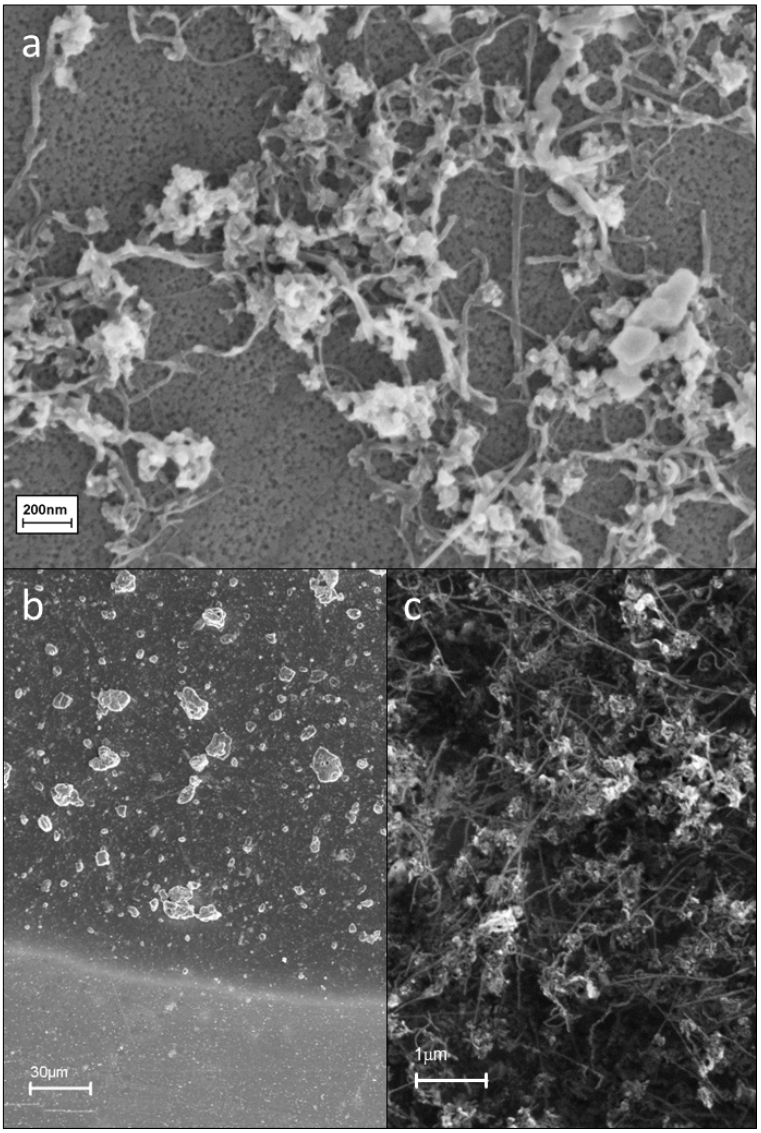

Figure 5.7: SEM of Xintek CNTs (a) and surface of field emission device made using them (b, c).

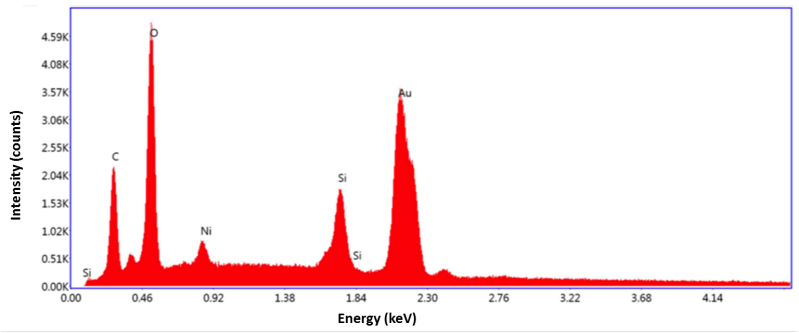

Figure 5.8: EDS spectrum of surface of emitter device printed with Xintek XNA-SP-36150 CNT material.

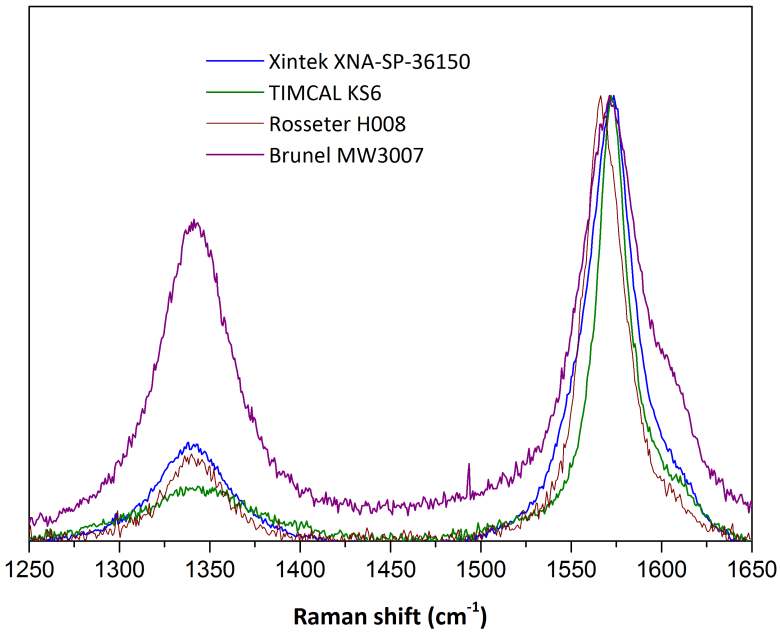

Figure 5.9: Raman spectra of emitter materials showing G and D bands.

Table 5.2: Results of Raman spectroscopy.

Manufacturer/material	**Purity**	I_D/I_G
TIMCAL KS6	99%	0.12
Rosseter Holdings H008	40-60%	0.20
Brunel University MW3007	90%	0.72
Xintek XNA-SP-36150	88%	0.22

Table 5.3 summarises the emitter devices used in this chapter. In each case the emitter material and silica binder concentrations are given, with the remainder of the ink composed of the same vehicle described in section 2.5.1. Full formulations are included in appendix B.

Table 5.3: Formulations of inks used in this chapter.

Ink	Emitter material	Mass fraction	
		Emitter	Binder
KS6-1	TIMCAL KS6	0.0205	0.0702
H008-1	Rosseter H008	0.0017	0.0659
MW3007-5	Brunel MW3007	0.0023	0.0300
X-3	Xintek XNA-SP	0.0046	0.0829

5.3 Results

Figure 5.10 shows the *J-E* curves and accompanying Fowler-Nordheim plots of the best-performing device made with each material, with the results summarised in table 5.4. The Rosseter H008 exhibited relatively poor performance, as expected from the low proportion of CNTs in the material and the low aspect ratio of the individual CNTs. An impractically high applied field was therefore required to achieve a low emission current. The Brunel-grown MW3007 CNTs, despite having high aspect ratio, gave a similar emission current density of 0.9 $mA{\cdot}cm^{-2}$, but at an even higher applied field. The graphite flake material gave significantly better performance than both, with higher emission current density at a lower applied field.

Ultimately the Xintek CNTs gave the best performance, giving the highest emission current of 6.7 $mA{\cdot}cm^{-2}$ at the lowest applied field. The material had both high purity and aspect ratio, and the individual CNTs are small enough to stand vertically on the substrate so that their geometric field enhancement factor can be realised. Figure 5.11 shows an SEM image taken at a low angle of 2.8° relative to the substrate surface, allowing the morphology of the deposited material to be seen. Disordered CNTs can be seen to protrude from a cluster of material on the substrate surface.

By contrast the Brunel-grown MWNTs are found to lie flat on the substrate surface, as seen in figure 5.12. A break in the CNT indicates damage has occurred since the device was printed.

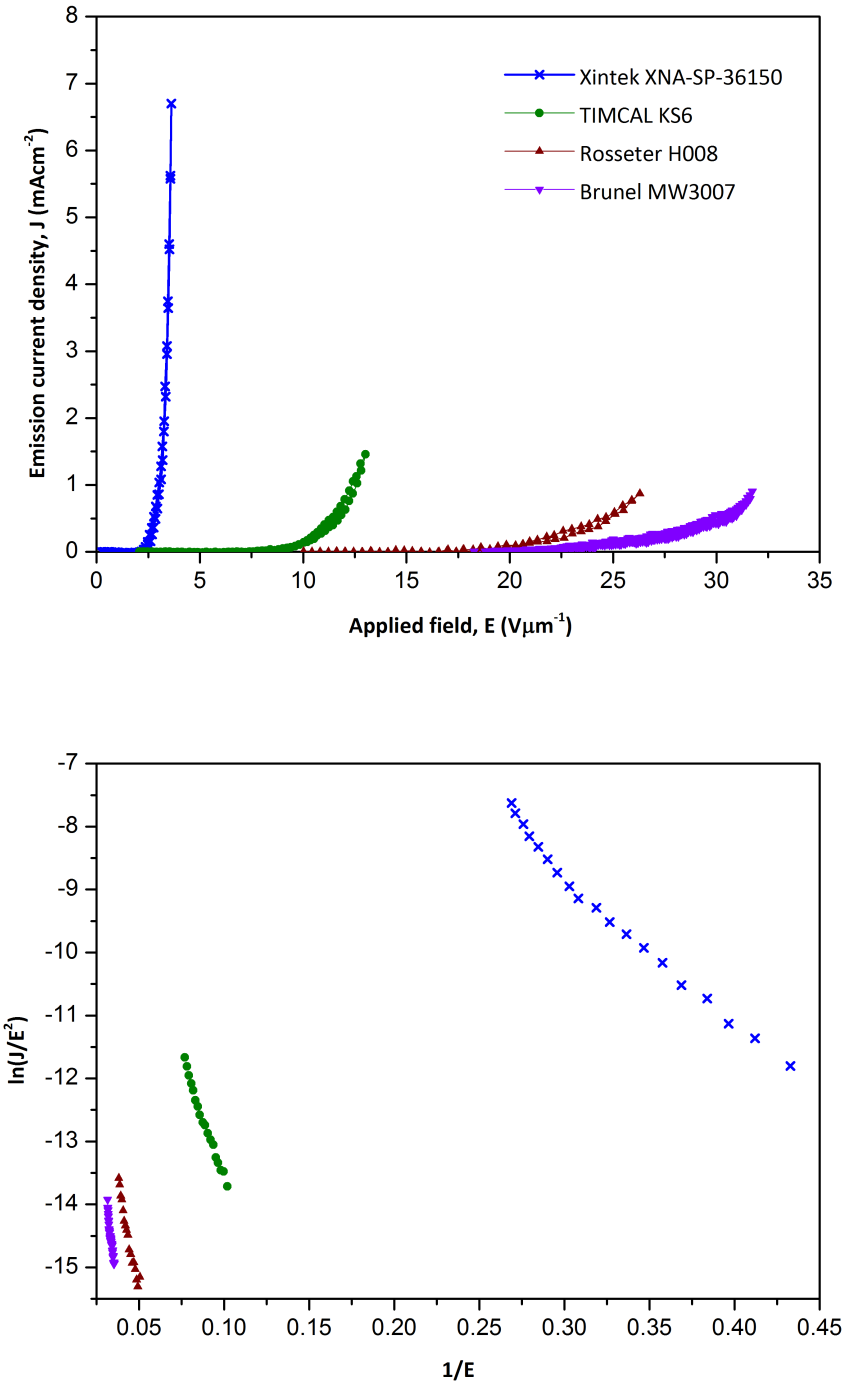

Figure 5.10: FE performance of emitters fabricated with different nanostructured carbon materials.

Table 5.4: FE test results from different emitter materials .

Material	**Max. current density** ($mA \cdot cm^{-2}$)	**Applied field** ($V \cdot \mu m^{-1}$)
TIMCAL KS6	1.46	13.0
Rosseter H008	0.87	26.3
Brunel MW3007	0.90	31.7
Xintek XNA-SP-36150	6.70	3.61

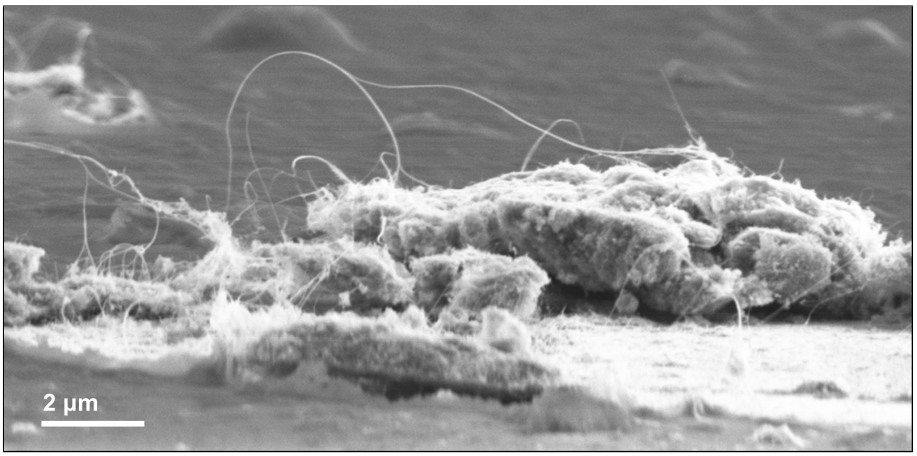

Figure 5.11: Low-angle SEM of Xintek XNA-SP-36150 CNT-based device showing nanotubes protruding from substrate.

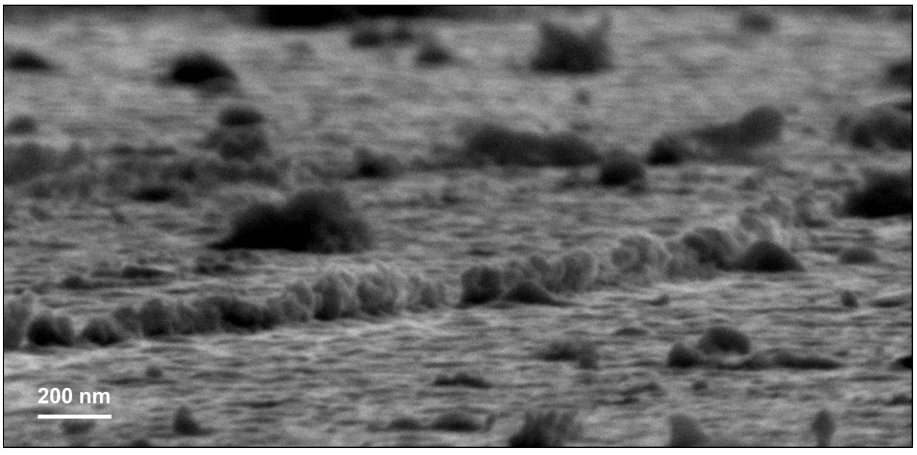

Figure 5.12: Low-angle SEM of Brunel-grown CNT-based device showing nanotubes lying flat on substrate.

5.4 Conclusions

Four emitter materials have been studied with the objective of assessing the best material to fabricate emission devices capable of high current density. The Xintek CNTs demonstrated superior performance compared to the other materials, giving higher emission current density at a lower applied field. Although these CNTs dispersed poorly, it was found that the resulting network of clusters on the substrate surface had a three-dimensional structure, allowing CNTs to protrude significantly from the surface and exhibit a high field enhancement factor despite their random orientation. As a result of this experiment, the Xintek XNA-SP-36150 CNT material was selected for experiments performed thereafter.

Chapter 6

Optimisation

6.1 Introduction

Having identified a suitable CNT material, experiments were conducted to optimise the fabricated emission device. This section includes results from a series of tests designed to assess the effect of several parameters on the field emission behaviour of the device, including the manufacturing technique, CNT and binder content of the ink, substrate material and the geometry of the device. The operating life of the device was also assessed.

6.2 Fabrication methods

A small number of trials with an EPD method were performed in the early part of the project with two MEng students. Several CNT species were used, with the best results from a suspension of the Xintek material incorporating the silica binder from the ink formulation, using PVP as a dispersing agent [143] [155]. Deposition was performed using the method described in section 2.5.5.

Initial trials used the same Au/NiCr/glass substrates as the printed emitters fabricated at the time. As with printed inks, best results were achieved with addition of the silica binder material. Figure 6.1 shows a *J-E* curve from a field emission test of the best performing EPD device made using the Xintek t-MWNT material and silica binder on an Au/NiCr/glass substrate, with the corresponding Fowler-Nordheim plot. EPD was found to be a promising method of fabricating emission devices easily when compared to screen printing, requiring fewer steps to prepare a suspension. Additionally, the use of a delicate mesh in screen printing meant the equipment was more vulnerable to damage and required frequent careful cleaning. By contrast, the working parts used in the EPD technique consisted only of electrodes and a beaker, which were low cost and easily replaced. However, it was found that

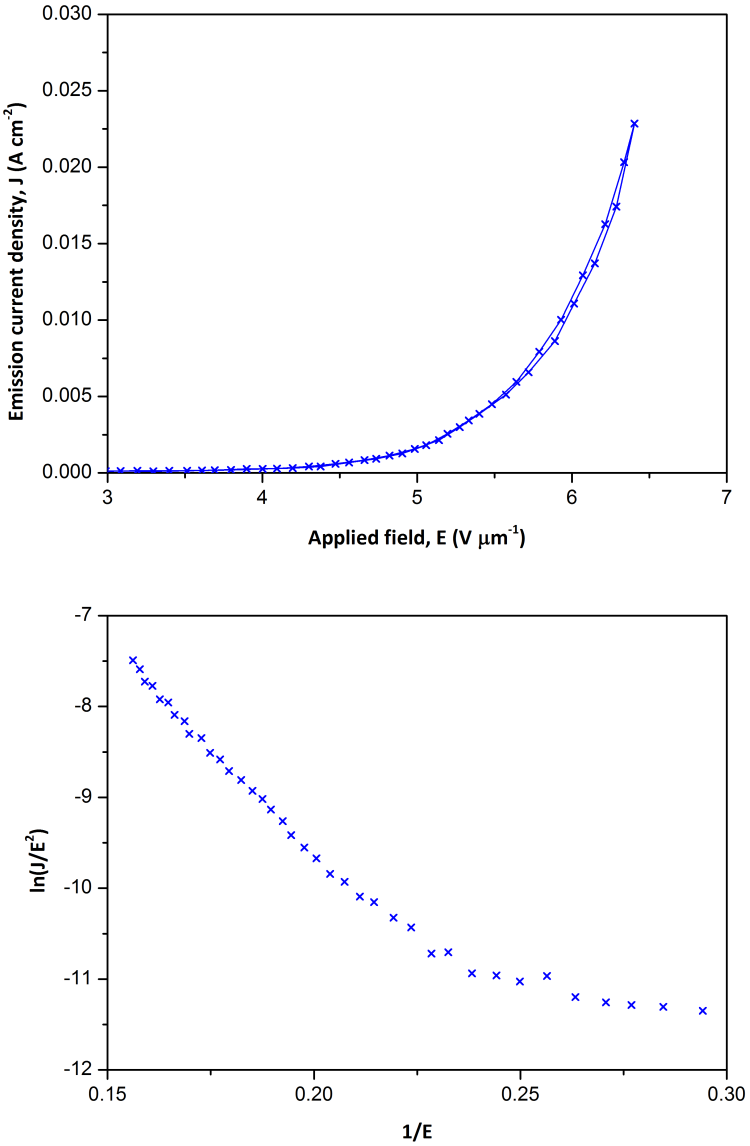

Figure 6.1: *J-E* plot from test of field emission device fabricated by EPD (top) with corresponding Fowler-Nordheim plot (bottom).

the characteristics of CNT suspensions used in EPD changed as they were used, giving declining deposition, and resulted in large quantities of CNT material in suspension being discarded. The technique was also difficult to control with addition of the binder material,with lower deposition rates and uneven deposition observed.

When printed emitters on a copper substrate began to give current densities exceeding those observed using Au/NiCr/glass substrates, EPD was attempted with copper substrates but it was found that the developed deposition method did not translate simply. The cost of gold-coated glass substrates is considerably higher than copper, and for the best-performing CNT material studied here the cost of the discarded material from EPD experiments was appreciable. As one of the project requirements (section 1.1.1) was that the device should be made using low cost techniques, screen printing was determined to be the better method.

Results from the literature have demonstrated the potential of EPD as a technique for depositing CNTs for field emission applications, including similar CNTs to those used here [156]. The principle difference here is the use of the dielectric binder material.

6.3 Emitter/binder concentration

The proportion of CNT loading in the ink formulation is an easily controlled variable with a potentially very large effect on device performance. A large number of emitting sites is desirable, which would suggest devices printed using an ink with a higher CNT concentration will give more emission current density at a given applied field. However, previous research suggests that closely-packed CNTs on a surface shield each other and result in a lower field enhancement factor. Simulations and experiment suggest that for vertically-orientated CNTs grown by PECVD an optimum is found when the CNTs are situated at intervals of 2–5 times their own lengths. This assumes CNTs are of uniform height and have direct electrical contact with the substrate. In a printed emitter the CNTs are of different lengths, randomly orientated and may have a conducting path to the substrate through one or more other CNTs [152]. In this work, the CNTs are also surrounded by a dielectric matrix. Although a thicker deposited layer will mean a poorer electrical connection from the substrate to the emitting tip, having more CNTs present is expected to give longer life as the nanotubes are damaged or ablated by residual gas sputtering, ohmic heating and breakdown events.

In a practical sense, inks become more difficult to work with at higher CNT concentrations, exhibiting more agglomeration and clogging the print screen more quickly, requiring more frequent cleaning. Cleaning necessarily involves discarding CNT material, which is hazardous, and for a commercial device increases manufacturing cost through disposal overheads as well as wastage.

In this section an experiment investigating the dependence of field emission performance

Table 6.1: Formulation of ink Mk-4.

Component	Weight (g)	Mass fraction
CNT	0.0529	0.0074
PVP	0.0104	0.0015
Silica binder	0.4880	0.0697
Polymer gel	4.300	0.6143
Butoxyethanol	1.792	0.2560
Octanol	0.3582	0.0512
Total	7	1

on the ratio of emitter to binder material is described. The inks used here were formulated to all give a printed emitter with the same total combined weight of emitter and binder material remaining after heat treatment, but with varying ratios of the two. Six inks were made, denoted Mk-1 to Mk-6 in order of increasing CNT concentration. In table 6.1, reproduced from section 2.5.1, the full formulation of ink Mk-4 is shown.

All the inks used in this section were made using the methods described in section 2.5.1, using the same basic vehicle of polymer gel, butoxyethanol and octanol with varying amounts of CNT and binder material to give the desired dry product. The quantity of dispersant was controlled to remain at 20 % of the CNT weight in each ink. A summary of the ink compositions is given in table 6.2, with full formulations in Appendix B. The materials were assessed in terms of concentration in the ink formulations and the proportion of the calculated dry emitter/binder product remaining after heat treatment at 450 °C, with the expectation that field emission performance would correlate with the emitter/binder ratio.

Table 6.2: Summary of inks used in concentration experiments.

Ink	Emitter mass fraction		Binder mass fraction		Emitter/binder
	Ink	Dry product	Ink	Dry product	ratio
Mk-1	0.0018	0.1385	0.1392	0.8615	0.1607
Mk-2	0.0038	0.2921	0.1150	0.7079	0.4126
Mk-3	0.0056	0.4318	0.0923	0.5682	0.7598
Mk-4	0.0075	0.5715	0.0698	0.4285	1.3338
Mk-5	0.0092	0.7081	0.0473	0.2919	2.4261
Mk-6	0.0112	0.8587	0.0229	0.1413	6.0766

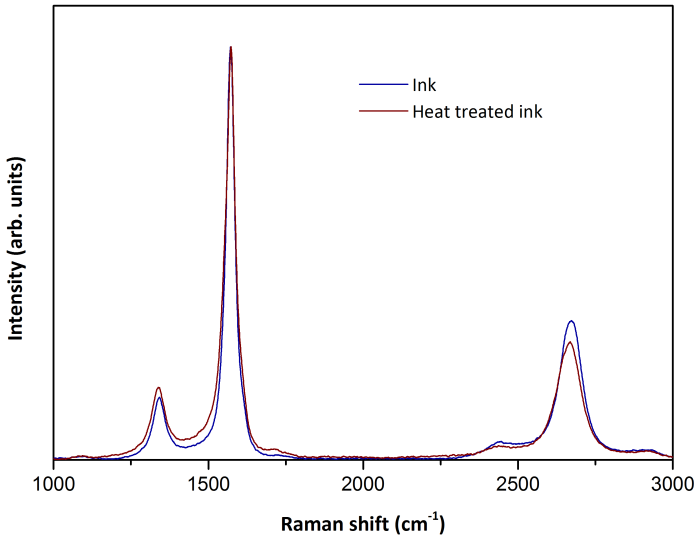

Figure 6.2: Raman spectra of Xintek MWNT-based ink before and after heat treatment in hydrogen atmosphere.

Figure 6.2 shows Raman spectra of the Xintek CNT-based ink before and after heat treatment in hydrogen. Comparing the I_D/I_G ratios of the spectra as described in section 2.6.2, an increase from 0.141 to 0.165 is seen. This implies that the structure of the CNTs is affected by the heat treatment process.

Field emission testing was performed as described in section 3.6.1, repeatedly cycling the applied voltage before incrementally increasing. The anode-cathode gap was set to 400 μm. For each ink, three field emission devices were tested. In figure 6.3 field emission test results from the 10th cycle with a maximum applied voltage of 4 kV are plotted as a function of the CNT mass fraction in the ink. *J-E* curves for an emitter made using each ink are included in appendix D.1. In each case an arithmetic mean has been taken of the results for devices made with the ink, with the error bars representing the standard deviation. The series resistor acts to reduce the maximum applied field for emission devices exhibiting higher emission current densities. However, a trend is established showing that higher emission current densities are achieved from devices printed using inks with higher CNT concentrations. Mean turn-on field is also plotted, and in this case the data does not indicate that the CNT concentration has a significant effect. Threshold field is shown to have a linear correlation with CNT concentration, however. Contrary to expectation, the measured parameters did not have a linear correlation with the ratio of emitter to binder material.

TGA was performed on a sample of the Xintek 36150 t-MWNTs in their as-bought state

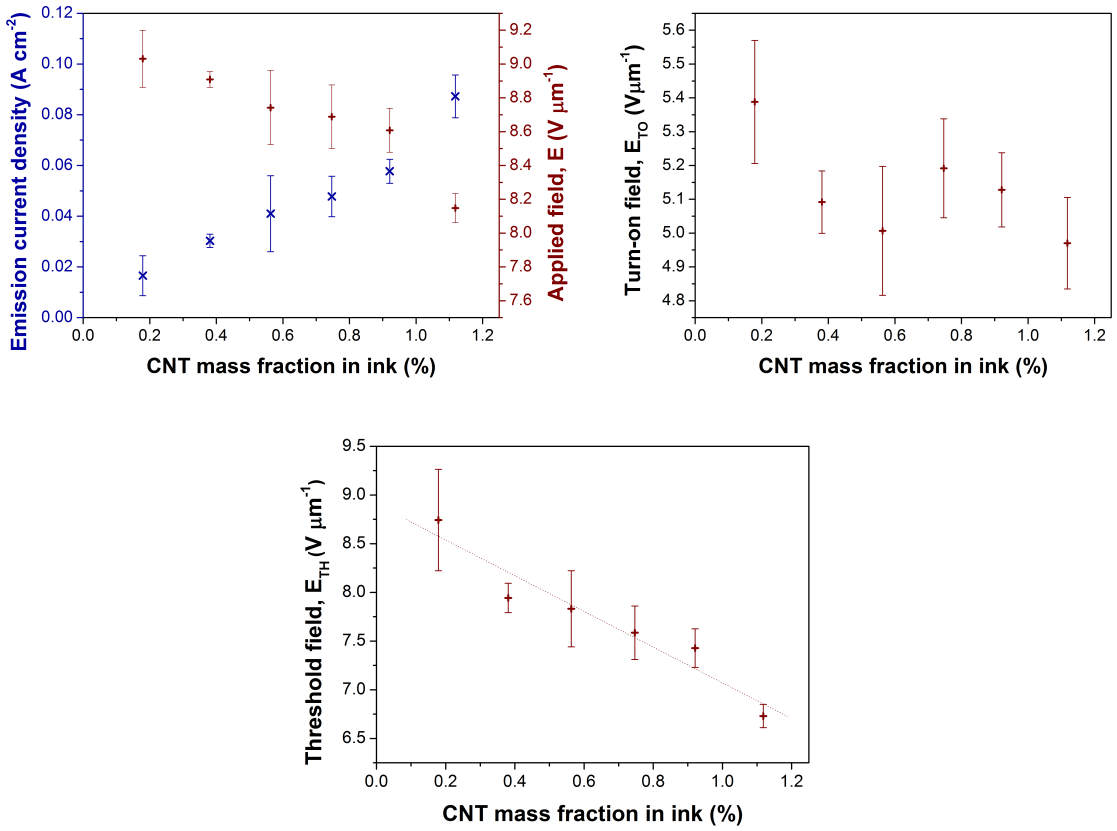

Figure 6.3: Peak emission current density and applied field, turn-on field and threshold field plotted as a function of CNT ink concentration by mass.

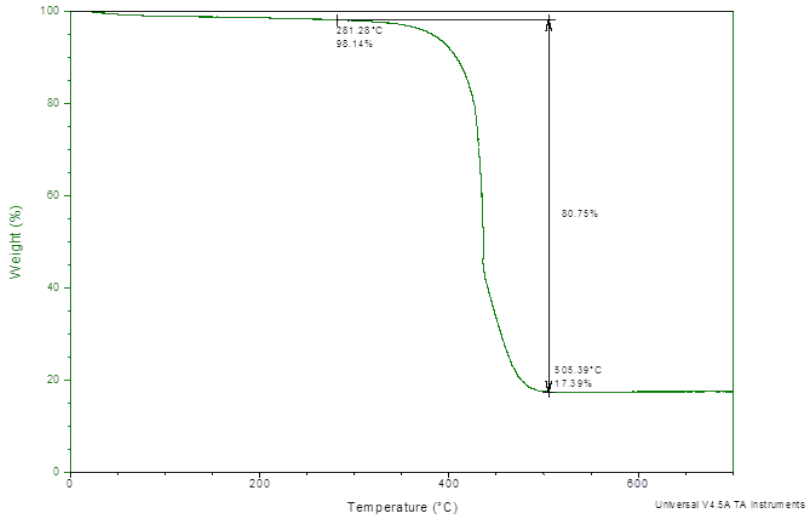

Figure 6.4: Plot of TGA of raw CNT powder.

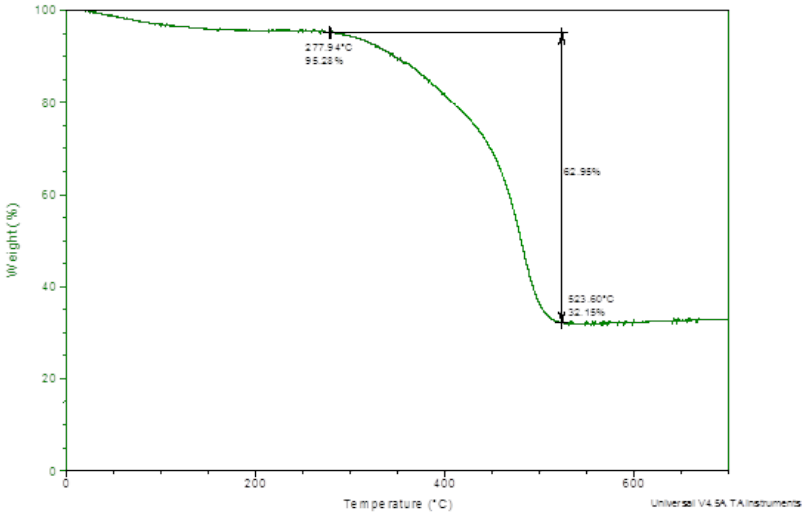

Figure 6.5: Plot of TGA data from ink Mk-5.

using a ramp rate of 5 °C/minute in air. Figure 6.4 shows the resulting plot. It can be seen that the CNTs burn off between 300-500 °C leaving a residue that remains unchanged with further temperature increase.

To analyse the inks used to fabricate field emission devices, samples were placed on glass microscope slides and dried on a hot-plate using the same temperature profile as the emission devices. The resulting product was then separated from the slide and TGA performed using the same ramp rate and atmosphere as the raw CNTs. Figure 6.5 shows TGA data from the Mk-5 ink. Results from the other inks are included in appendix E.

Table 6.3: Results of TGA of ink samples.

Ink	Mass loss %	Remaining %
Mk-1	36.85	66.79
Mk-2	54.29	37.81
Mk-3	48.52	46.12
Mk-4	63.56	31.08
Mk-5	62.95	32.15
Mk-6	72.68	21.8

Table 6.3 shows calculated results from the TGA data. From section 2.5.6 and equation 2.1 it can be calculated that the CNT and silica proportion of the remaining ink components at 250 °C is between 20-23%. The other components are expected to be removed as temperature rises, leaving only the CNTs and silica. The data shows only one ink with a

remaining mass consistent with this model, and significant variation between the inks. The developed process therefore does not result in the removal of undesired ink components, and is a suggested area for further work.

The Xintek t-MWNT material forms clusters of densely packed CNTs on the surface of the emitter. To analyse the clusters images of the devices were captured using an optical microscope (figure 6.6), and an automatic particle count was performed using ImageJ [157]. Corresponding SEM images are shown in figure 6.7. In both figures one example of an emitter made with each ink is shown.

The data in figure 6.8 gathered using the particle count function shows that increasing the CNT concentration of the ink results in a greater density of clusters on the emitter, with a corresponding increase in coverage. However, the size of the clusters is shown not to be a function of CNT concentration, with no trend exhibited. As this behaviour was not observed in other emitter materials it is therefore likely that the cluster size is a result of the CNT properties.

EDS mapping of an emitter printed with the Mk-4 ink on a copper substrate (figure 6.9) found that silicon and carbon were present across the emitter surface but concentrated in the clusters. The non-uniform distribution of silicon suggests that the binder is unevenly distributed within the clusters.

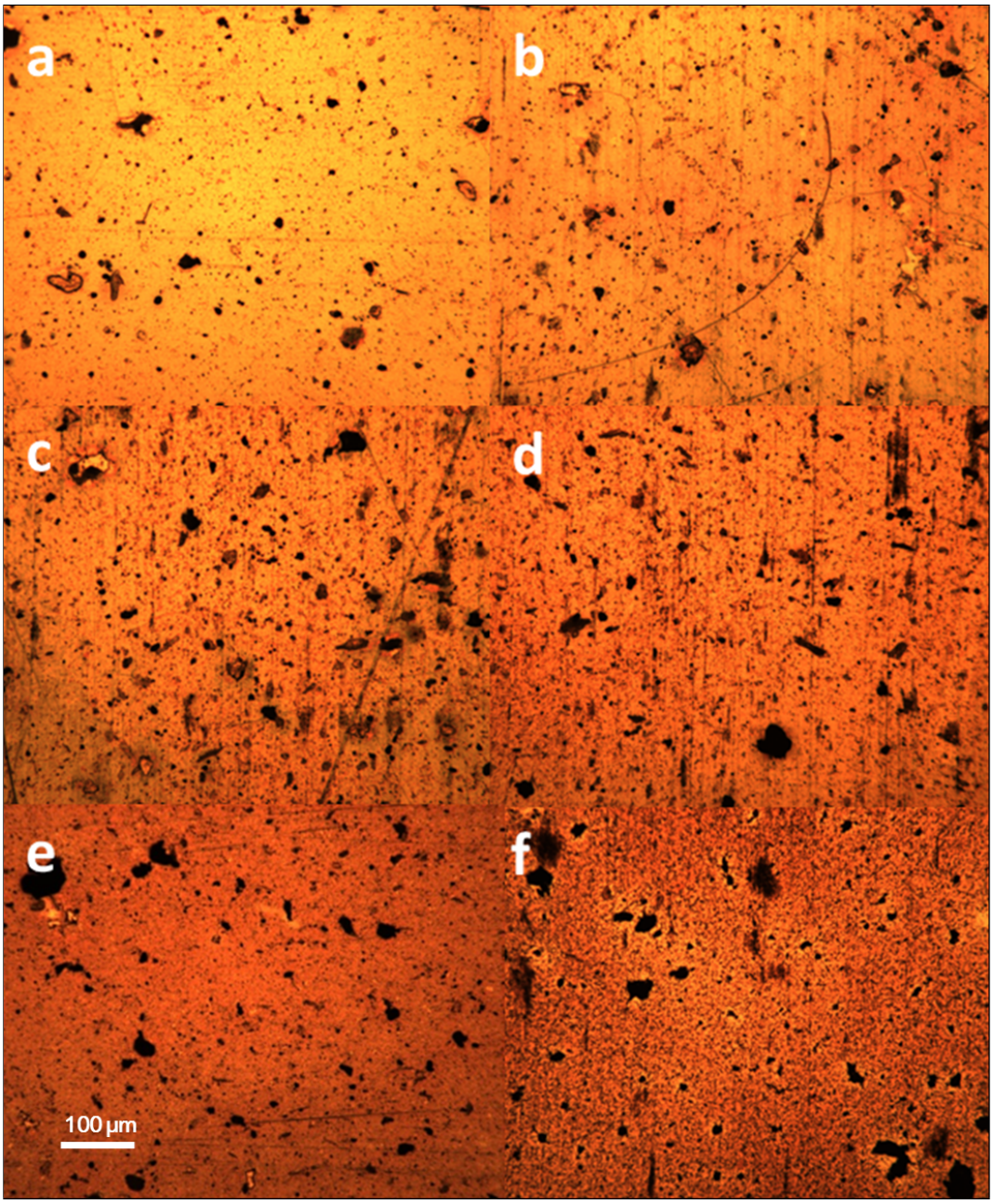

Figure 6.6: Optical microscope images of surfaces of emission devices printed with different inks (a) Mk-1 (b) Mk-2 (c) Mk-3 (d) Mk-4 (e) Mk-5 (f) Mk-6.

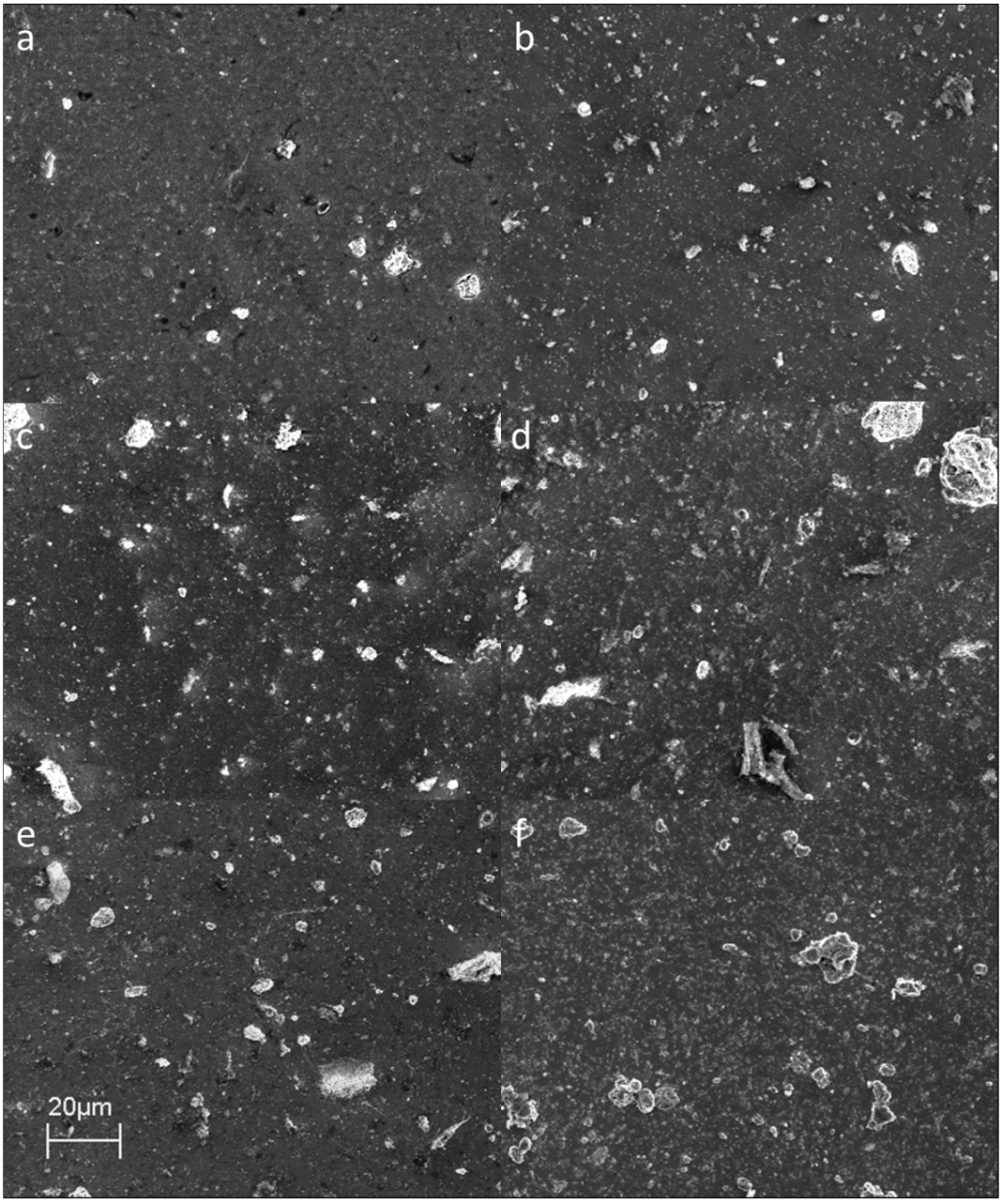

Figure 6.7: SEM images of surfaces of emission devices printed with different inks at 1000x magnification (a) Mk-1 (b) Mk-2 (c) Mk-3 (d) Mk-4 (e) Mk-5 (f) Mk-6.

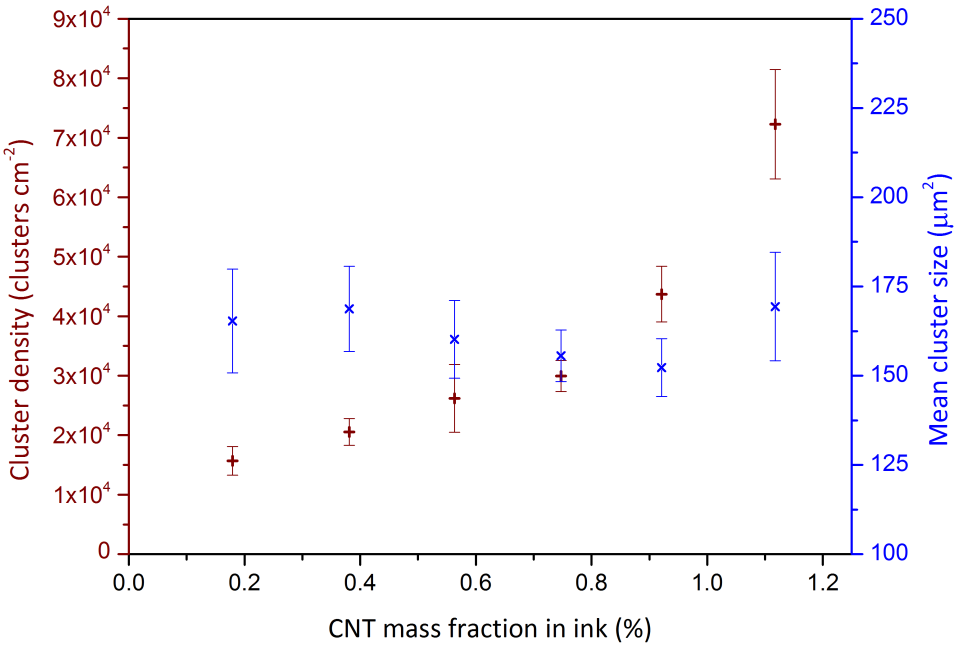

Figure 6.8: Cluster density and size vs. CNT concentration in ink.

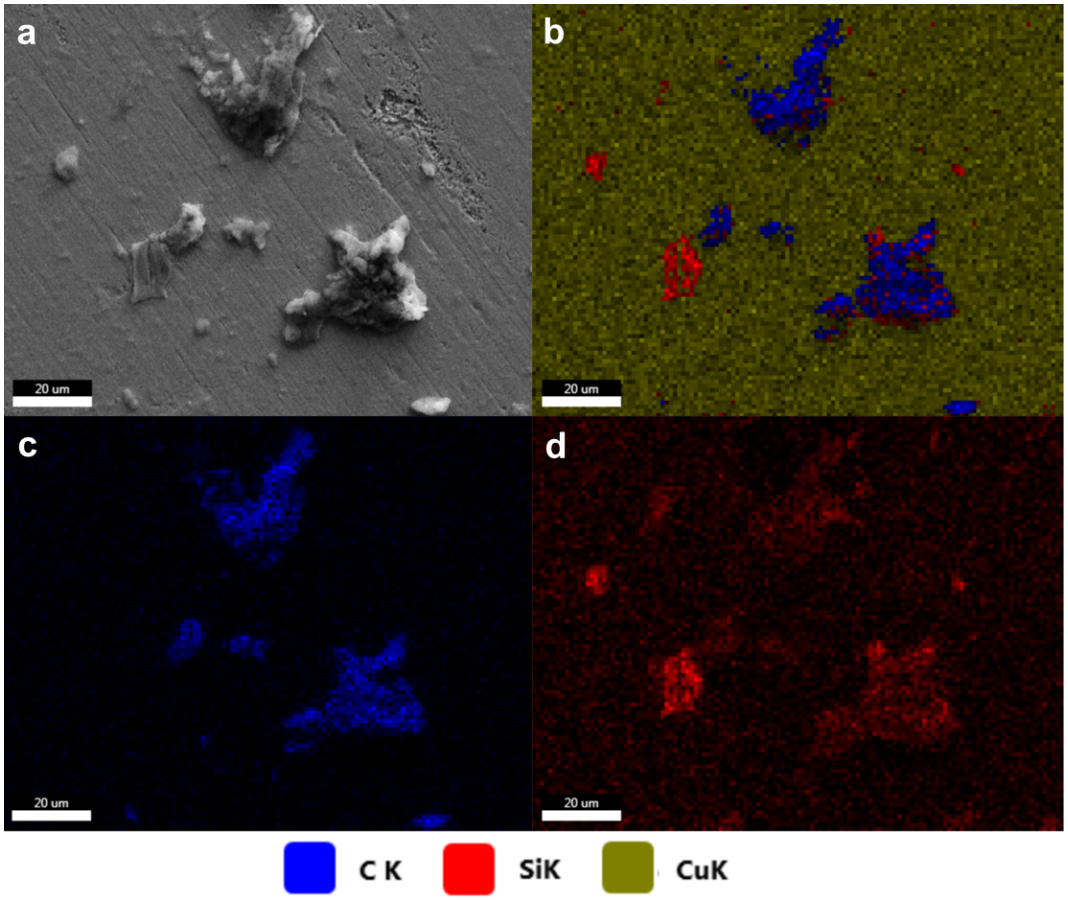

Figure 6.9: SEM image of clusters on emitter printed with Mk-4 ink (a), EDS map showing distribution of carbon, silicon and copper (b), distribution of carbon (c) and distribution of silicon (d).

6.4 Substrate materials

The substrate material of an emission device can have a significant impact on development of a commercial device. Vacuum electronics manufacturing techniques are well-established, meaning it is beneficial for a device to be compatible with existing processes and materials. Substrate materials used here were chosen based on criteria reflecting both the electronic properties and practical considerations. It is desirable to have a substrate that conducts well both thermally and electrically, but given that the scope of the project is to develop a inexpensive, scalable emission device, it is also important for the material to be readily available, easily fabricated in the correct dimensions, and not to require special treatment. It is also important that the screen printing process works well with the chosen material.

Substrate texture affects both the magnitudes and the directions of electric fields near the surface. Consequently a rough substrate has a defocusing effect on the electron beam [158]. To assess the roughness of the substrates R_a was measured using a Mitutoyo SJ-210 surface roughness tester performing 5 measurements over an evaluation length of 400 μm. In each case results from 5 samples were averaged. Substrate investigations were performed using inks made with the Xintek CNT material, and the standard emission test profile.

6.4.1 Au/NiCr/Glass

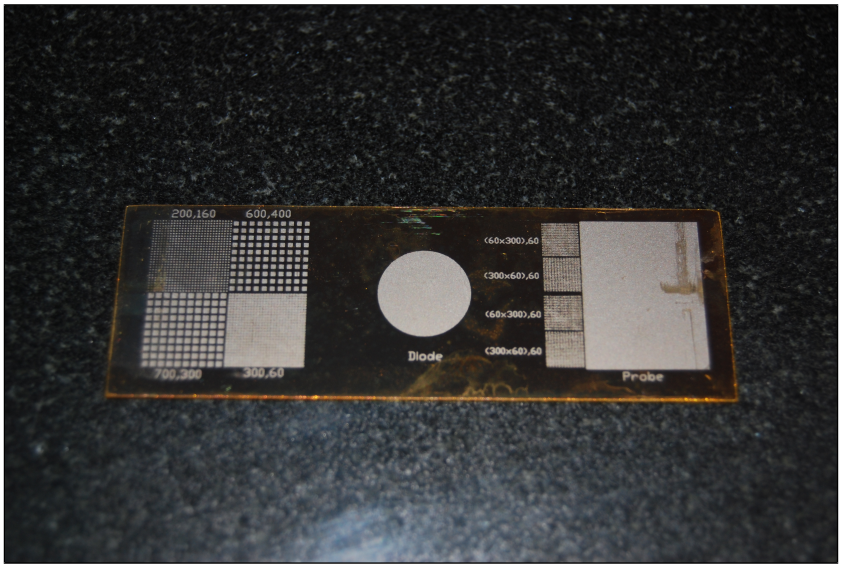

Figure 6.10: CNT-based emitter printed on Au/NiCr/glass substrate.

Gold-coated glass microscope slide substrates were tested first. The substrates were found to have $R_a \leqslant 10$ nm, were easy to print on and did not bend. A printed emitter is shown in figure 6.10.

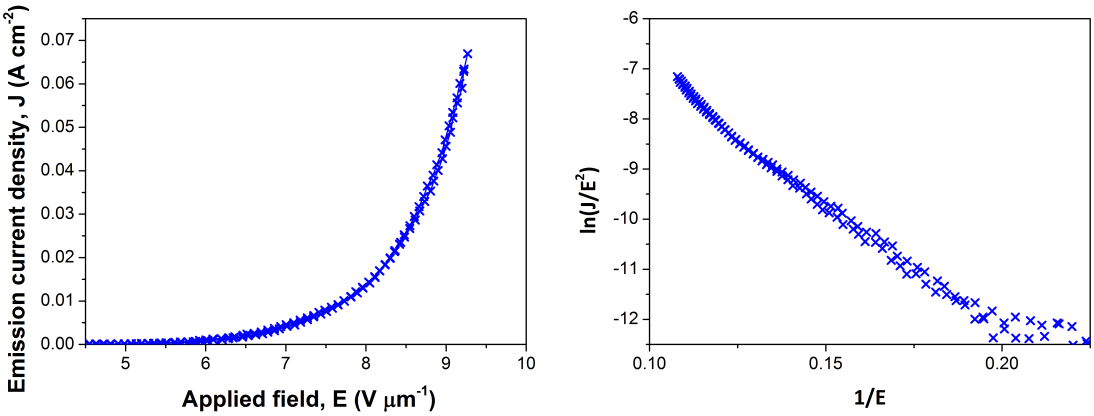

Figure 6.11: Final *J-E* cycle of CNT-based emitter printed on Au/NiCr/glass substrate with corresponding Fowler-Nordheim plot.

Table 6.4: Summary table for emitter printed on gold-coated glass substrate.

Ink	J_{max}	E	E_{TO}	E_{TH}
X-3	0.0669	9.268	5.28	7.81

Emission testing was performed using the standard test profile with a maximum PSU voltage of 4.4 kV. The *J-E* and Fowler-Nordheim plots in figure 6.11 are from the final cycle of an emission test of an emitter printed on Au/NiCr/glass substrate. The result is summarised in table 6.4.

6.4.2 Copper

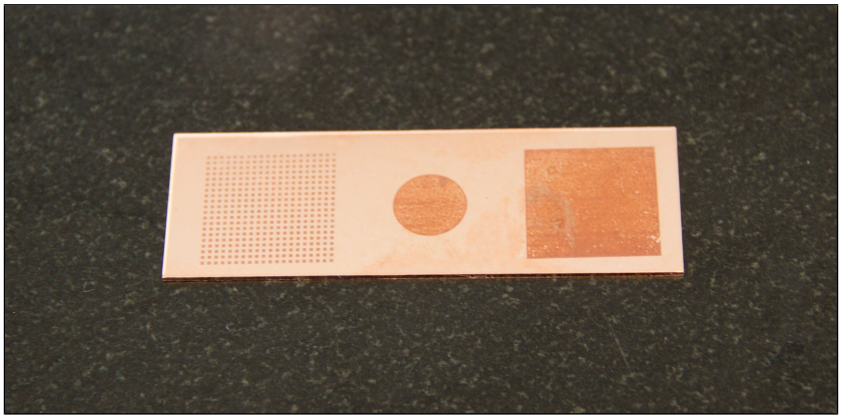

Figure 6.12: CNT-based emitter printed on copper substrate.

Table 6.5: Summary table for emitters printed on copper substrate.

Ink	J_{max} (A·cm^{-2})	E (V·μm^{-1})	E_{TO}	E_{TH}
X-3	0.119	8.6	4.9	7.0
Mk-4	0.063	9.3	5.0	7.8

The printing technique itself required little adaptation for use with copper substrates. However, different cleaning processes and an additional heat treatment step were required (section 2.5.7). Following heat treatment, the copper substrates were easily deformed and had to be handled with more care than the other substrate materials. A picture of a field emission device printed on a copper substrate is shown in figure 6.12, in which it can be seen that the colour in the printed areas differs from that of the gold-coated glass-based devices. Average R_a value for copper substrates was 26 nm.

Figure 6.13 shows the *J-E* curves and Fowler-Nordheim plots from the final cycle of standard emission tests for emitters made with two inks to allow comparison with the other substrate materials. Table 6.5 summarises the results. Although the copper substrate required an additional heat-treatment step to prepare the substrate before printing, it was selected as the preferred substrate for the majority of the experiments in the project as it was less expensive than gold-coated glass and performed well.

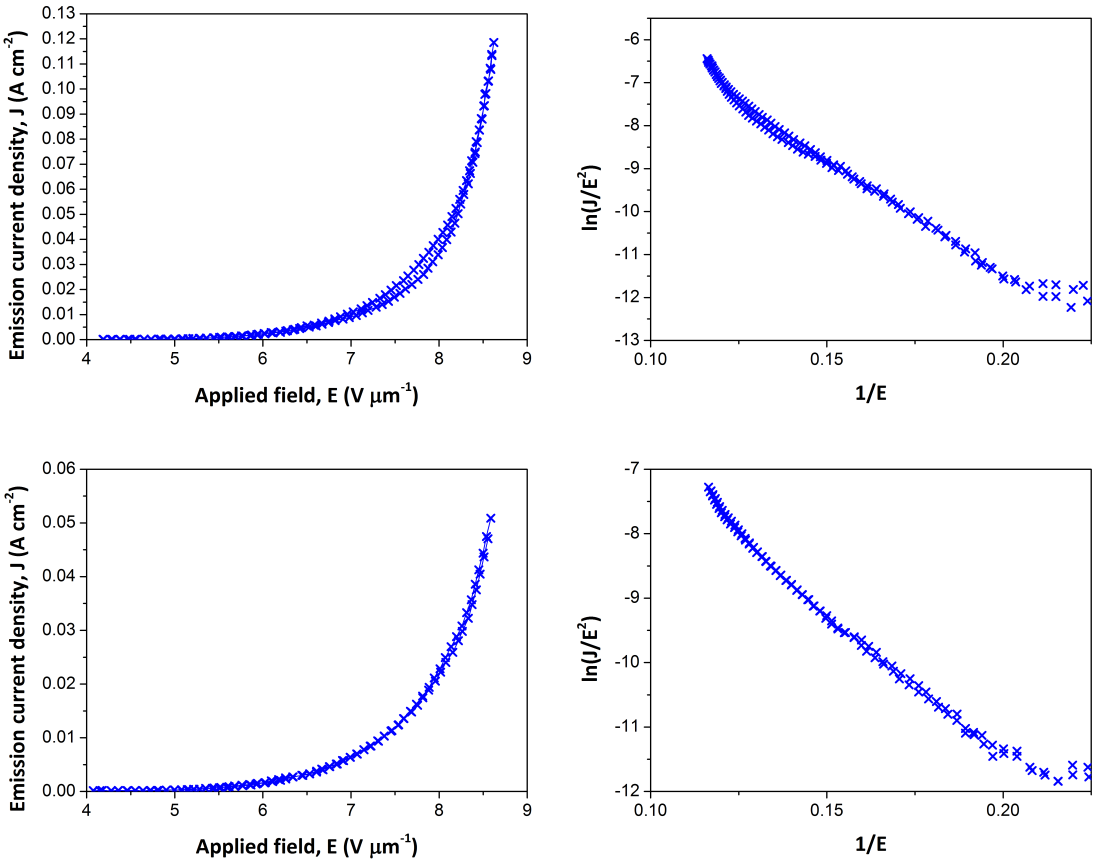

Figure 6.13: Final *J-E* cycle and corresponding Fowler-Nordheim plot from emission tests of emitters printed on copper substrates using X-3 ink (top), and Mk-4 ink (bottom).

6.4.3 Steel

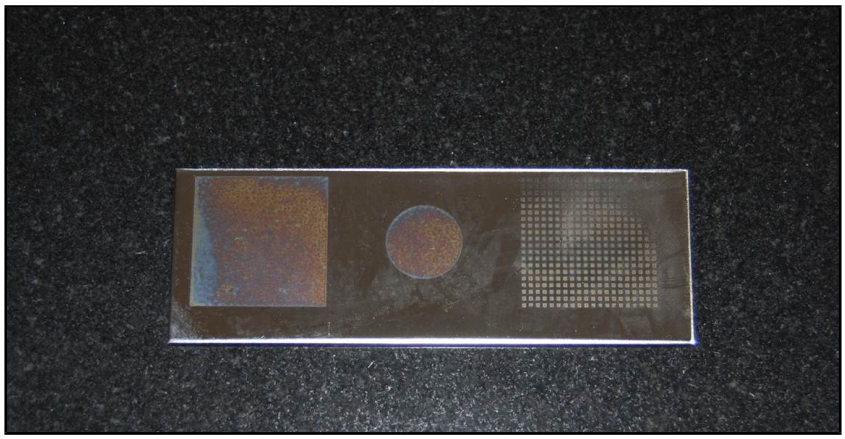

Figure 6.14: CNT-based emitter on steel substrate.

Some difficulty was experienced applying the printing technique to the stainless steel substrates. The picture in figure 6.14 shows a steel-based emission device. Again, the colour of the printed areas differs from those previously shown, in this case having variations in colour within the printed areas. The partial print seen towards the upper-right of the picture was a common problem, with few samples produced which were viable for emission testing. Steel substrates had $R_a \leqslant 10$ nm.

The *J-E* curve and Fowler-Nordheim plot from the final cycle of a standard emission test of a printed emitter on a steel substrate made using the Mk-4 ink is shown in figure 6.15, with results summarised in table 6.6. A change in the gradient of the Fowler-Nordheim plot occurs at a value corresponding to 8.0 $V{\cdot}\mu m^{-1}$, at which point an emission current of 7 $mA{\cdot}cm^{-2}$ was observed. The performance of the emitter was found to be comparable with that of a copper-based device made using the same ink.

Table 6.6: Summary table for emitter printed on stainless steel substrate.

Ink	J_{max} ($A{\cdot}cm^{-2}$)	E ($V{\cdot}\mu m^{-1}$)	E_{TO}	E_{TH}
Mk-4	0.040	9.6	5.1	8.48

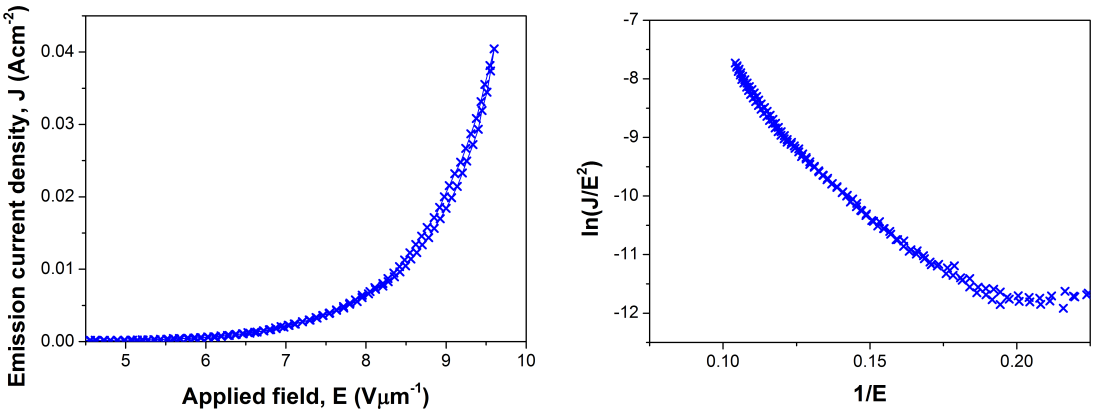

Figure 6.15: Final *J-E* cycle of field emission test of stainless steel-based emitter, with corresponding Fowler-Nordheim plot.

6.4.4 Molybdenum

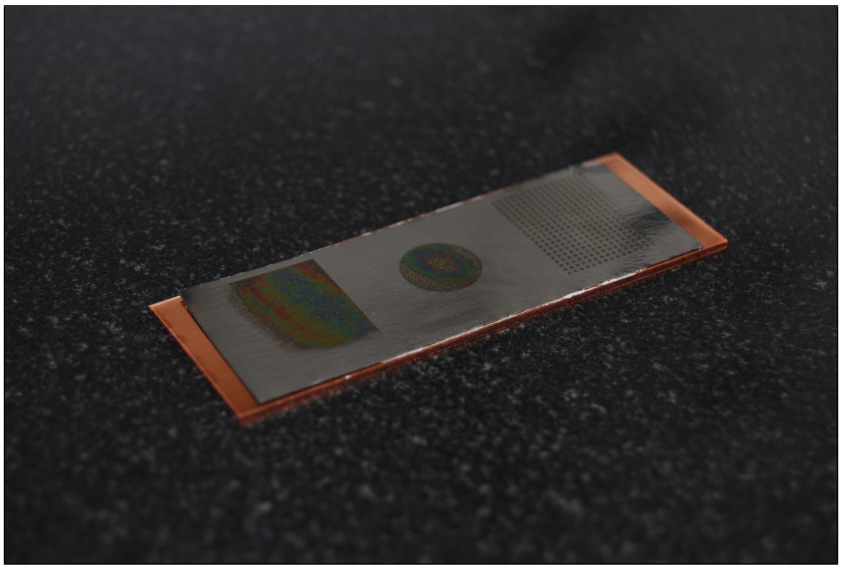

Figure 6.16: CNT-based emitter on molybdenum substrate.

The molybdenum substrates were considerably thinner than the other substrates used, having a thickness of 50 μm. The printing process was altered to accommodate the different dimensions, but was otherwise identical to the technique used with copper substrates. Figure 6.16 shows the molybdenum device mounted on a copper substrate for emission testing. As with the steel-based emitter, variations in colour can be seen in the printed areas. Average R_a value for molybdenum substrates was 32 nm.

Figure 6.17 shows the final *J-E* cycle of a standard automated field emission test of an

emitter made using the Mk-2 ink, with the results summarised in table 6.7. The molybdenum-based device was found to give a similar maximum current density to the copper-based devices printed using the same ink (section 6.3), despite the differences in substrate roughness, thickness, thermal and electrical conductivities, and the visual appearance of the printer material. However, the Fowler-Nordheim plot of the results shows instability occurring at values corresponding to 8.3 $V \cdot \mu m^{-1}$, at which point an emission current of 12 $mA \cdot cm^{-2}$ was recorded.

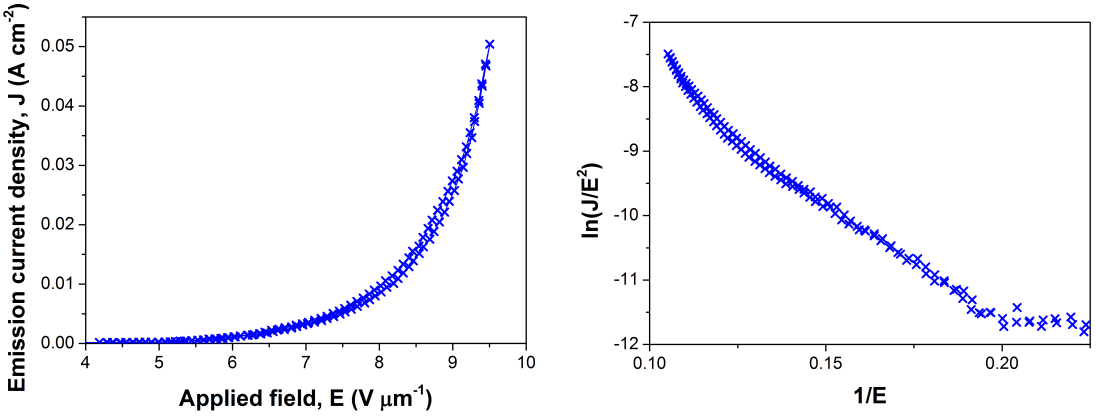

Figure 6.17: Final *J-E* cycle of field emission test of molybdenum-based emitter with corresponding Fowler-Nordheim plot.

Table 6.7: Summary table for emitter printed on molybdenum substrate.

Ink	J_{max} ($A \cdot cm^{-2}$)	E ($V \cdot \mu m^{-1}$)	E_{TO}	E_{TH}
Mk-4	0.050	9.5	4.8	8.1

6.4.5 Summary

The developed screen printing technique has been found to be applicable to four substrate materials. Comparing the copper and gold-coated glass substrates, a significant difference in emission current density is seen. The stainless steel emitter gave the poorest performance, as expected due to its electrical and thermal conductivities. The stainless steel substrates also had a lower R_a than the other solid metal substrates, which has been shown to decrease emission current density, and were difficult to use with the developed printing technique. Steel is a lower cost substrate material than the others tested, and requires less delicate handling than copper, and should therefore not be ruled out as a substrate for future investigation. Molybdenum is also of interest due to its widespread use in vacuum

electronics. Overall, the differences between the substrates was less pronounced than expected from their physical properties, suggesting the substrate material itself is not a limiting factor in device performance. Emission tests at higher duty may differentiate the substrate materials as dissipation of heat becomes more important.

While emission devices have been previously made using each of the substrate materials tested here [150] [79] [78], few studies apply the same technique to several materials. Where comparison are made the role of the substrate is under investigation due to its effect on CNT growth by CVD, as well as its electronic properties [159] [160].

6.5 Lifetime test

The lifetime test experiment was performed to assess how the emitter would perform if used in a commercial device. At the beginning of the test a current density of 39.2 $mA{\cdot}cm^{-2}$ was recorded at an applied field of 7.13 $V{\cdot}\mu m^{-1}$. Figures 6.18 shows photographs of the device surface and the anode taken after the test.

Figure 6.19 shows that the emission current density reduced sharply initially, before adopting a more gradual rate of decline as the test progressed. Emission current density after 10 hours was 35.2 $mA{\cdot}cm^{-2}$ at an applied field of 7.29 $V{\cdot}\mu m^{-1}$. Improving vacuum quality, particularly by reducing the partial pressure of oxygen, is expected to reduce damage to CNT tips during field emission and improve lifetime [21].

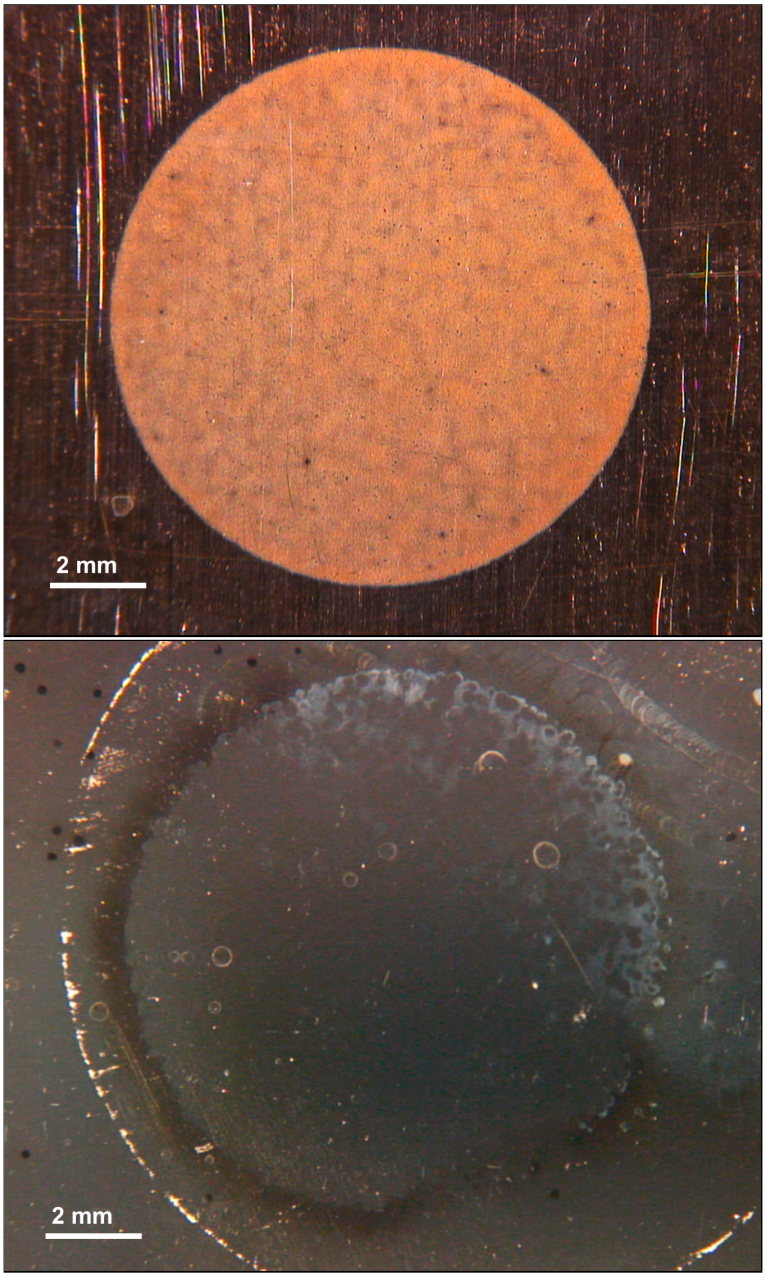

Figure 6.18: Top: field emission device used for lifetime test. Bottom: Anode surface after test.

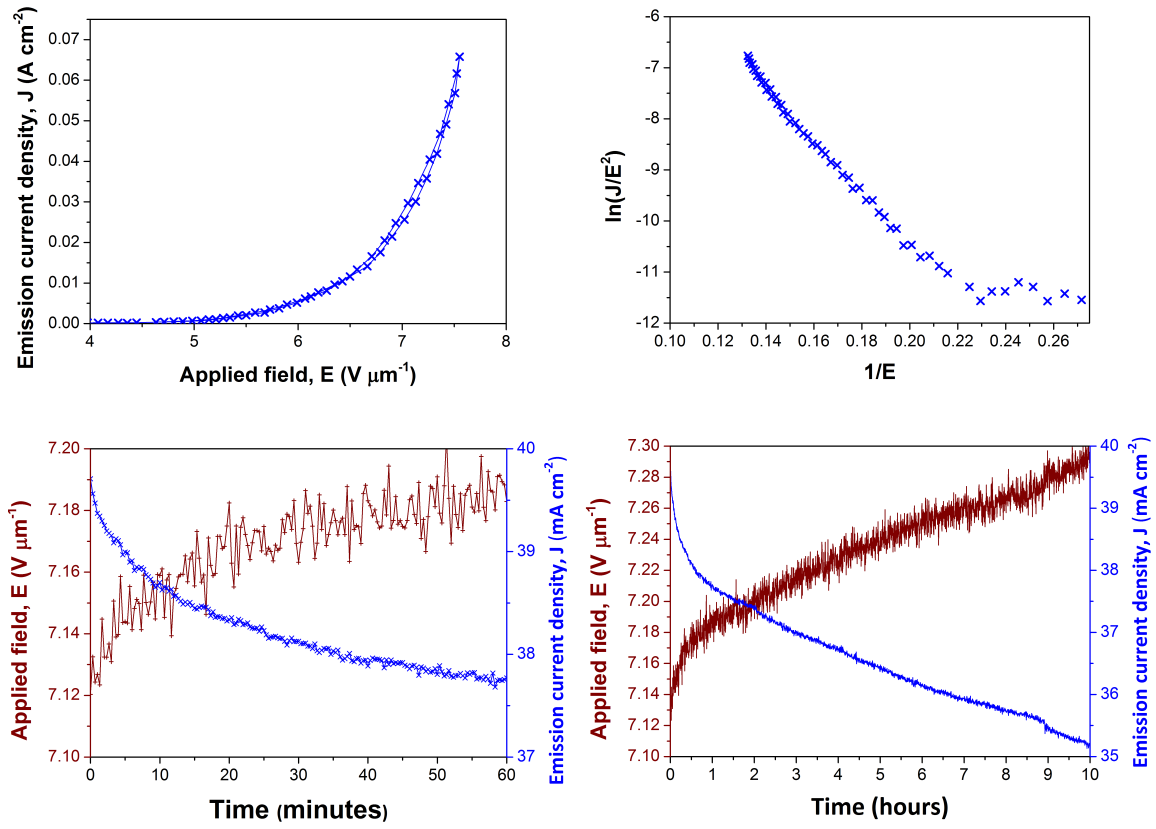

Figure 6.19: *J-E* curve and Fowler-Nordheim plot of emitter used for life test (top), and plot of data collected during life test, showing emission current density declining over time (bottom).

6.6 Device geometry

To assess whether emission test performance was affected by the geometry of the emitter, devices were printed with an array of small printed squares alongside the usual 1 cm^2 circular emitter. Both the array and circular emitter were printed as part of the standard print technique, with the array emitter at one end of the substrate. Emitters used for geometry investigations were printed with the Xintek CNT material on a copper substrate. The Mk-6 ink was used as it had the highest CNT concentration and was therefore most likely to exhibit the edge effect.

The array emitter consisted of a pattern of 400 squares (fig. 6.20). It was observed that the ink could run slightly between printing and drying, meaning the boundary of the printed area moved outward. This effect can be seen in the SEM image in figure 6.21. For the usual circular emitter the difference this effect has on the emitting area is negligible, but the increased total edge length of the array makes it significant. To accurately measure the printed area a high magnification photograph of an array emitter (figure 6.20) was analysed with ImageJ [157] and found to have an area of 1.40 cm^2.

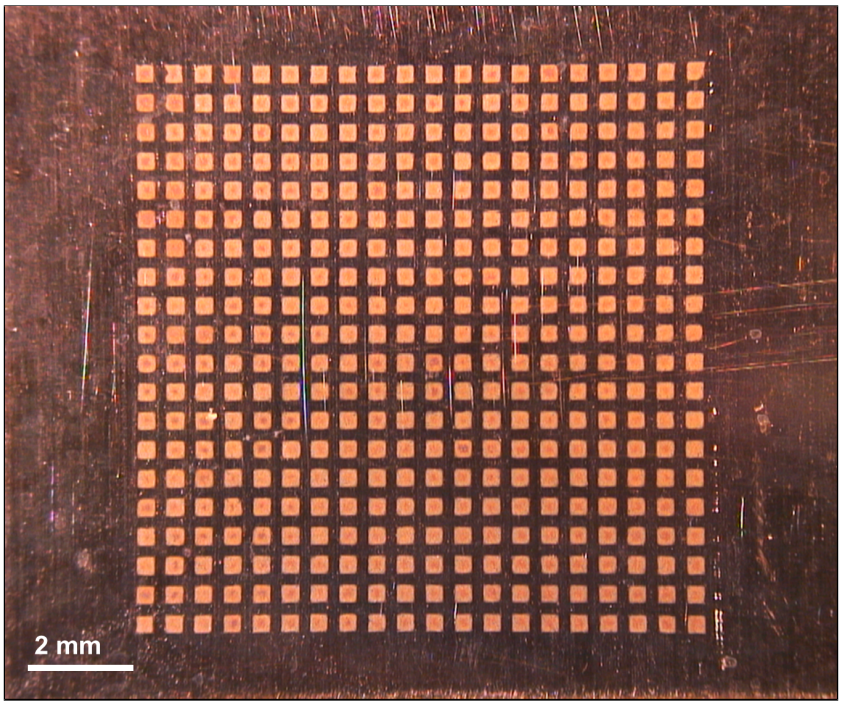

Figure 6.20: Photograph of array of printed squares used to test emitter geometry.

Results from emission tests of array emitters were compared with those from the circular emitter on the same sample. The results from an emission test of a square array emitter are presented in figure 6.22, with a similar Fowler-Nordheim plot to those obtained from tests of circular emitters. Figure 6.23 shows the results in comparison with results from an emission

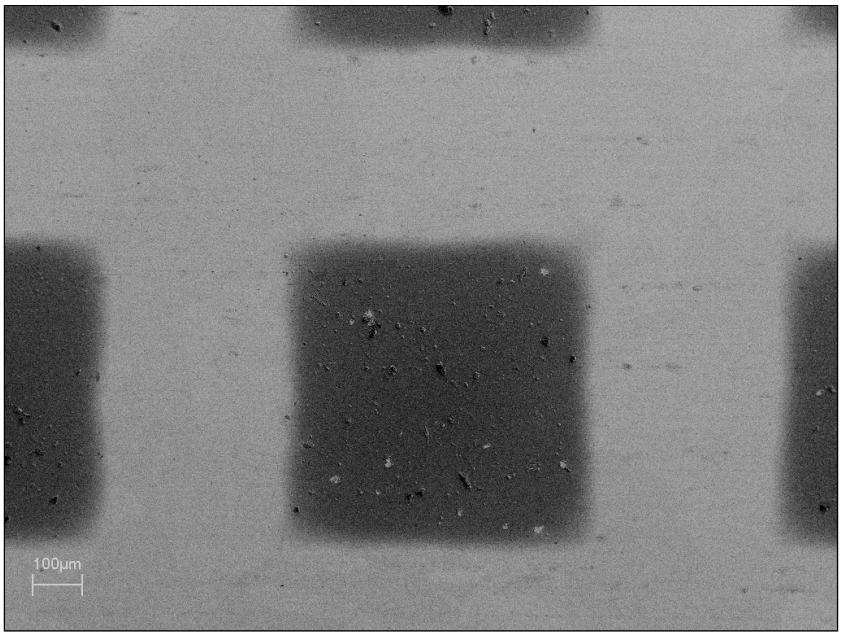

Figure 6.21: SEM of array of printed squares used to test emitter geometry.

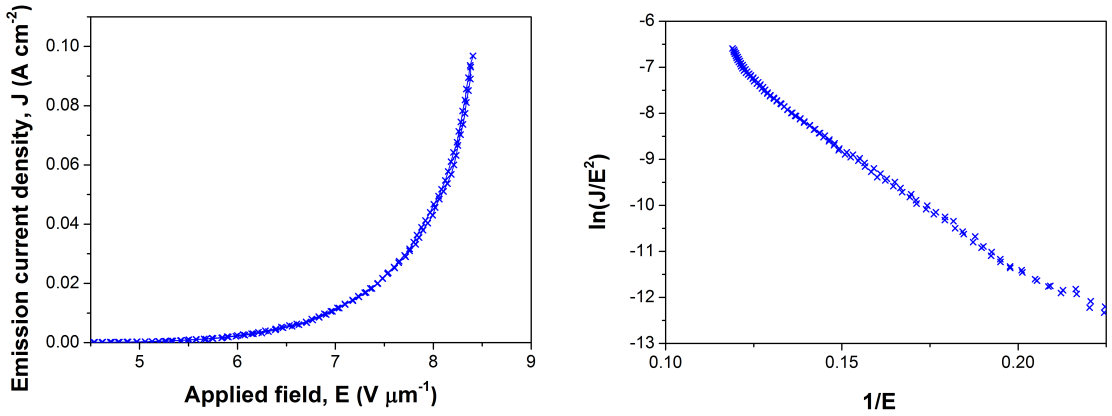

Figure 6.22: *J-E* plot from field emission test of square array emitter with corresponding Fowler-Nordheim plot.

test of the circular emitter from the same device, with results from a second device included in appendix D.2.

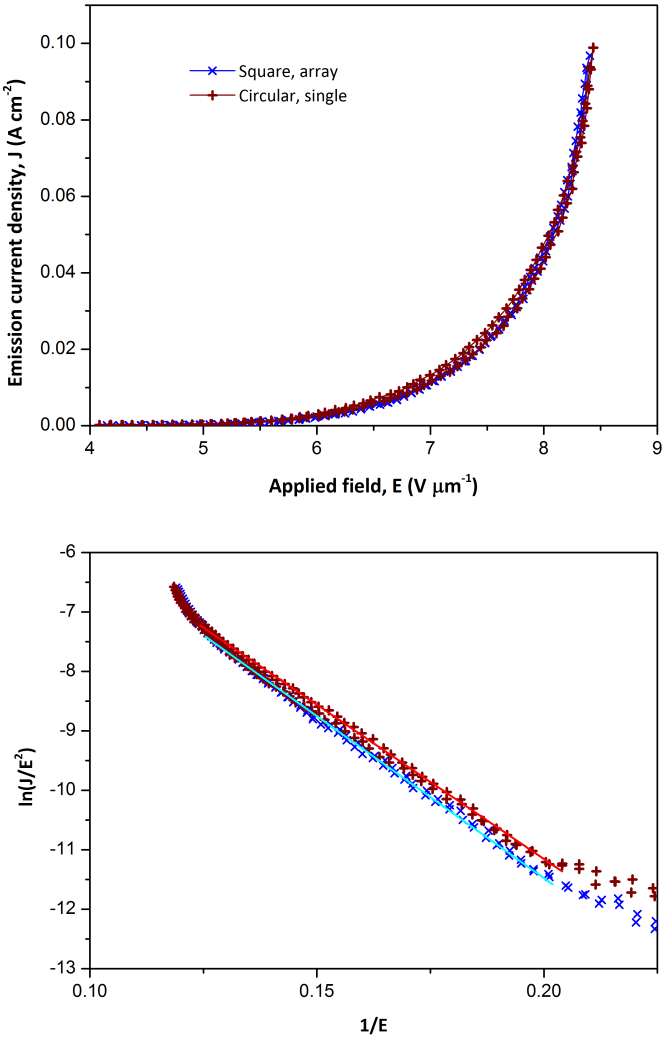

Figure 6.23: Comparison of *J-E* data from square array and circular emitter.

Table 6.8 summarises the results of emission testing. In this case, a value for the field enhancement factor is calculated as described in section 3.7.3 to compare the performance of the two emitters, using the gradients of regression lines fitted to the straight section of the Fowler-Nordheim plot (shown in figure 6.23). The results are more similar than would be expected if the edge effect was significant, with less variation than that found between different devices printed using the same ink. The onset of instability is estimated by examination of the Fowler-Nordheim plot and found to correspond to a field of 8.0 $V \cdot \mu m^{-1}$ for both devices, with an emission current of 44.0 $mA \cdot cm^{-2}$ measured for the array emitter

Table 6.8: Emission test results from emitters used for geometry test.

Geometry	β	J_{max} (A·cm^{-2})	E (V·μm^{-1})	E_{TO}	E_{TH}
Circular	1470	0.099	8.4	5.0	6.8
Array	1400	0.097	8.4	4.9	7.0

and 46.6 mA·cm^{-2} for the circular emitter, corresponding to the termination points of the displayed regression lines. The result shows that the current method can be used to make emission devices with larger surface area without compromising emission current density, as well as supporting the earlier result indicating that the device could be improved with a higher CNT concentration.

While results from previous studies have demonstrated the edge effect [10] [161], in these cases CNTs were grown by CVD, were well aligned, closely-packed, and of similar length, meaning the geometric field enhancement factor of the CNTs was not exhibited, except where a CNT had few neighbours. In the present work a very different arrangement of CNTs is present, and while the shading effect is likely to prevent a large number of CNTs in a cluster participating in field emission, the emission sites themselves are not sufficiently closely-spaced for shading to occur. Therefore, smaller clusters, or a uniform deposited layer, and a higher concentration of CNTs is expected to give a higher emission current density.

6.7 Conclusions

Optimisation of emitters based on the Xintek CNT material has been investigated in this chapter. EPD has been used to deposit the same CNT species and binder material as used with screen printing. However, practical considerations meant the screen printing method was favoured. The developed printing method has been applied to four substrate materials.

The surfaces of the printed emitter devices have been shown to be composed of clusters of densely-packed CNTs, with the concentration of the CNT material in the ink positively correlated with the number of clusters per unit area, but not their size. CNT concentration also has an effect on the emission current density of a printed emitter, with emitters with higher ratio of CNT to binder material exhibiting higher emission current densities.

Finally, the geometry of the printed emitters has been demonstrated to have no effect, with an array of smaller printed squares giving similar emission current density per unit area than a single circular area. It is concluded from this that emission sites are not of sufficient density to exhibit the edge effect, and that an increase in CNT concentration would

be beneficial to field emission performance.

Chapter 7

Conclusions

7.1 Final summary and discussion

At the outset of the project the objectives were to develop a field emission cathode fabricated by screen printing nanostructured carbon materials with a dielectric binder, to develop a method of testing the cathodes and to identify the factors affecting performance to enable optimisation of the device.

A fabrication process has been developed producing field emission cathodes by screen printing inks based on commercially available CNTs, and incorporating a dielectric binder. Performance was found to depend strongly on CNT material, as expected. The screen printing process is scalable and simple, with standard vacuum electronics manufacturing techniques used. The use of several substrate materials has been demonstrated. The developed test setup has a variable anode-cathode separation and a pulsed power supply with maximum voltage of 4.5 kV and variable pulse width and PRF. The fabricated field emission cathodes have been tested using a duty profile designed to simulate the application of a multi-cathode CT scanner for airport baggage scanning.

Characterisation of the fabricated devices showed that increased emission current density is correlated with increased CNT concentration in the ink, but with decreasing silica binder concentration. The best-performing CNT material was found to form clusters on the substrate surface, with EDS-mapping suggesting the binder was not uniformly dispersed. Protruding nanotubes were identified as the emission sites, and were shown to exhibit damage as a result of field emission testing, with longer CNTs observed lying flat on the substrate surface after the test. It is unknown whether these CNTs still participate in field emission by aligning under the application of an electric field. Although the presence of these CNTs indicates some degree of adhesion to the substrate, carbon was found to have been deposited on the anode.

Whilst the addition of a dielectric material to CNT-based field emission devices has been

shown in the literature to have beneficial effects on device performance [162], the effect of the binder in the present work is unclear. A study in which t-MWNTs were coated with a nanoscale layer of silica found improvements in terms of emission current density and lifetime [82], and also found the silica to have a protective effect, but required significant processing of the CNTs to achieve the coating. Compared to the work presented here, a higher CNT concentration was used, suggesting that the silica binder used here may be of benefit if similar concentrations are used.

Historically, studies of screen printed CNT-based field emission devices are dominated by work related to development of displays, which have a different set of objectives to that presented here. Above the level required to excite a phosphor screen with adequate brightness, high emission current density is not a concern. Instead, it is beneficial to achieve a modest emission current density at a lower applied field. More recently, the focus of the work has shifted, in some cases resulting in high-current screen printed cathodes. In a study performed at SAIT, a patterned emitter was fabricated by screen-printing a well-dispersed paste of SWNTs, which formed a thick layer. An emission current density of 25 $mA{\cdot}cm^{-2}$ was observed at an applied field of 2 $V{\cdot}\mu m^{-1}$ [32]. While higher emission current densities have been demonstrated in the present work, a substantially higher field was applied. Although the use of a thick deposited layer has been shown to give good results in this case, this cannot necessarily be expected to have the same effect with the addition of a dielectric binder. The use of SWNTs may be expected to improve results, but have been shown to degrade more quickly than MWNTs [163].

EPD has been used with similar CNTs to give very high current densities. A high density layer of CNTs has been deposited with vertically-aligned protruding CNTs [44]. While these emitters have found application in CT scanners, the low manufacturing cost of the devices fabricated in the present work would make them more attractive for a baggage scanner with several hundred cathodes, if the required current density can be achieved.

The greatest degree of control over CNT height, placement and orientation is achieved using CVD techniques [164]. For example, arrays of uniformly spaced CNTs of height 3 μm and diameter 30 nm have been achieved with PECVD [25]. Height anisotropy is minimised with CVD, in this case to 6 %, which has been shown to reduce heating during emission and consequently improve stability and lifetime [11]. For the device presented here, the random positioning and alignment of the deposited CNTs results in a broad distribution of exhibited geometric field enhancement factors among the emitting tips on the surface [152]. Although there appear to be a large number of CNTs per cluster, it is likely that emission is dominated by the small number that protrude. Consequently screen printing techniques are unlikely to compete with CVD on emission current density alone, but are lower cost and scalable.

7.2 Further work

The results in chapter 6 suggest that improvements can be made by increasing the concentration of CNTs in the ink formulation, which will require work to improve dispersion of the CNT material in the ink vehicle. Further improvements could be achieved with simple alterations to the device. The copper substrate gave the best performance of the substrates tested. However, higher grades of copper are available. Oxygen-free, high conductivity (OFHC) copper is commonly used in applications where good thermal and electrical conductivity are of paramount importance, especially vacuum electronics.

The results presented here also suggest that increasing the CNT concentration will allow increased emission current density. This necessitates investigation into the ink formulation to improve the dispersion of the CNT material. Studies using ink with much higher CNT concentrations suggest this can be achieved [165]. In the present work, the observation of densely packed clusters along with the practical difficulties experienced with higher concentration inks indicate that the dispersion of the CNTs in the ink vehicle is poor. Whilst the technique of using a centrifugal mixer was convenient and quick, and visually homogenised the inks, alternative methods may mix the ink more thoroughly. Equally, the fact that devices printed with different emitter materials gave a more uniform dispersion suggests that the ink vehicle requires modifying to optimise it for use with the Xintek CNTs. At higher concentrations the increase in emission current density would be limited by the shading effect, and contact resistance between the CNTs and the substrate, with investigation required to quantify these effects.This is also expected to affect the lifetime of the device, with the expectation that a device printed with a higher concentration of CNTs will deteriorate at a slower rate. Further work must also be carried out to separate the effect of the CNT and binder concentration. The ink formulation and processing techniques must also be optimised to ensure that all material, other than the CNTs and silica binder are removed.

It is likely that in a vacuum electronics application a triode configuration would be used, rather than the diode configuration used in this work. Investigations using this configuration therefore represent a logical next step. Work is underway to adapt the developed test setup to function as a triode.

Vacuum electronics devices such as TWTs typically operate under vacuum of 10^{-7} Pa (10^{-9} mbar). To achieve this the devices are baked at 450 °C for several days in UHV while being actively pumped to remove residual gases and water vapour. This process was not applied to the field emission devices made as part of this project. It has previously been found that the process benefits CNT-based cathodes [78], and therefore it is expected that performing a similar process on the screen printed cathodes will improve performance, particularly with respect to stability and lifetime.

Although material has been found to be deposited on the anode, the underlying process has not been characterised. An understanding of the degradation mechanism of the emitters is an important part of improving the fabrication process. It is also desirable to identify other commercially available CNT species which offer comparable or improved performance.

The silica binder is expected to have a protective effect on the CNTs during emission [83]. Further lifetime tests on emitters printed with differing CNT and binder concentrations are necessary to establish whether this is the case, and to quantify the effect. As the CNT/binder ratio has been shown to adversely affect emission current density, it is desirable to minimise the quantity of binder. The introduction of a dielectric material is also expected to have an effect on the conducting path, both between CNTs and at the substrate boundary, and to affect the potential barrier between the emitting tips and vacuum. An understanding of these processes is key to further development of the device. TEM study is required to examine the interaction between the silica and CNTs. The method used to synthesise the binder material has been shown to produce a porous film which traps water molecules from the atmosphere, which may be a source of instability in the emission behaviour. A device with this property is undesirable, requiring storage in vacuum and a lengthy conditioning process before use, as is the case with thermionic dispenser cathodes. Several similar sol-gel processes result in a silica film with lower porosity by altering the catalyst and heat treatment temperature, which merit investigation [166]. TEM may also be used to investigate the contact between the CNTs and the substrate, which will also be affected by the presence of the binder.

Appendix A

Published work

A.1 HiPerNano, May 2011

On 10th May, a poster entitled “Screen Printing Carbon Nanotubes for Field Emission Devices” was presented by the author at the HiPerNano event hosted by the Knowledge Transfer Network at the Royal Academy of Engineering. The submitted abstract and poster are reproduced below.

Screen Printing Carbon Nanotubes for Field Emission Devices

Edward Boughton[1,2] Wenhui Song[1], Benjamin Jones[2], Robert Bulpett[2], Sabina Orlowska[3], Geoffrey Sheehy[3], Michael Waite[3,] Mike Miller[3]

1. *Wolfson Centre for Materials Processing, Brunel University, Uxbridge, West London, UK*
2. *Experimental Techniques Centre, Brunel University, Uxbridge, West London, UK*
3. *TMD Technologies Ltd., Hayes, Middlesex, UK*

Abstract

Electron sources have applications in x-ray scanners, displays, microwave amplifiers and electric propulsion for space missions. Currently, these technologies use thermionic electron emission, in which a filament of a low work function material is heated to high temperature to give electrons enough energy to overcome the potential barrier and escape the material. An accelerating voltage draws off the electron beam. By contrast, field electron emission is a process by which electrons are able to escape without additional thermal energy. Field emission ordinarily occurs only at very high electric fields. However, a sharp tip concentrates electric field lines, meaning the local field strength may be several orders of magnitude higher [1]. Field emission can therefore occur from a sharp tip at lower applied fields. The extent to which the required field is lowered is measured by the field enhancement factor, β, and is proportional to the aspect ratio of the tip [2,3]. Carbon nanotubes (CNTs) are 1-dimensional tubes composed of graphene sheets of hexagonally-arranged carbon atoms. This study aims to exploit the high aspect ratio, small size and ballistic conductivity of multiwalled carbon nanotubes (MWNTs) to fabricate a field emission electron source with low turn-on field, a large number of individual emission sites and high current density. A method of fabricating a field emission cathode by screen-printing CNT-containing inks is used to compare several CNT species. A field emission cathode with current density of 5mAcm^{-2} DC and field enhancement factor β of ~1920 has been fabricated.

References

1. A. Buldum and J.P. Lu, Physical Review Letters 91, 23 (2003)
2. W.A. de Heer, A. Chatelain and D. Ugarte, Science 270, 1179 (1995).

Figure A.1: Abstract submitted to HiPerNano 2011.

A.2 10th International Conference on Materials Chemistry (MC10), July 2011

From 3-7th July the international Materials Chemistry 10 conference was attended at Manchester University. A poster entitled "Screen Printing Carbon Nanotubes for Field Emission Devices" was presented by the author. The submitted abstract and poster are reproduced below.

Screen Printing Carbon Nanotubes for Field Emission Devices

Abstract

Electron sources have applications in x-ray scanners, displays, microwave amplifiers and electric propulsion for space missions. Currently, these technologies use thermionic electron emission, in which a filament of a low work function material is heated to high temperature to give electrons enough energy to overcome the potential barrier and escape the material. An accelerating voltage draws off the electron beam. By contrast, field electron emission is a process by which electrons are able to escape without additional thermal energy. Field emission ordinarily occurs only at very high electric fields. However, a sharp tip concentrates electric field lines, meaning the local field strength may be several orders of magnitude higher [1]. Field emission can therefore occur from a sharp tip at lower applied fields. The extent to which the required field is lowered is measured by the field enhancement factor, β, and is proportional to the aspect ratio of the tip [2,3]. Carbon nanotubes (CNTs) are 1-dimensional tubes composed of graphene sheets of hexagonally-arranged carbon atoms. This study aims to exploit the high aspect ratio, small size and ballistic conductivity of multiwalled carbon nanotubes (MWNTs) to fabricate a field emission electron source with low turn-on field, a large number of individual emission sites and high current density. A method of fabricating a field emission cathode by screen-printing CNT-containing inks is used to compare several CNT species. A field emission cathode with current density of 5mAcm^{-2} DC and field enhancement factor β of ~1920 has been fabricated.

References

1. A. Buldum and J.P. Lu, Physical Review Letters 91, 23 (2003)
2. W.A. de Heer, A. Chatelain and D. Ugarte, Science 270, 1179 (1995).
3. K. L. Aplin, B. J. Kent, W. Song and C. Castelli, Acta Astronautica, 2009, 64, 875-881.

Figure A.2: Abstract submitted to MC10.

Screen printing carbon nanotubes for field emission devices

Edward Boughton[1,2], Wenhui Song[1], Benjamin Jones[2], Robert Bulpett[2], Sabina Orlowska[3], Geoff Sheehy[3], Michael Waite[3], Mike Miller[3]

1. Wolfson Centre for Materials Processing, Brunel University, Uxbridge, Middlesex, UK
2. Experimental Techniques Centre, Brunel University, Uxbridge, Middlesex, UK
3. TMD Technologies Ltd., Hayes, Middlesex, UK

Introduction

Currently, electron beams are produced by heating a cathode to the point where electrons have enough energy to overcome the work function, ϕ. In field emission, the potential barrier is lowered by the strength of the applied field only. Because this requires very high fields, current research focuses on exploiting the local increase in field strength which occurs around a sharp tip. The field enhancement factor, β, measures the degree to which this effect occurs and is related to the aspect ratio of the tip.

Because no heat is required, a field emission electron source can be smaller, lighter, more efficient and have a faster response time than a thermionic filament source, which is advantageous to x-ray machine and high-powered microwave tube applications.

Materials

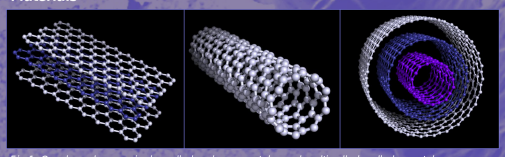

Fig 1: Graphene layers, single-walled carbon nanotube and multiwalled-walled nanotube

Multiwalled Carbon nanotubes (MWCNTs) are composed of graphene sheets of hexagonally-arranged carbon atoms rolled-up into nanostructured tubes (fig. 1). Their small size, high aspect ratio and ballistic conductivity mean there is the potential to fabricate a field emission device with low turn-on field, a large number of individual emission sites and high current density [1,2].

Type A:
Process: Arc-discharge
Length: 200-300nm
Avg. diameter: 8.4nm
Purity: Low. Also includes nano-onions, graphite and amorphous carbon.

Type B:
Process: Chemical Vapour Deposition (CVD)
Length: ~300μm
Avg. diameter: ~100nm
Purity: 90%

Type C:
Process: CVD
Length: >10μm
Avg. diameter: 7nm
Purity: 88%

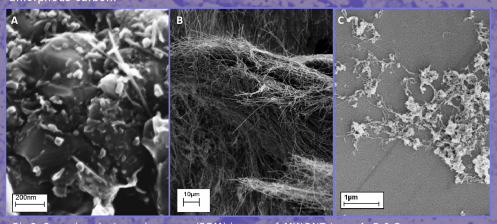

Fig 2: Scanning electron microscope (SEM) images of MWCNT types A, B & C

Fabrication

The MWCNTs are suspended in solvent by ultrasonication. The addition of further solvents and binders results in thick black ink. A screen printer is used to apply a thin layer of the ink to a gold-coated glass slide in the desired pattern. Sintering at 450° C in air improves the adhesion of the MWCNTs to the substrate and drives off undesired ink components.

References

1. W.A. de Heer, A. Chatelain and D. Ugarte, Science 270, 1179(1995).
2. K. Aplin, B. Kent, W. Song and C. Castelli, Acta Astronautica, 64, 875(2009)

Testing

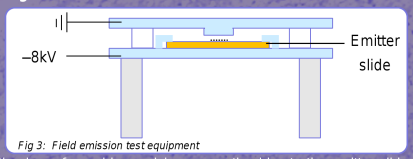

Fig 3: Field emission test equipment

Testing is performed by applying a negative bias to the emitter slide of up to 8kV, relative to an anode which is separated from the emitter by a gap of 200μm in vacuum of 10^{-6} mbar. Bias is increased gradually and the observed emission current recorded using an integrated microammeter.

Results

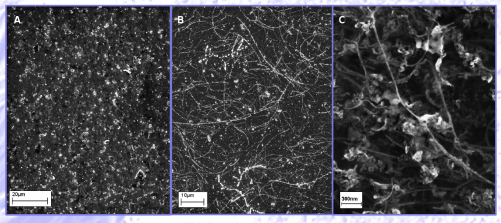

Fig 4: SEM images of field emitters fabricated using CNT types A, B & C

Fig. 5 shows that type C nanotubes produce the best emitter, with the highest maximum emission current density of 5mAcm^{-2} and a lower turn-on field among the emitters tested. Analysis of the data gives a field enhancement factor for this emitter of 1920. Although type B MWCNTs have the potential to give high β, figure 3 shows that the nanotubes lie flat on the surface. Few sharp tips therefore protrude, and the field enhancement factor is lower than expected.

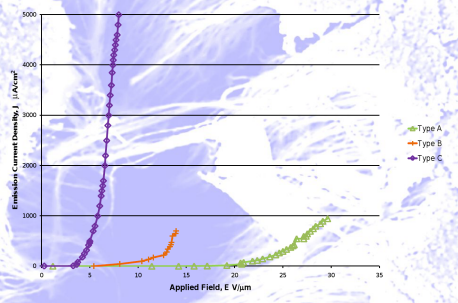

Fig 5: Plot of field emission performance of printed emitters

Summary

The superiority of the type C material over type B is attributed to their small size, which allows them to protrude from the surface. The performance of the type A material suffers as a result of the low MWCNT purity. A phosphor screen must be used to evaluate the emitter's uniformity and pulsed-mode testing must be performed to assess the suitability of the material for real-world applications.

Acknowledgement: Thanks to EPSRC and TMD Technologies Ltd. for financial support. Contact: wenhui.song@brunel.ac.uk, edward.boughton@brunel.ac.uk

A.3 R2i conference, June 2012

On 19th June, a poster entitled “Screen Printing Carbon Nanotubes for Field Emission Devices” was presented by Wenhui Song and Sabina Orlowska at the R2i conference at Loughborough University. The submitted abstract and poster are reproduced below.

Screen Printing Carbon Nanotubes for Field Emission Devices

Abstract

Electron sources have applications in x-ray scanners, displays, microwave amplifiers and electric propulsion for space missions. Currently, these technologies use thermionic electron emission, in which a filament of a low work function material is heated to high temperature to give electrons enough energy to overcome the potential barrier and escape the material. An accelerating voltage draws off the electron beam. By contrast, field electron emission is a process by which electrons are able to escape without additional thermal energy. Field emission ordinarily occurs only at very high electric fields. However, around a sharp tip electric field lines concentrate, meaning that the local electric field may be several orders of magnitude higher locally than macroscopically [1]. This effect allows field emission to occur from a sharp tip at significantly lower applied fields. The extent to which the required field is lowered is measured by the field enhancement factor, β, and is proportional to the aspect ratio of the tip [2,3]. Carbon nanotubes (CNTs) are 1-dimensional tubes composed of graphene sheets of hexagonally-arranged carbon atoms. The work presented here aims to exploit the high aspect ratio, small size and ballistic conductivity of multiwalled carbon nanotubes (MWNTs) to fabricate a field emission electron source with low turn-on field, a large number of individual emission sites and high current density. A method of fabricating a field emission cathode by screen-printing CNT-containing inks is used to produce a device capable of current density of over 60mAcm^{-2}.

References

1. A. Buldum and J.P. Lu, Physical Review Letters 91, 23 (2003)
2. W.A. de Heer, A. Chatelain and D. Ugarte, Science 270, 1179 (1995).
3. K. L. Aplin, B. J. Kent, W. Song and C. Castelli, Acta Astronautica, 2009, 64, 875-881.

Figure A.4: Abstract submitted to r2i 2012.

Screen printing carbon nanotubes for field emission devices

Edward Boughton[1,2], Wenhui Song[1], Benjamin Jones[2], Robert Bulpett[2], Sabina Orlowska[3], Geoff Sheehy[3], Michael Waite[3], Mike Miller[3]

1. Wolfson Centre for Materials Processing, Brunel University, Uxbridge, Middlesex, UK
2. Experimental Techniques Centre, Brunel University, Uxbridge, Middlesex, UK
3. TMD Technologies Ltd., Hayes, Middlesex, UK

Introduction

Currently, electron beams are produced by heating a cathode to the point where electrons have enough energy to overcome the work function of the material. In field emission, the potential barrier is lowered by the strength of the applied field only. Because this requires very high fields, current research focuses on exploiting the local increase in field strength which occurs around a sharp tip. The field enhancement factor, β, measures the degree to which this effect occurs and is related to the aspect ratio of the tip.

Because no heat is required, a field emission electron source can be smaller, lighter, more efficient and have a faster response time than a thermionic filament source, which is advantageous to x-ray machine and high-powered microwave tube applications.

Materials & Processing

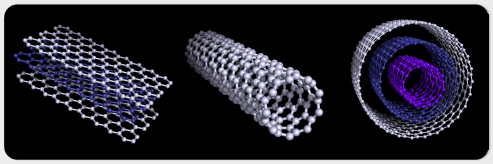

Fig 1: Graphene layers, single-walled carbon nanotube and multi-walled nanotube.

Multiwalled Carbon nanotubes (MWCNTs) are composed of graphene sheets of hexagonally-arranged carbon atoms rolled-up into nanostructured tubes (fig. 1). Their small size, high aspect ratio and ballistic conductivity mean there is the potential to fabricate a field emission device with low turn-on field, a large number of individual emission sites and high current density [1,2].

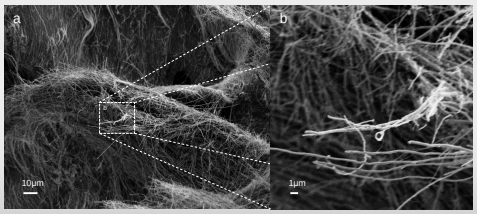

Fig 2: Multiwalled carbon nanotubes.

The MWCNTs are suspended in solvent and incorporated into a thick black ink. A screen printer is used to apply a thin patterned layer of the ink to a metallic substrate. Sintering improves the adhesion of the MWCNTs to the substrate and drives off undesired ink components.

References

1. W.A. de Heer, A. Chatelain and D. Ugarte, Science 270, 1179(1995).
2. K. Aplin, B. Kent, W. Song and C. Castelli, Acta Astronautica, 64, 875(2009)

Testing

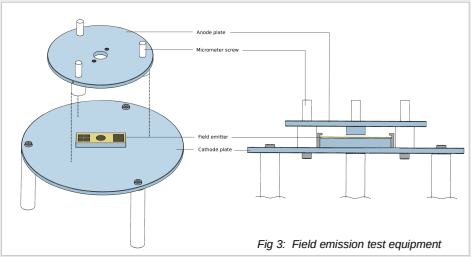

Fig 3: Field emission test equipment

Testing is performed by cyclically applying a high voltage across a gap of 250μm in vacuum of 10^{-4} Pa. A solid state switch allows the field to be pulsed and a ZnO phosphor-coated screen allows emission uniformity to be assessed. The field is increased gradually and the observed emission current recorded.

Results

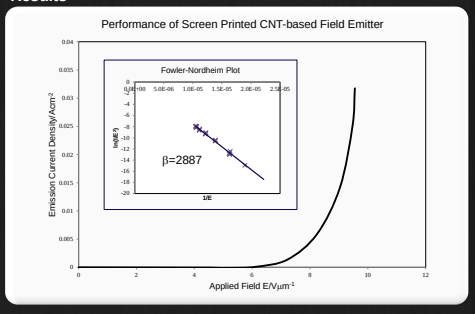

Fig 4: Plot of field emission performance of printed emitter. Inset: Fowler-Nordheim plot.

Fig. 4 shows a plot of emission current per unit area against applied electric field. The shape of the curve is typical for a field emission device. The Fowler-Nordheim plot shows a straight line, again indicating field emission, and allows the field enhancement factor, β, to be calculated.

Fig 5: Phosphor-coated anode showing uniform emission at 6V/μm⁻¹.

Summary

A field emission device has been fabricated with field enhancement factor of 2887 and a maximum emission current density in excess of 30mAcm^{-2}. Further work will focus on increasing the maximum current.

Acknowledgement: Thanks to EPSRC and TMD Technologies Ltd. for financial support. Contact: wenhui.song@brunel.ac.uk, edward.boughton@brunel.ac.uk

Figure A.5: Poster presented at r2i.

A.4 UKSAF Winter Meeting, Jan 2013

On 9th January a poster entitled “Screen printing carbon nanotubes for field emission devices” was presented by the author at the UKSAF Winter Meeting held at the Diamond Light Source, Harwell. The submitted abstract and poster are reproduced below.

Screen Printing Carbon Nanotubes for Field Emission Devices

Edward Boughton[1,2] Wenhui Song[1], Benjamin Jones[2], Robert Bulpett[2], Geoff Sheehy[3], Michael Waite[3]

1. *Wolfson Centre for Materials Processing, Brunel University, Uxbridge, West London, UK*
2. *Experimental Techniques Centre, Brunel University, Uxbridge, West London, UK*
3. *TMD Technologies Ltd., Hayes, Middlesex, UK*

Abstract

Electron sources have applications in x-ray scanners, displays, microwave amplifiers and electric propulsion for space missions. Currently, these technologies use thermionic electron emission, in which a cathode surface with a low work function is heated to high temperature to give electrons enough energy to overcome the potential barrier and escape the material. An accelerating voltage draws off the electron beam. By contrast, field electron emission is a process by which electrons are able to escape without additional thermal energy. Field emission ordinarily occurs only at very high electric fields. However, a sharp tip concentrates electric field lines, meaning the local field strength may be several orders of magnitude higher. Field emission can therefore occur from a sharp tip at lower applied fields. The extent to which the required field is lowered is proportional to the aspect ratio of the tip. Carbon nanotubes (CNTs) are 1-dimensional tubes composed of graphene sheets of hexagonally-arranged carbon atoms. This study aims to exploit the high aspect ratio, small size and ballistic conductivity of multiwalled carbon nanotubes (MWNTs) to fabricate a field emission electron source with low turn-on field, a large number of individual emission sites and high current density. A method of fabricating a field emission cathode by screen-printing CNT-containing inks is presented, along with results demonstrating the device’s performance.

Presenter: Edward Boughton

Acknowledgement: Our gratitude to EPSRC and TMD Technologies Limited for the financial support.

Figure A.6: Abstract submitted to UKSAF.

Screen printing carbon nanotubes for field emission devices

Edward Boughton[1,2], Wenhui Song[1], Benjamin Jones[2], Robert Bulpett[2], Sabina Orlowska[3], Geoff Sheehy[3], Michael Waite[3], Mike Miller[3]

1. Wolfson Centre for Materials Processing, Brunel University, Uxbridge, Middlesex, UK
2. Experimental Techniques Centre, Brunel University, Uxbridge, Middlesex, UK
3. TMD Technologies Ltd., Hayes, Middlesex, UK

Introduction

Currently, electron beams are produced by heating a cathode to the point where electrons have enough energy to overcome the work function of the material. In field emission, the potential barrier is lowered by the strength of the applied field only. Because this requires very high fields, current research focuses on exploiting the local increase in field strength which occurs around a sharp tip. The field enhancement factor, β, measures the degree to which this effect occurs and is related to the aspect ratio of the tip.

Because no heat is required, a field emission electron source can be smaller, lighter, more efficient and have a faster response time than a thermionic filament source, which is advantageous to x-ray machine and high-powered microwave tube applications.

Materials & Processing

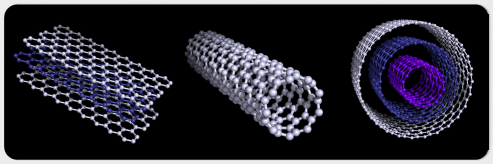

Fig 1: Graphene layers, single-walled carbon nanotube and multi-walled nanotube.

Multiwalled Carbon nanotubes (MWCNTs) are composed of graphene sheets of hexagonally-arranged carbon atoms rolled-up into nanostructured tubes (fig. 1). Their small size, high aspect ratio and ballistic conductivity mean there is the potential to fabricate a field emission device with low turn-on field, a large number of individual emission sites and high current density [1,2].

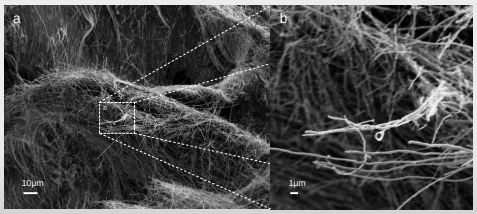

Fig 2: Multiwalled carbon nanotubes.

The MWCNTs are suspended in solvent and incorporated into a thick black ink. A screen printer is used to apply a thin patterned layer of the ink to a metallic substrate. Sintering improves the adhesion of the MWCNTs to the substrate and drives off undesired ink components.

References

1. W.A. de Heer, A. Chatelain and D. Ugarte, Science 270, 1179(1995).
2. K. Aplin, B. Kent, W. Song and C. Castelli, Acta Astronautica, 64, 875(2009)

Testing

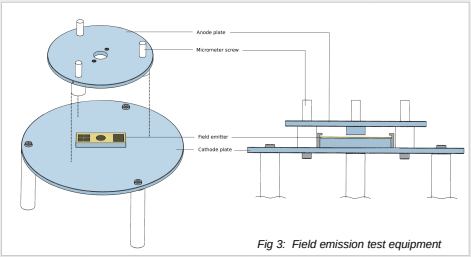

Fig 3: Field emission test equipment

Testing is performed by cyclically applying a high voltage across a gap of 250μm in vacuum of 10^{-4} Pa. A solid state switch allows the field to be pulsed and a ZnO phosphor-coated screen allows emission uniformity to be assessed. The field is increased gradually and the observed emission current recorded.

Results

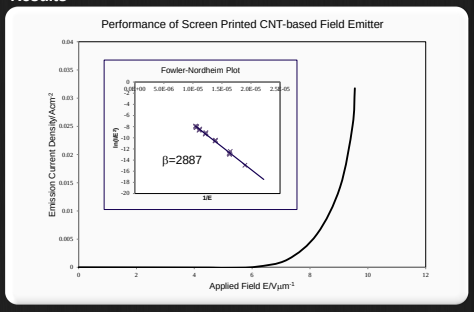

Fig 4: Plot of field emission performance of printed emitter. Inset: Fowler-Nordheim plot.

Fig. 4 shows a plot of emission current per unit area against applied electric field. The shape of the curve is typical for a field emission device. The Fowler-Nordheim plot shows a straight line, again indicating field emission, and allows the field enhancement factor, β, to be calculated.

Fig 5: Phosphor-coated anode showing uniform emission at 6V/μm⁻¹.

Summary

A field emission device has been fabricated with field enhancement factor of 2887 and a maximum emission current density in excess of 30mAcm^{-2}. Further work will focus on increasing the maximum current.

Acknowledgement: Thanks to EPSRC and TMD Technologies Ltd. for financial support. Contact: wenhui.song@brunel.ac.uk, edward.boughton@brunel.ac.uk

Figure A.7: Poster presented at UKSAF winter meeting.

A.5 National Vacuum Electronics Conference 2013 (NVEC13), June 2013

On 25th June 2013 an oral presentation entitled “A screen-printed carbon nanotube-based field emission device” was given by the author at the National Vacuum Electronics Conference at Queen Mary University, London. The submitted abstract is reproduced below.

A screen-printed carbon nanotube-based field emission device

Edward Boughton[1,2,3], Wenhui Song[1], Benjamin Jones[2], Robert Bulpett[2], Hugh Levinson[3], Geoff Sheehy[3], Michael Waite[3]

1. *Wolfson Centre for Materials Processing, Brunel University, Uxbridge, West London, UK*
2. *Experimental Techniques Centre, Brunel University, Uxbridge, West London, UK*
3. *TMD Technologies Ltd., Hayes, Middlesex, UK*

Currently, most vacuum electronics technologies use thermionic electron sources, in which a low work function material is heated to high temperature. By contrast, field electron emission is a process by which electrons are able to escape without additional thermal energy. Field emission ordinarily occurs only at very high electric fields. However, around a sharp tip the local electric field may be several orders of magnitude higher than macroscopically. This effect allows field emission to occur from a sharp tip at significantly lower applied fields. The extent to which the required field is lowered is related to the aspect ratio of the tip. Carbon nanotubes (CNTs) are 1-dimensional tubes composed of graphene sheets of hexagonally-arranged carbon atoms. A screen-printing technique has been developed which exploits the high aspect ratio, small size and ballistic conductivity of multiwalled carbon nanotubes (MWNTs) to fabricate a field emission electron source with low turn-on field, a large number of individual emission sites and high current density. The device has the advantage over thermionic cathodes of requiring fewer connections, has no warm-up time and can be fabricated on a number of substrate materials.

Figure A.8: Abstract submitted to NVEC.

A.6 International Vacuum Electronics Conference 2016 (IVEC), April 2016

On 19th April 2016 a paper entitled ”A Large-Area, Screen-Printed Nanostructured Carbon-Based Field Emission Cathode” was presented by the author at the International Vacuum Electronics Conference held by IEEE in Monterey, CA [167]. The paper is reproduced below.

A Large-Area, Screen-Printed Nanostructured Carbon-Based Field Emission Cathode

Edward Boughton
TMD Technologies Ltd., Hayes, Middlesex, UK, UB3 1DQ
The Wolfson Centre for Materials Processing/Experimental Techniques Centre, Brunel University, London, UK UB8 3PH

Abstract: *A method of screen printing carbon nanotubes (CNTs) in a dielectric binder to produce low-cost, large area field emission electron sources is presented. Imaging under the scanning electron microscope (SEM) shows the nanotubes forming dense clusters on the substrate surface with protruding CNTs in random orientations. The printed device gives an emission current of 45 mAcm^{-2} at an applied field of 6.5 Vμm^{-1} and can be fabricated using several substrate materials.*

Keywords: field emission; carbon nanotube; CNT; screen printing; nanostructured.

Introduction

Field emission sources have been investigated as alternatives for thermionic electron sources in x-ray machines and high-powered microwave devices. Potential advantages include rapid switching, no warm-up time and greater efficiency in a smaller, lighter package with fewer electrical connections. A variety of field emission technologies based on nanostructured carbon materials have been developed since the first observation of field emission from carbon nanotubes, some of which are finding application in commercial devices [1]. Principle challenges in fabricating field emission devices from nanostructured carbon stem from the requirement to align emitting tips to optimize geometric field enhancement factor, while maintaining sufficient spacing to prevent the screening effect [2][3]. Methods giving the greatest control over these parameters and therefore the highest emission current density suffer from a lack of scalability or rely on intensive processing techniques.

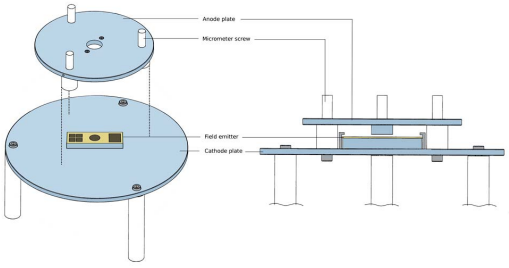

Figure 1: Field emission test configuration.

Presented here are the results of investigations to fabricate large-area, low-cost field emission electron sources capable of useful emission current densities.

Experimental

Commercially available carbon nanotubes were suspended in solvent by sonication with the aid of a dispersant. A dielectric binder and polymer gel were added and the resulting ink was screen printed on both solid metal and gold-coated glass substrates. Heat treatment was performed at 450 °C in hydrogen atmosphere. The printed field emission devices were circular with an area of 1 cm^2.

Emission testing was performed in a diode configuration using parallel plates with an adjustable gap (figure 1). A phosphor-coated transparent anode was used to assess emitter uniformity and a solid copper anode for high current testing. A MOSFET-based power supply circuit was used to apply 0-8 kV square pulses at pulse widths from 70 μs to 2 ms. Results shown use an anode-cathode gap of 400 um and pulse width of 85 μs. Scanning electron microscopy (SEM) was performed using a Zeiss Supra 35 VP.

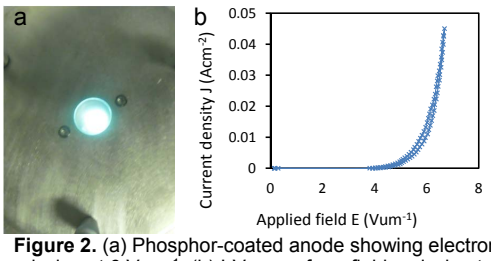

Figure 2. (a) Phosphor-coated anode showing electron emission at 6 Vμm^{-1}. (b) I-V curve from field emission test of printed emitter.

Results and discussion

Figure 2 shows a photograph of a phosphor-coated anode while the printed field emission electron source is under test. Although lower applied fields showed emission from several distinct sites on the device, emission was close to uniform at 6 Vμm^{-1}. Also shown is a typical I-V curve from field emission testing of the printed emitters. It can be seen that an emission current density of 45 mAcm^{-2} was drawn at an applied field of 6.5 Vμm^{-1}.

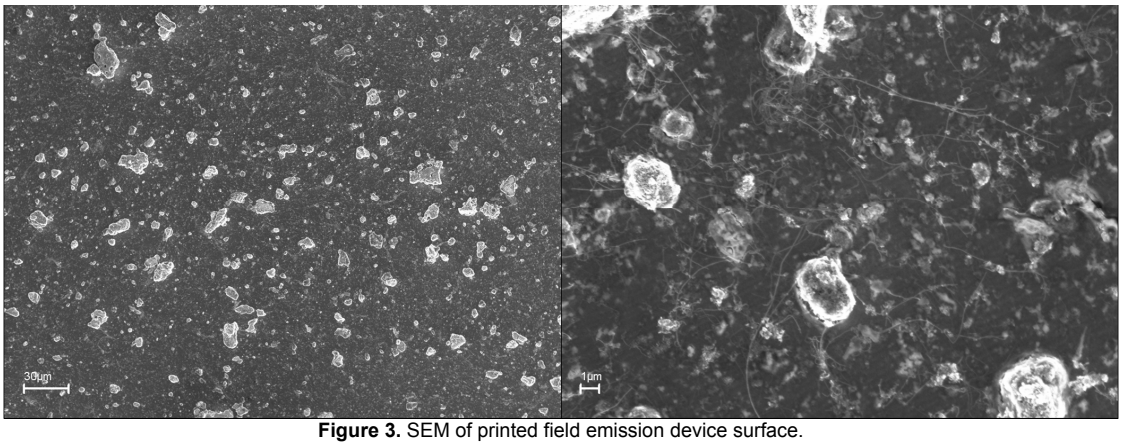

Figure 3. SEM of printed field emission device surface.

SEM examination (figure 3) shows the CNTs are arranged on the substrate surface in clusters with maximum dimension of 25 µm in the substrate plane. Protruding CNTs have no common axis of alignment.

Conclusions

A method of fabricating field emission electron sources by screen printing carbon nanotubes has been developed. Examination by SEM showed the nanotubes were arranged in clusters on the substrate surface with no vertical alignment exhibited. The printed devices are capable of high current density.

Acknowledgements

The work presented was performed as part of an EPSRC-funded project.

References

1. Filip, V., L. D. Filip, and F. Okuyama, Journal of Instrumentation, 2013, 8.
2. De Jonge, N., and J. M. Bonard, Philosophical Transactions of the Royal Society A-Mathematical Physics and Engineering Sciences, 2004, 362(1823): 2239-2266.
3. Bocharov, G. S., A. V. Eletskii, and T.J. Sommerer, Technical Physics, 2011, 56(4): 540-545.

Figure A.9: Paper presented at IVEC [167]. *© 2016 IEEE. Reprinted, with permission, from E. Boughton, A large-area, screen-printed nanostructured carbon-based field emission cathode, 2016 IEEE International Vacuum Electronics Conference (IVEC), April 2016*.

Appendix B

Ink formulations

Table B.1: Formulations of inks with component quantities expressed as mass fraction.

Ink	G1	H008	MW3007	X-3
Material	TIMCAL KS6	Rosseter H008	Brunel MW3007	Xintek XNA-SP
Section	5	5	5	5, 6.4.1
Emitter	0.0205	0.0017	0.0023	0.0046
PVP	-	-	-	0.0009
Binder	0.0702	0.0659	0.0300	0.0829
Polymer gel	0.6062	0.5689	0.5337	0.6077
Butoxyethanol	0.2526	0.2370	0.2224	0.2532
Octanol	0.0505	0.0474	0.0445	0.0506
IPA	-	0.0790	0.1913	-

Table B.2: Formulations of Xintek XNA-SP-36150 CNT-based inks used in section 6.3 with component quantities expressed as mass fraction.

	Mk-1	Mk-2	Mk-3	Mk-4	Mk-5	Mk-6
Emitter	0.0018	0.0038	0.0056	0.0075	0.0092	0.0112
PVP	0.0003	0.0007	0.0011	0.0015	0.0018	0.0022
Binder	0.1392	0.1150	0.0923	0.0698	0.0473	0.0229
Polymer gel	0.5706	0.5872	0.6004	0.6140	0.6287	0.6425
Butoxyethanol	0.2401	0.2443	0.2503	0.2559	0.2607	0.2678
Octanol	0.0479	0.0490	0.0503	0.0513	0.0523	0.0534

Appendix C

Test rig

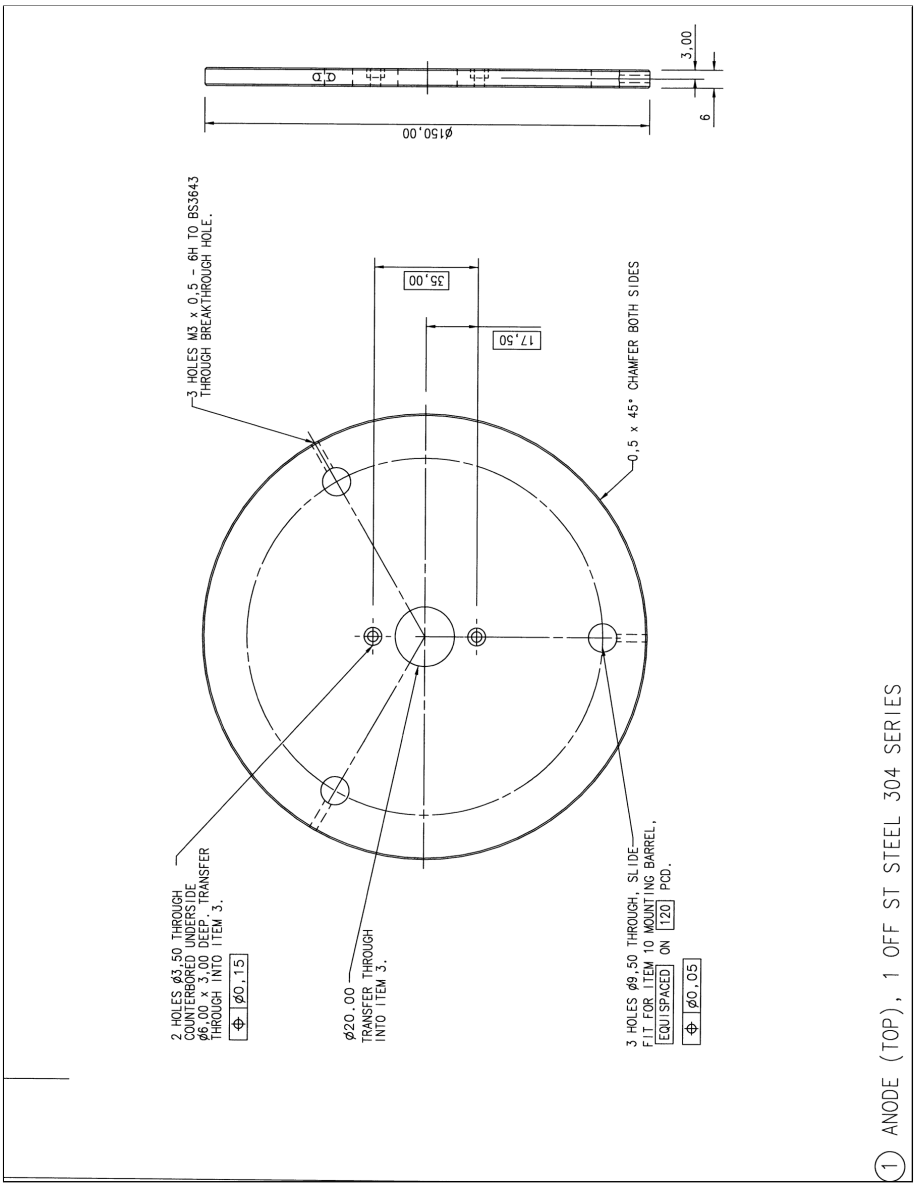

Figure C.1: Field emission test rig item 1: anode plate.

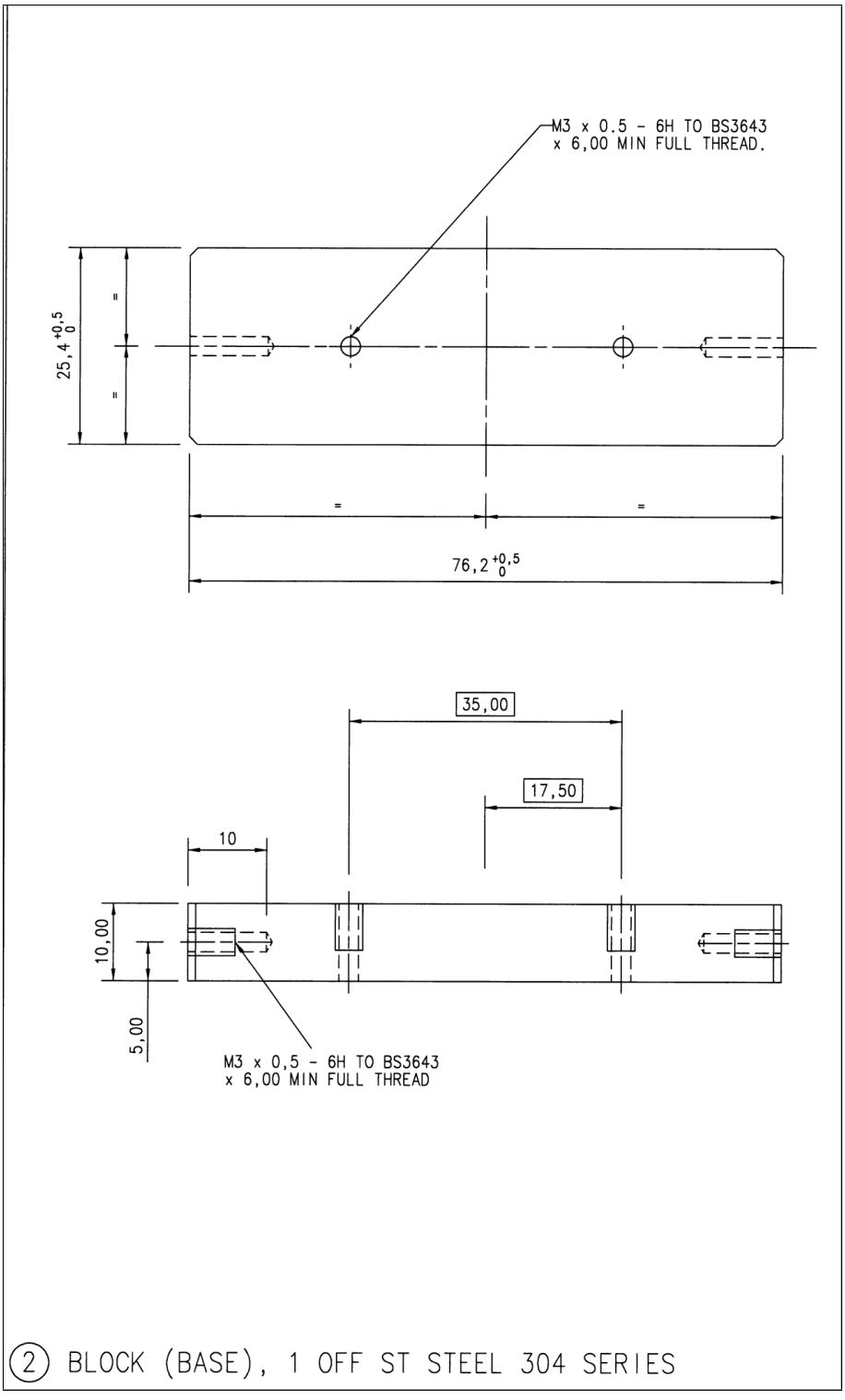

Figure C.2: Field emission test rig item 2: field emission device holding block.

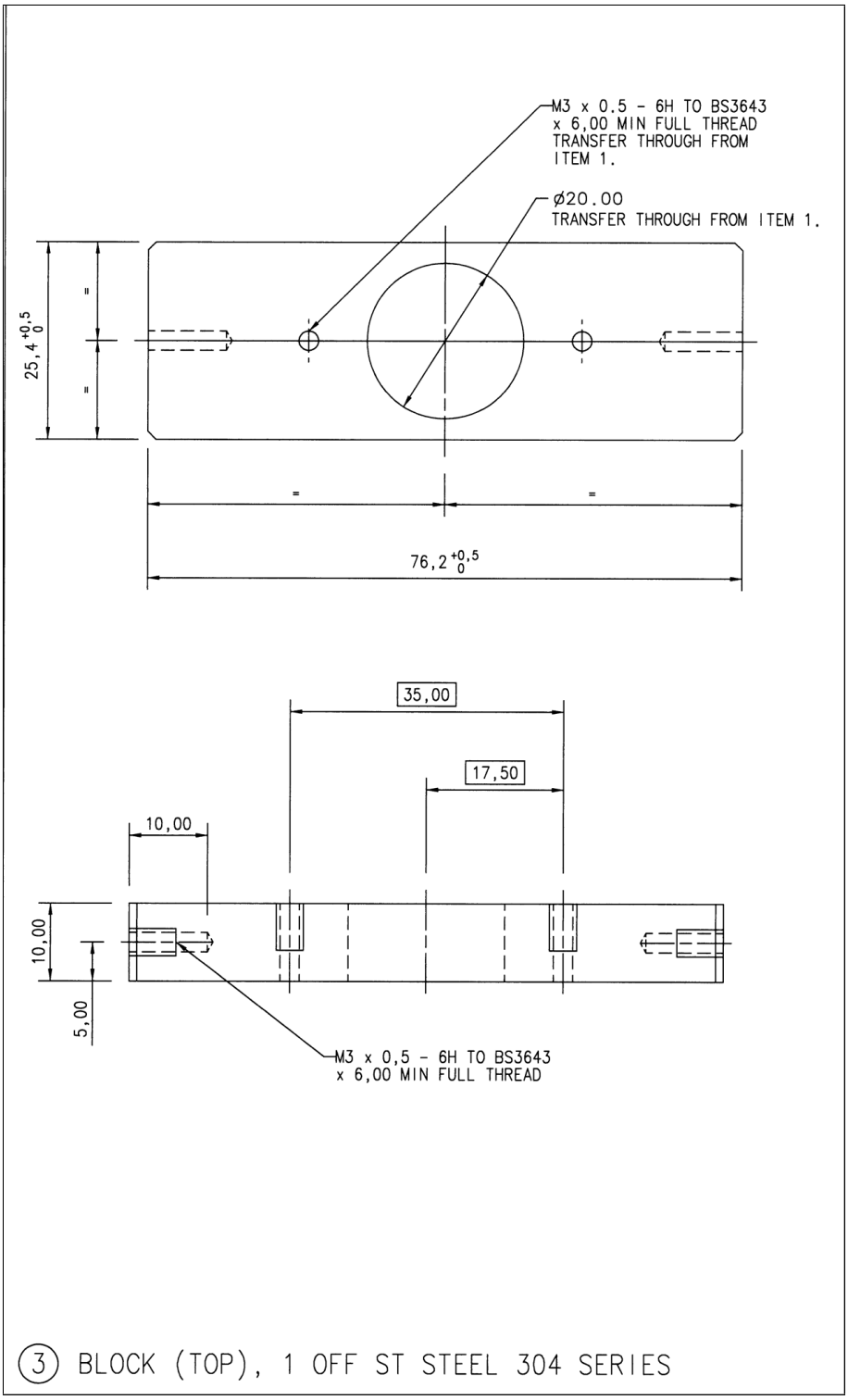

Figure C.3: Field emission test rig item 3: anode plate holding block.

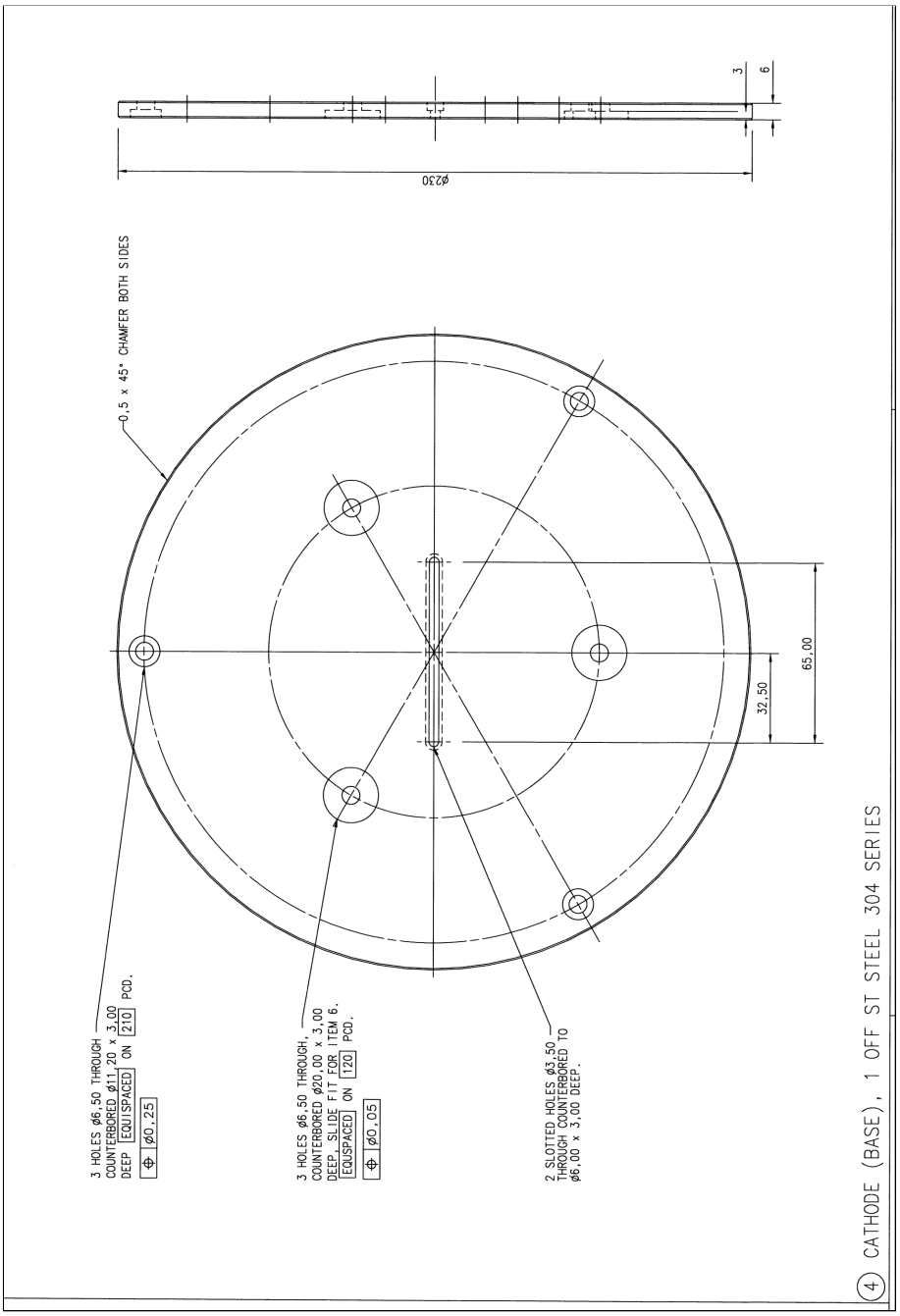

Figure C.4: Field emission test rig item 4: cathode plate.

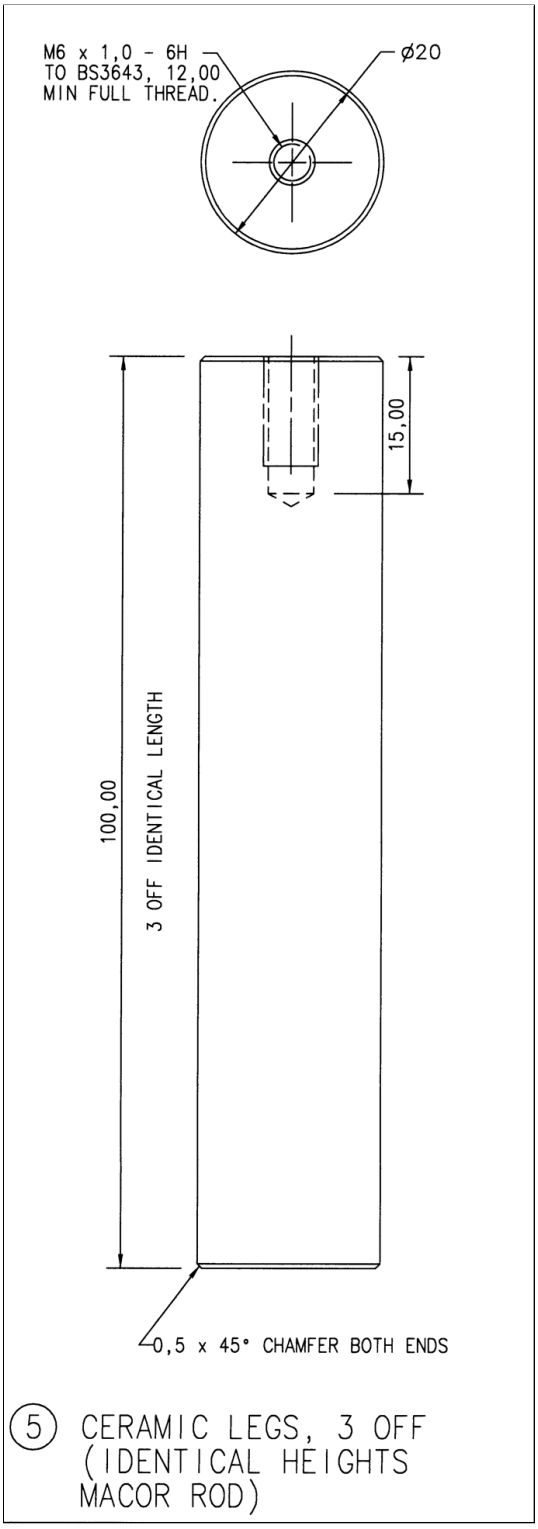

Figure C.5: Field emission test rig item 5: cathode plate leg.

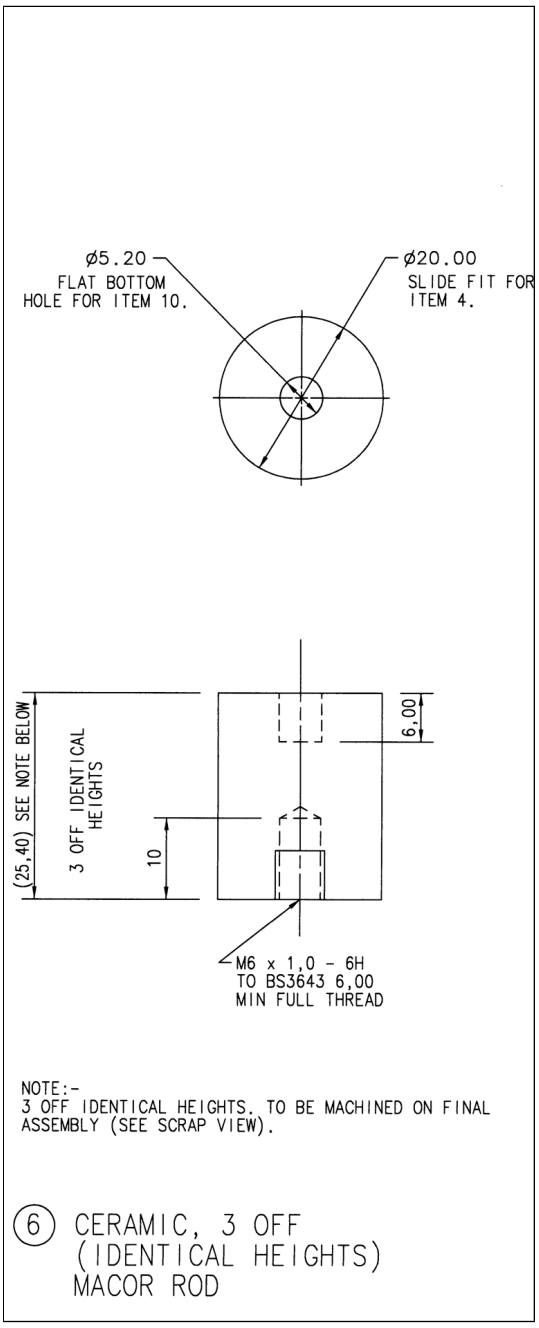

Figure C.6: Field emission test rig item 6: anode plate leg.

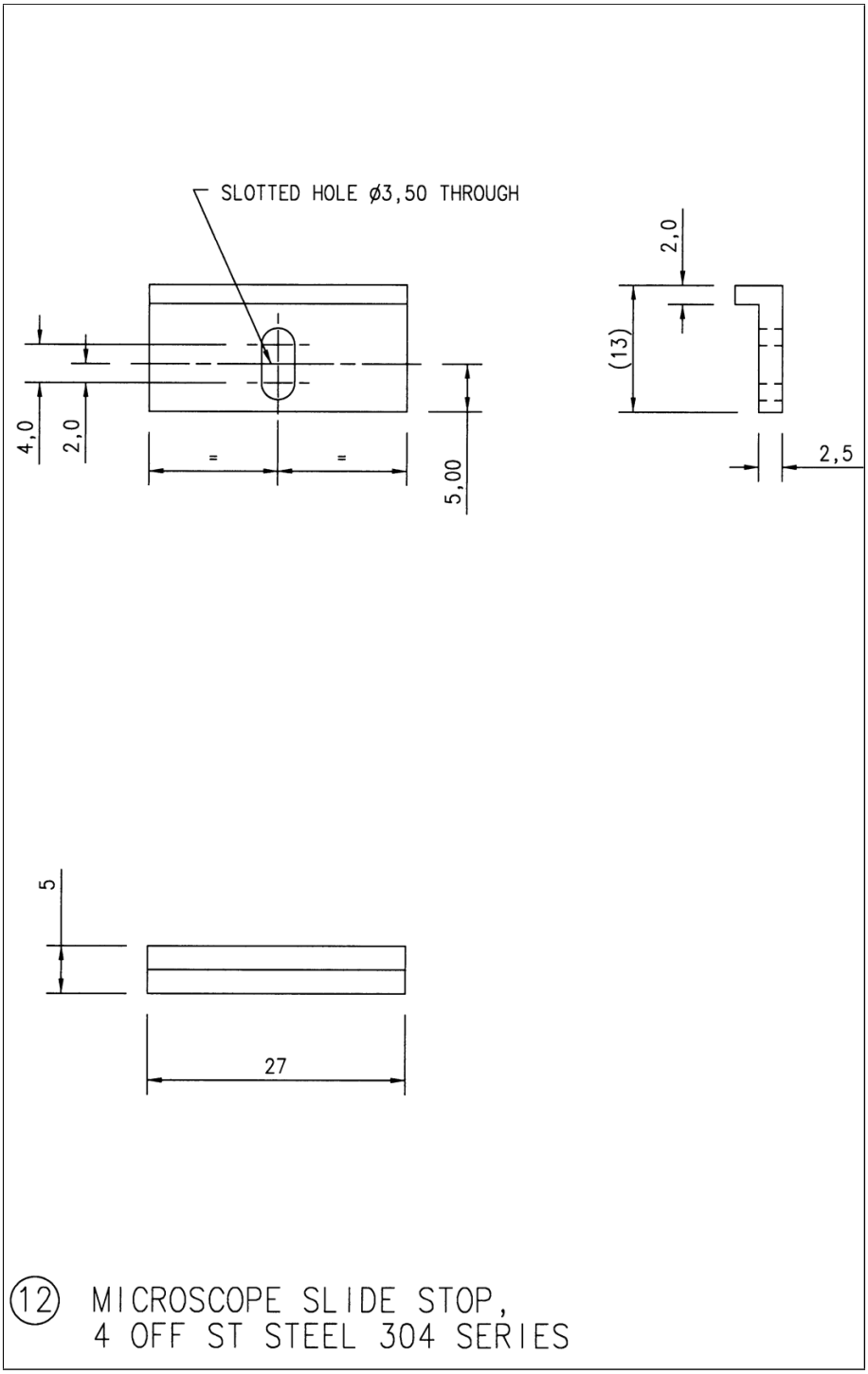

Figure C.7: Field emission test rig item 12: FE device/anode retaining clip.

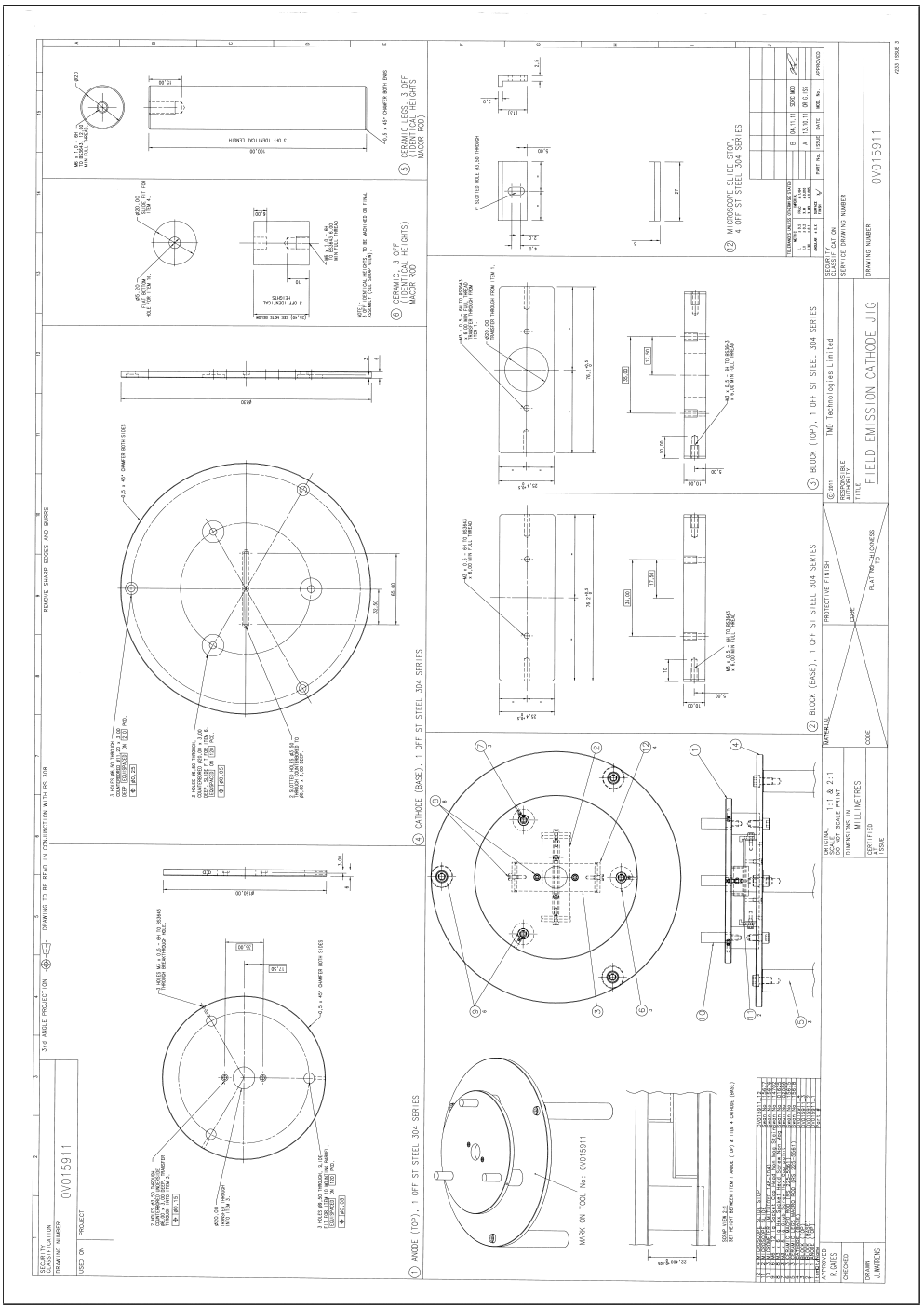

Figure C.8: Technical drawing of second-generation test rig design. *Drawing by Jonathan Warrens, TMD Technologies Ltd*.

Appendix D

Example FE test results

D.1 Concentration study

Examples of collected test data for field emission devices printed with each of the six inks used in section 6.3 are included here. Maximum applied voltage was 4 kV.

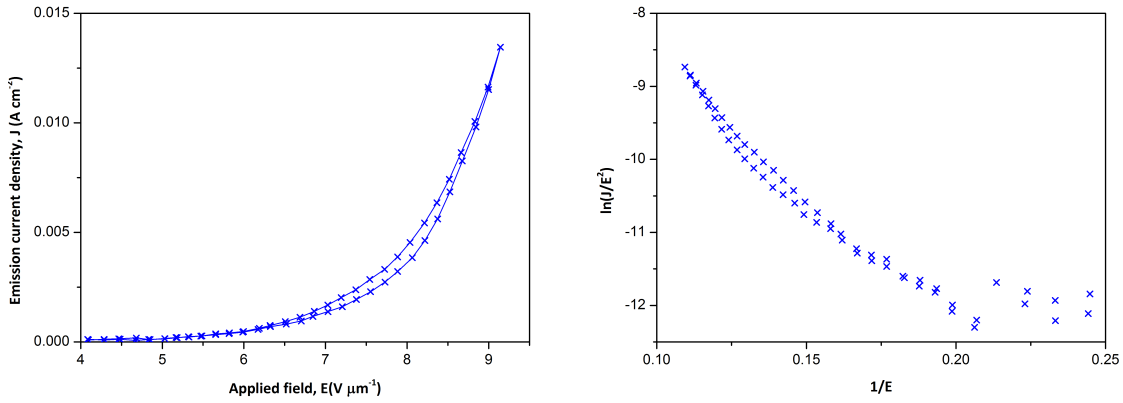

Figure D.1: Emission test results from emission device printed using Mk-1 ink.

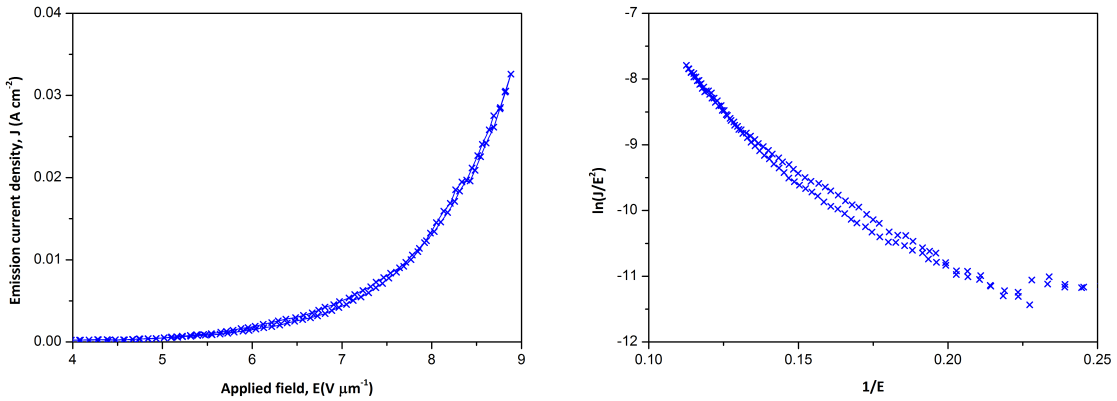

Figure D.2: Emission test results from emission device printed using Mk-2 ink.

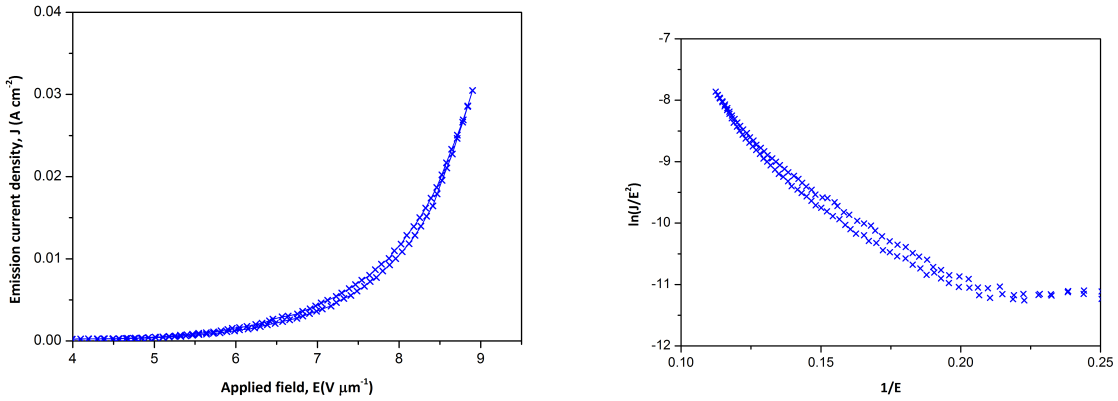

Figure D.3: Emission test results from emission device printed using Mk-3 ink.

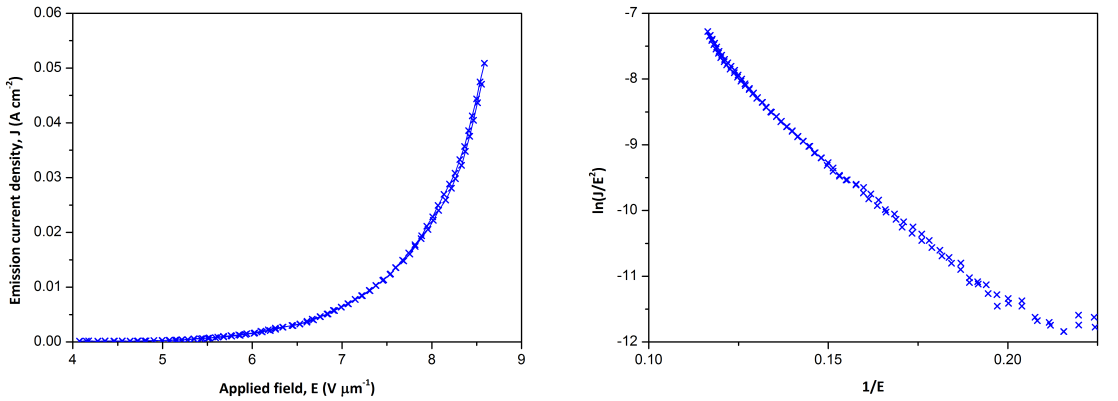

Figure D.4: Emission test results from emission device printed using Mk-4 ink.

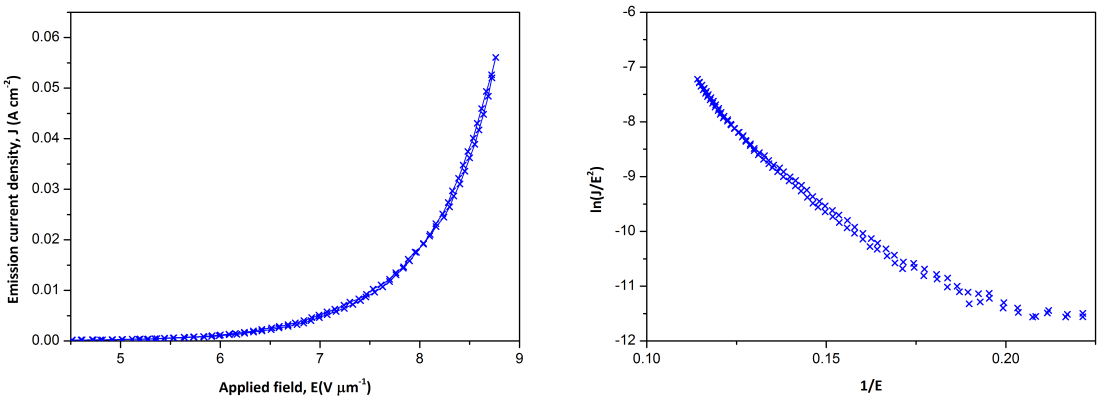

Figure D.5: Emission test results from emission device printed using Mk-5 ink.

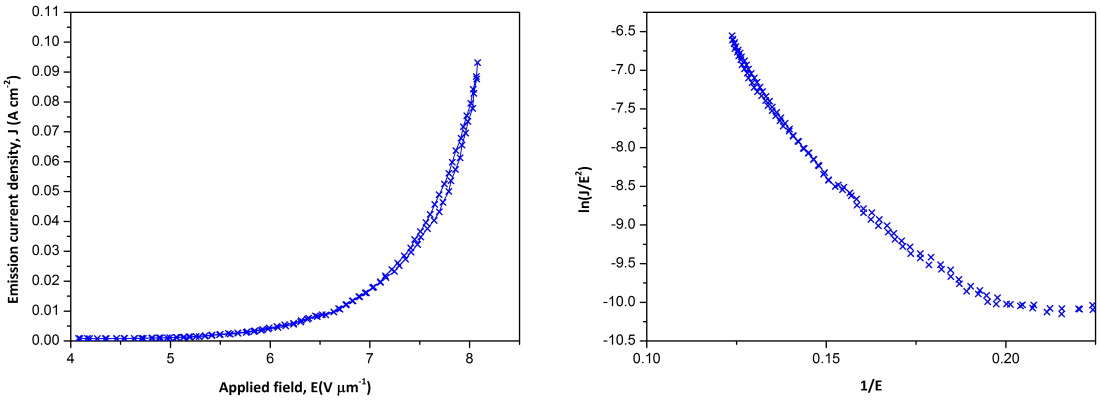

Figure D.6: Emission test results from emission device printed using Mk-6 ink.

D.2 Geometry test

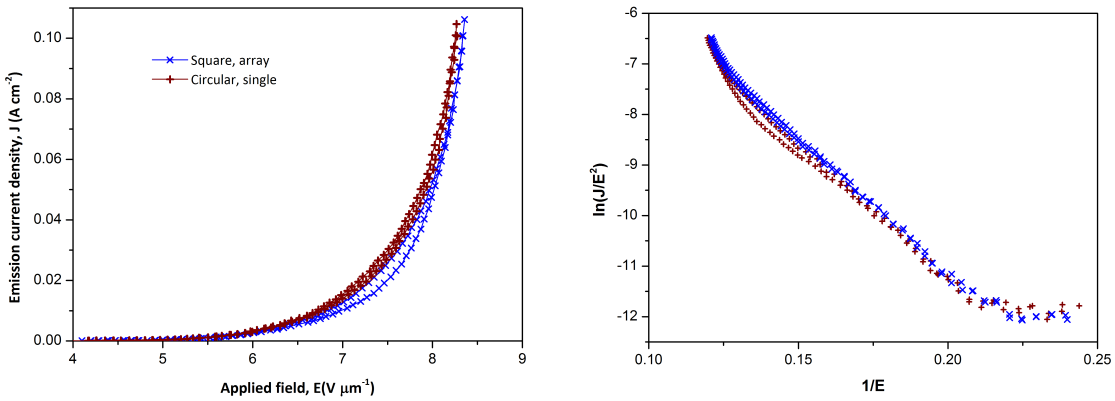

Figure D.7: Emission test results from emission devices printed with different geometries.

Appendix E

TGA results

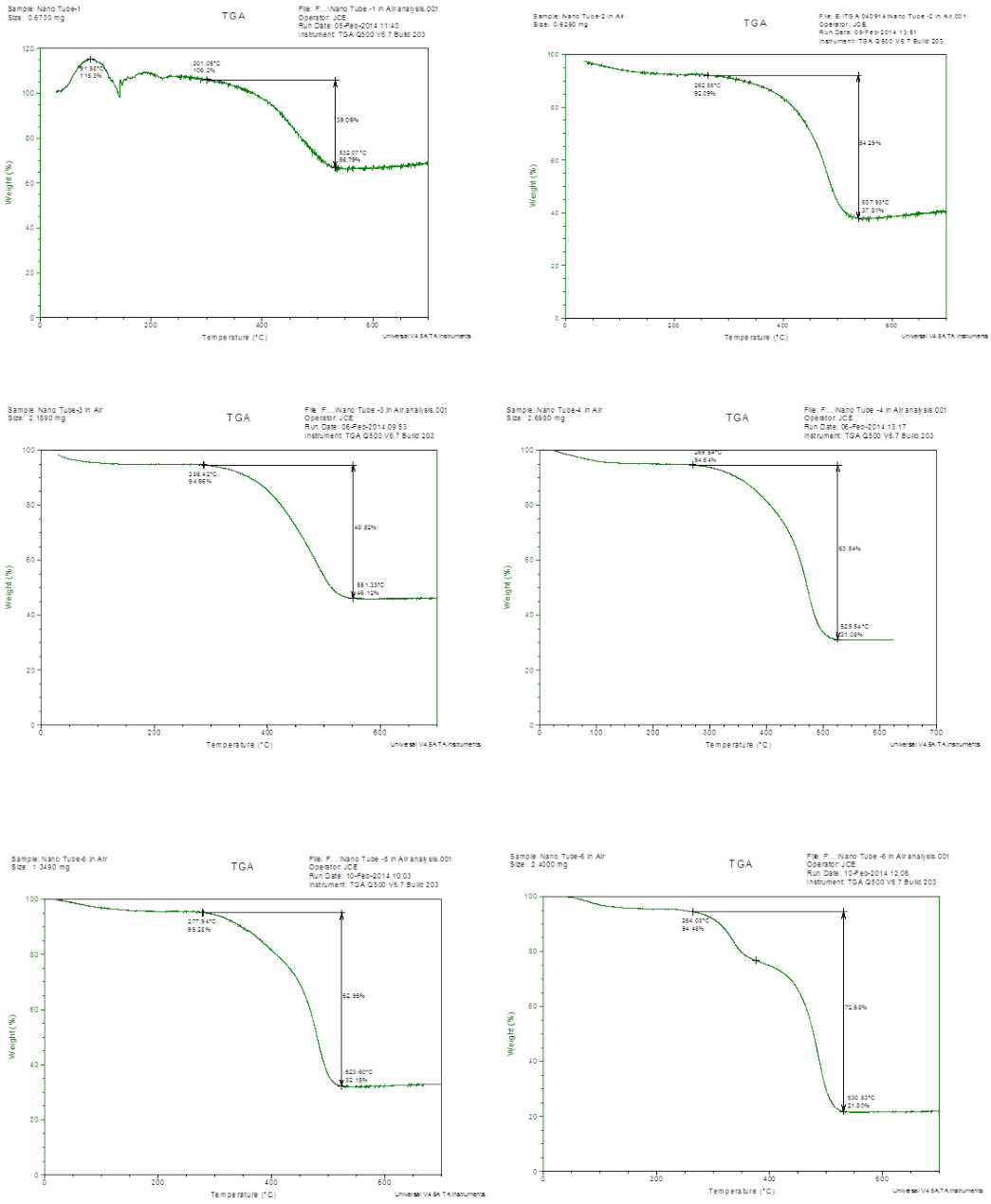

Figure E.1: Plot of TGA data from inks Mk1-6.

References

[1] Richardson, O.W., *On the negative radiation from hot platinum ...* Univ. Press, Cambridge, 1901.

[2] Kaye, G. and Laby, T., *Tables of Physical and Chemical Constants (16th edition 1995). 4.3 Work Function*. Longman, 1995.

[3] Pelletier, J. and Pomot, C., Work function of sintered lanthanum hexaboride. *Applied Physics Letters* **34**(4).

[4] Fowler, R. and Nordheim, L., Electron emission in intense electric fields. *Proceedings of the Royal Society, London A* **119**(781) (1928) 173.

[5] Utsumi, T., Vacuum microelectronics: what's new and exciting. *IEEE Transactions on Electron Devices* **38**(10) (1991) 2276.

[6] Eletskii, A.V. and Bocharov, G.S., Emission properties of carbon nanotubes and cathodes on their basis. *Plasma Sources Science & Technology* **18**(3) (2009) 034013.

[7] Kim, H.J. *et al.*, Growth of carbon nanotube field emitters on single strand carbon fiber: a linear electron source. *Nanotechnology* **22**(9) (2011) 095602.

[8] Yonathan, P., Kim, H.T. and Yoon, D.H., Field emission from multi-walled carbon nanotubes with various fillers. *Materials Letters* **62**(17-18) (2008) 2795.

[9] Bocharov, G.S., Eletskii, A.V. and Sommerer, T.J., Optimization of the parameters of a carbon nanotube-based field-emission cathode. *Technical Physics* **56**(4) (2011) 540.

[10] Silan, J.L. *et al.*, Investigation of carbon nanotube field emitter geometry for increased current density. *Solid-State Electronics* **54**(12) (2010) 1543.

[11] Dionne, M., Coulombe, S. and Meunier, J.L., Screening effects between field-enhancing patterned carbon nanotubes: A numerical study. *IEEE Transactions on Electron Devices* **55**(6) (2008) 1298.

[12] Smith, R.C. and Silva, S.R.P., Interpretation of the field enhancement factor for electron emission from carbon nanotubes. *Journal of Applied Physics* **106**(1) (2009) 014314.

[13] Smith, R.C. and Silva, S.R.P., Maximizing the electron field emission performance of carbon nanotube arrays. *Applied Physics Letters* **94**(13) (2009) 133104.

[14] Liu, H., Kato, S. and Saito, Y., Effect of cathode-anode distance on field emission properties for carbon nanotube film emitters. *Japanese Journal of Applied Physics* **48**(1) (2009) 015007.

[15] Asaka, K., Nakahara, H. and Saito, Y., Nanowelding of a multiwalled carbon nanotube to metal surface and its electron field emission properties. *Applied Physics Letters* **92**(2) (2008) 023114.

[16] Spindt, C.A. *et al.*, Physical properties of thin-film field emission cathodes with molybdenum cones. *Journal of Applied Physics* **47**(12) (1976) 5248.

[17] de Heer, W.A., Chatelain, A. and Ugarte, D., A carbon nanotube field-emission electron source. *Science* **270**(5239) (1995) 1179.

[18] Xu, N. and Huq, S., Novel cold cathode materials and applications. *Materials Science & Engineering R-Reports* **48**(2-5) (2005) 47.

[19] de Jonge, N. and Bonard, J., Carbon nanotube electron sources and applications. *Philosophical Transactions of the Royal Society A-Mathematical Physical and Engineering Sciences* **362**(1823) (2004) 2239.

[20] Chen, P.Y. *et al.*, Space charge effects in field emission nanodevices. *Nanotechnology* **20**(40) (2009) 405202.

[21] Hata, K., Takakura, A. and Saito, Y., Field emission from multiwall carbon nanotubes in controlled ambient gases, H-2, CO, N-2 and O-2. *Ultramicroscopy* **95**(1-4) (2003) 107.

[22] Dean, K. and Chalamala, B., Current saturation mechanisms in carbon nanotube field emitters. *Applied Physics Letters* **76**(3) (2000) 375.

[23] Milne, W. *et al.*, Carbon nanotubes as field emission sources. *Journal of Materials Chemistry* **14**(6) (2004) 933.

[24] Mann, M., Milne, W.I. and Teo, K.B.K., *Preparation of Patterned CNT Emitters*. Carbon Nanotube and Related Field Emitters, Wiley-VCH Verlag GmbH & Co. KGaA, 2010. 23–40.

[25] Milne, W.I. *et al.*, Aligned carbon nanotubes/fibers for applications in vacuum microwave amplifiers. *Journal of Vacuum Science & Technology B* **24**(1) (2006) 345.

[26] Legagneux, P. *et al.*, Carbon nanotube based cathodes for microwave amplifiers. In *2009 IEEE International Vacuum Electronics Conference*, 80–81.

[27] Li, C. *et al.*, High emission current density, vertically aligned carbon nanotube mesh, field emitter array. *Applied Physics Letters* **97**(11) (2010) 113107.

[28] Krivchenko, V.A. *et al.*, Nanocrystalline graphite: Promising material for high current field emission cathodes. *Journal of Applied Physics* **107**(1) (2010) 014315.

[29] Krivchenko, V.A. *et al.*, Studying the morphology of nanocrystalline graphite field-emission cathode grown on a diamond grid. *Technical Physics Letters* **36**(1) (2010) 23.

[30] Zhang, Y. *et al.*, Optimize the field emission character of a vertical few-layer graphene sheet by manipulating the morphology. *Nanotechnology* **23**(1) (2012) 015202.

[31] Green, M.J., Analysis and measurement of carbon nanotube dispersions: nanodispersion versus macrodispersion. *Polymer International* **59**(10) (2010) 1319.

[32] Kim, Y. *et al.*, Activation-free printed carbon nanotube field emitters. *Nanotechnology* **22**(43).

[33] Lee, J.H. *et al.*, Optimization of field emission properties from multi-walled carbon nanotubes using ceramic fillers. *Applied Physics A-Materials Science & Processing* **93**(2) (2008) 511.

[34] Lee, H.J. *et al.*, Enhanced surface morphologies of screen-printed carbon nanotube films by heat treatment and their field-emission properties. *Carbon* **44**(13) (2006) 2625.

[35] Song, J.W. *et al.*, The production of transparent carbon nanotube field emitters using inkjet printing. *Physica E-Low-Dimensional Systems & Nanostructures* **41**(8) (2009) 1513.

[36] Tuck, R. *et al.*, The pFED - a viable route to large field emission displays. In *Vacuum Nanoelectronics Conference, 2005. IVNC 2005. Technical Digest of the 18th International*, 80–81.

[37] Taylor, W. *et al.*, Printed FEDs-technical advances and manufacturing cost modelling. In *Vacuum Microelectronics Conference, 2001. IVMC 2001. Proceedings of the 14th International*, 177–180.

[38] Waite, M.S. *et al.*, Alternative field electron emission characteristics from graphite-insulator composite layers. In *Vacuum Nanoelectronics Conference, 2005. IVNC 2005. Technical Digest of the 18th International*, 332–333.

[39] Burden, A. *et al.*, Incorporating consumer-priced field-emitting inks into arrays of triode devices. *Solid-State Electronics* **45**(6) (2001) 987.

[40] Boccaccini, A.R. *et al.*, Electrophoretic deposition of carbon nanotubes. *Carbon* **44**(15) (2006) 3149.

[41] Boccaccini, A.R. *et al.*, Electrophoretic deposition of carbon nanotube-ceramic nanocomposites. *Journal of the European Ceramic Society* **30**(5) (2010) 1115.

[42] Chavez-Valdez, A., Shaffer, M.S.P. and Boccaccini, A.R., Applications of Graphene Electrophoretic Deposition. A Review. *Journal of Physical Chemistry B* **117**(6) (2013) 1502.

[43] Oh, S.J. *et al.*, Liquid-phase fabrication of patterned carbon nanotube field emission cathodes. *Applied Physics Letters* **84**(19) (2004) 3738.

[44] Calderon-Colon, X. *et al.*, A carbon nanotube field emission cathode with high current density and long-term stability. *Nanotechnology* **20**(32) (2009) 325707.

[45] Cao, G. *et al.*, A dynamic micro-CT scanner based on a carbon nanotube field emission x-ray source. *Physics in Medicine and Biology* **54**(8) (2009) 2323.

[46] Zhu, W. *et al.*, Large current density from carbon nanotube field emitters. *Applied Physics Letters* **75**(6) (1999) 873.

[47] Shiffler, D. *et al.*, A high-current, large-area, carbon nanotube cathode. *IEEE Transactions on Plasma Science* **32**(5) (2004) 2152.

[48] Qian, M. *et al.*, A comparative study of field emission properties of carbon nanotube films prepared by vacuum filtration and screen-printing. *Applied Surface Science* **256**(14) (2010) 4642.

[49] Baby, T.T. and Ramaprabhu, S., Cold field emission from hydrogen exfoliated graphene composites. *Applied Physics Letters* **98**(18) (2011) 183111.

[50] Chen, G. *et al.*, Field emission characteristics of point emitters fabricated by a multi-walled carbon nanotube yarn. *Nanotechnology* **20**(31) (2009) 315201.

[51] Houdellier, F. *et al.*, New carbon cone nanotip for use in a highly coherent cold field emission electron microscope. *Carbon* **50**(5) (2012) 2037.

[52] Zhang, J. *et al.*, Efficient fabrication of carbon nanotube point electron sources by dielectrophoresis. *Advanced Materials* **16**(14) (2004) 1219.

[53] Kim, W.J. *et al.*, Better than 10 mA Field Emission from an Isolated Structure Emitter of a Metal Oxide/CNT Composite. *Acs Nano* **5**(1) (2011) 429.

[54] Pan, L. *et al.*, Field emission properties of titanium carbide coated carbon nanotube arrays. *Advanced Engineering Materials* **9**(7) (2007) 584.

[55] Sharma, H. *et al.*, Enhanced electron emission from titanium coated multiwalled carbon nanotubes. *Thin Solid Films* **518**(23) (2010) 6915.

[56] Uh, H.S., Park, S. and Kim, B., Enhanced field emission properties from titanium-coated carbon nanotubes. *Diamond and Related Materials* **19**(5-6) (2010) 586.

[57] Nakayama, Y., *Surface Coating of CNT Emitters.* Carbon Nanotube and Related Field Emitters, Wiley-VCH Verlag GmbH & Co. KGaA, 2010. 163–175.

[58] Kumar, K.S. *et al.*, Improved field emission from Cs coated carbon nanotubes. In *Vacuum Electronics Conference (IVEC), 2011 IEEE International*, 99–100. ID: 1.

[59] Suzuki, S. *et al.*, Work functions and valence band states of pristine and Cs-intercalated single-walled carbon nanotube bundles. *Applied Physics Letters* **76**(26) (2000) 4007.

[60] Wadhawan, A., Stallcup, R. and Perez, J., Effects of Cs deposition on the field-emission properties of single-walled carbon-nanotube bundles. *Applied Physics Letters* **78**(1) (2001) 108.

[61] Yu, J. and Chua, D.H.C., Effective electron emitters by molybdenum oxide-coated carbon nanotubes core-shell nanostructures. *Journal of Materials Science* **46**(14) (2011) 4858.

[62] Lee, S.Y. *et al.*, The roles of ruthenium nanoparticles decorated on thin multi-walled carbon nanotubes in the enhancement of field emission properties. *Applied Physics Letters* **100**(2) (2012) 023102.

[63] Yu, K. *et al.*, Significant improvement of field emission by depositing zinc oxide nanostructures on screen-printed carbon nanotube films. *Applied Physics Letters* **88**(15) (2006) 153123.

[64] Rakhi, R.B., Sethupathi, K. and Ramaprabhu, S., Electron field emitters based on multi-walled carbon nanotubes coated with conducting polymer/metal/metal-oxide composites. *Journal of Experimental Nanoscience* **4**(1) (2009) 67.

[65] Vink, T.J. *et al.*, Enhanced field emission from printed carbon nanotubes by mechanical surface modification. *Applied Physics Letters* **83**(17) (2003) 3552.

[66] Zeng, F.G. *et al.*, A novel mechanical approach to improve the field emission characteristics of printed CNT films. *Materials Letters* **60**(19) (2006) 2399.

[67] Wang, Q.H. *et al.*, Field emission from nanotube bundle emitters at low fields. *Applied Physics Letters* **70**(24) (1997) 3308.

[68] Feng, T. *et al.*, Surface modification of printed carbon nanotubes and its application of field emission. *Surface Review and Letters* **12**(5-6) (2005) 733.

[69] Wang, W.P. *et al.*, Field emission characteristics of carbon nanotubes post-treated with high-density Ar plasma. *Applied Surface Science* **256**(7) (2010) 2184.

[70] Liu, J.L. *et al.*, Improved field emission property of graphene paper by plasma treatment. *Applied Physics Letters* **97**(3).

[71] Kim, D.H., Kim, C.D. and Lee, H.R., Effects of the ion irradiation of screen-printed carbon nanotubes for use in field emission display applications. *Carbon* **42**(8-9) (2004) 1807.

[72] Kyung, S.J. *et al.*, Improvement of electron field emission from carbon nanotubes by Ar neutral beam treatment. *Carbon* **46**(10) (2008) 1316.

[73] Kyung, S.J. *et al.*, The effect of atmospheric pressure plasma treatment on the field emission characteristics of screen printed carbon nanotubes. *Carbon* **45**(3) (2007) 649.

[74] Yu, J. *et al.*, Field emission characteristics of screen-printed carbon nanotubes cold cathode by hydrogen plasma treatment. *Applied Surface Science* **258**(2) (2011) 738.

[75] Lee, H.J. *et al.*, Improvement of field emission from printed carbon nanotubes by a critical bias field. *Journal of Applied Physics* **98**(1) (2005) 016107.

[76] Ren, H. *et al.*, Effect of surface treatment on printed carbon nanotube field emitters. *Surface and Interface Analysis* **36**(5-6) (2004) 485.

[77] Shang, X.F. *et al.*, The enhanced field-emission properties of screen-printed single-wall carbon-nanotube film by electrostatic field. *Applied Surface Science* **256**(7) (2010) 2005.

[78] Read, M. *et al.*, Carbon nanotube-based cathodes for microwave tubes. In *Pulsed Power Plasma Science, 2001. IEEE Conference Record - Abstracts*, 161. ID: 1.

[79] Lahiri, I. *et al.*, Enhanced field emission from multi-walled carbon nanotubes grown on pure copper substrate. *Carbon* **48**(5) (2010) 1531.

[80] Wu, C., Xing, W. and Li, Y., Field emission characteristics of FED with carbon nanotube field emitters using improved cathode electrode. *Manufacturing Processes and Systems, Pts 1-2* **148-149** (2011) 1315.

[81] Peng, Y., Hu, Y. and Wang, H., Fabrication of carbon nanotube field emission film by electrophoresis deposition and sintering. *Colloids and Surfaces A-Physicochemical and Engineering Aspects* **329**(3) (2008) 161.

[82] Moon, J.S. *et al.*, Enhanced field emission properties of thin-multiwalled carbon nanotubes: Role of SiOx coating. *Journal of Applied Physics* **100**(10) (2006) 104303.

[83] Jeong, H.J. *et al.*, All-carbon nanotube-based flexible field-emission devices: from cathode to anode. *Advanced Functional Materials* **21**(8) (2011) 1526.

[84] Kurihara, K. *et al.*, Carbon loss induced by plasma beam irradiation in porous silica films. *Journal of Applied Physics* **101**(11) (2007) 113301.

[85] Kim, T.S. *et al.*, Simulations of the dielectric constant of bonding materials and field emission properties of CNT cathodes. *Metals and Materials International* **12**(4) (2006) 339.

[86] Brioude, A. *et al.*, Synthesis of sheathed carbon nanotube tips by the sol-gel technique. *Applied Surface Science* **221**(1-4) (2004) 4.

[87] Bajic, S. and Latham, R.V., Enhanced cold-cathode emission using composite resin carbon coatings. *Journal of Physics D-Applied Physics* **21**(1) (1988) 200.

[88] Di, Y. *et al.*, Field emission from carbon nanotube and tetrapod-like ZnO compound cathode fabricated by spin-coating method. *Applied Surface Science* **255**(8) (2009) 4636.

[89] Hwang, J.O. *et al.*, Vertical ZnO nanowires/graphene hybrids for transparent and flexible field emission. *Journal of Materials Chemistry* **21**(10) (2011) 3432.

[90] Devan, R.S. *et al.*, One-dimensional metal-oxide nanostructures: recent developments in synthesis, characterization, and applications. *Advanced Functional Materials* **22**(16) (2012) 3326.

[91] Cathode white paper, available at www.tmd.co.uk.

[92] Falce, L.R., Dispenser cathodes: The current state of the technology. In *1983 International Electron Devices Meeting*, volume 29, 448–451.

[93] Orlowska, S. In *2007 National Vacuum Electronics Conference (NVEC)*.

[94] Zhao, J. *et al.*, Scandate dispenser cathode fabrication for a high-aspect-ratio high-current-density sheet beam electron gun. *IEEE Transactions on Electron Devices* **59**(6) (2012) 1792.

[95] Liu, H. *et al.*, Effect of patterned and aligned carbon nanotubes on field emission properties. *Vacuum* **86**(7) (2012) 933.

[96] Oostrom, A.V., Field emission cathodes. *Journal of Applied Physics* **33**(10) (1962) 2917.

[97] Whaley, D. *et al.*, Application of field emitter arrays to microwave power amplifiers. *IEEE Transactions on Plasma Science* **28**(3) (2000) 727.

[98] Makishima, H. *et al.*, Design and performance of traveling-wave tubes using field emitter array cathodes. *Applied Surface Science* **146**(1-4) (1999) 230.

[99] Whaley, D. *et al.*, High average power field emitter cathode and testbed for X/Ku-band cold cathode TWT. In *2013 IEEE 14th International Vacuum Electronics Conference (IVEC)*, 1–2.

[100] Sanborn, G. *et al.*, A thin film triode type carbon nanotube field emission cathode. *Applied Physics A-Materials Science & Processing* **110**(1) (2013) 99.

[101] Teo, K. *et al.*, Microwave devices - Carbon nanotubes as cold cathodes. *Nature* **437**(7061) (2005) 968.

[102] Manohara, H. *et al.*, Field emission testing of carbon nanotubes for THz frequency vacuum micro-tube sources. *Reliability, Testing and Characterization of Mems/moems Iii* **5343** (2004) 227.

[103] Ulisse, G. *et al.*, Carbon nanotubes electron source. In *2013 IEEE 14th International Vacuum Electronics Conference (IVEC)*, 1–2.

[104] Lee, Y.Z. *et al.*, Carbon nanotube based X-ray sources: Applications in pre-clinical and medical imaging. *Nuclear Instruments & Methods in Physics Research Section A-Accelerators Spectrometers Detectors and Associated Equipment* **648** (2011) S281.

[105] Ruedenauer, F.G., Field emission devices for space applications. *Surface and Interface Analysis* **39**(2-3) (2007) 116.

[106] Kent, B.J. *et al.*, Space applications of micro fabricated field emitters. In *2005 International Vacuum Nanoelectronics Conference*, 82.

[107] Balsiger, H. *et al.*, Rosina – Rosetta orbiter spectrometer for ion and neutral analysis. *Space Science Reviews* **128**(1) (2007) 745.

[108] Sheridan, S. *et al.*, A carbon nano tube electron impact ionisation source for low-power, compact spacecraft mass spectrometers. *Advances in Space Research* **49**(8) (2012) 1245.

[109] Getty, S.A. *et al.*, Integration of a carbon nanotube field emission electron gun for a miniaturized time-of-flight mass spectrometer. In *Proceedings of SPIE - The International Society for Optical Engineering*, volume 7318.

[110] Zou, R. *et al.*, Improved emission uniformity and stability of printed carbon nanotubes in electrolyte. *Applied Surface Science* **255**(20) (2009) 8672.

[111] Chen, G. *et al.*, Carbon nanotubes cathode of field emission lamp prepared by electrophoretic deposition. *2012 International Conference on Future Energy, Environment, and Materials, Pt a* **16** (2012) 240.

[112] Donaldson, K. *et al.*, Asbestos, carbon nanotubes and the pleural mesothelium: a review of the hypothesis regarding the role of long fibre retention in the parietal pleura, inflammation and mesothelioma. *Particle and Fibre Toxicology* **7** (2010) 5.

[113] *Using nanomaterials at work*. Health and Safety Executive, 2013.

[114] Lee, C. *et al.*, Measurement of the elastic properties and intrinsic strength of monolayer graphene. *Science* **321**(5887) (2008) 385.

[115] Obraztsov, A., Volkov, A. and Pavlovskii, I., Mechanism of field emission from carbon materials. *Jetp Letters* **68**(1) (1998) 59.

[116] Novoselov, K.S. *et al.*, Electric field effect in atomically thin carbon films. *Science* **306**(5696) (2004) 666.

[117] Qian, M. *et al.*, Electron field emission from screen-printed graphene films. *Nanotechnology* **20**(42).

[118] Iijima, S., Helical microtubules of graphitic carbon. *Nature* **354**(6348) (1991) 56.

[119] White, C.T. and Todorov, T.N., Carbon nanotubes as long ballistic conductors. *Nature* **393**(6682) (1998) 240.

[120] Eletskii, A.V., Transport properties of carbon nanotubes. *Physics-Uspekhi* **52**(3) (2009) 209.

[121] del Carmen Camacho, M. *et al.*, Mechanical properties and durability of CNT cement composites. *Materials* **7**(3) (2014) 1640.

[122] Kruss, S. *et al.*, Carbon nanotubes as optical biomedical sensors. *Advanced Drug Delivery Reviews* **65**(15) (2013) 1933.

[123] Nicola, M.P., On the strength of the carbon nanotube-based space elevator cable: from nanomechanics to megamechanics. *Journal of Physics: Condensed Matter* **18**(33) (2006) S1971.

[124] Saito, Y., *Structures and Synthesis of Carbon Nanotubes*. Carbon Nanotube and Related Field Emitters, Wiley-VCH Verlag GmbH & Co. KGaA, 2010; 2010. 1–14.

[125] Bonard, J. *et al.*, Field emission properties of multiwalled carbon nanotubes. *Ultramicroscopy* **73**(1-4) (1998) 7.

[126] Takakura, A. *et al.*, Energy distributions of field emitted electrons from a multi-wall carbon nanotube. *Ultramicroscopy* **95**(1-4) (2003) 139.

[127] Xu, Z. *et al.*, Field emission of individual carbon nanotube with in situ tip image and real work function. *Applied Physics Letters* **87**(16) (2005) 163106.

[128] Zajec, B. *et al.*, Ring-shaped field emission patterns from carbon nanotube films. *Carbon* **49**(10) (2011) 3332.

[129] Purcell, S. *et al.*, Hot nanotubes: Stable heating of individual multiwall carbon nanotubes to 2000 K induced by the field-emission current. *Physical Review Letters* **88**(10) (2002) 105502.

[130] Rinzler, A.G. *et al.*, Unraveling nanotubes - field-emission from an atomic wire. *Science* **269**(5230) (1995) 1550.

[131] Hsieh, Y.C. *et al.*, Thermal analysis of multi-walled carbon nanotubes by Kissinger's corrected kinetic equation. *Aerosol and Air Quality Research* **10**(3) (2010) 212.

[132] Sveningsson, M. *et al.*, Quantifying temperature-enhanced electron field emission from individual carbon nanotubes. *Physical Review B* **72**(8) (2005) 085429.

[133] Charbonnier, F. *et al.*, Nottingham effect in field and T-F emission: heating and cooling domains, and inversion temperature. *Physical Review Letters* **13**(13) (1964) 397.

[134] Liu, W.W. *et al.*, Synthesis and characterization of graphene and carbon nanotubes: A review on the past and recent developments. *Journal of Industrial and Engineering Chemistry* **20**(4) (2014) 1171.

[135] Lan, Y., Wang, Y. and Ren, Z.F., Physics and applications of aligned carbon nanotubes. *Advances in Physics* **60**(4) (2011) 553.

[136] Shiratori, Y. *et al.*, One-step formation of aligned carbon nanotube field emitters at 400 degrees C. *Applied Physics Letters* **82**(15) (2003) 2485.

[137] Chen, Y. and Zhang, J., Chemical vapor deposition growth of single-walled carbon nanotubes with controlled structures for nanodevice applications. *Accounts of Chemical Research* **47**(8) (2014) 2273.

[138] Tan, L.L. *et al.*, Growth of carbon nanotubes over non-metallic based catalysts: A review on the recent developments. *Catalysis Today* **217** (2013) 1.

[139] Dijon, J. *et al.*, How to switch from a tip to base growth mechanism in carbon nanotube growth by catalytic chemical vapour deposition. *Carbon* **48**(13) (2010) 3953.

[140] Szabo, A. *et al.*, Synthesis methods of carbon nanotubes and related materials. *Materials* **3**(5) (2010) 3092.

[141] Ro, J.C. and Chung, I.J., Sol-gel kinetics of tetraethylorthosilicate (TEOS) in acid catalyst. *Journal of Non-Crystalline Solids* **110**(1) (1989) 26.

[142] Asomoza, M. *et al.*, Hydrolysis catalyst effect on sol-gel silica structure. *Materials Letters* **36**(5-6) (1998) 249.

[143] Kielty, J., Carbon nanotube-based field emitters for use in an ion engine. Master's thesis, Brunel University, 2011.

[144] Kaye, G. and Laby, T., *Tables of Physical and Chemical Constants (16th edition 1995). 2.3.7 Thermal conductivities*. Longman, 1995.

[145] Kaye, G. and Laby, T., *Tables of Physical and Chemical Constants (16th edition 1995). 2.6.1 Electrical resistivities*. Longman, 1995.

[146] Hiramatsu, M., Kondo, H. and Hori, M., *Graphene nanowalls*. New Progress on Graphene Research, Prof. Jian Ru Gong (Ed.), InTech, DOI: 10.5772/51528. Available from: http://www.intechopen.com/books/new-progress-on-graphene-research/graphene-nanowalls, 2013. I–XXIV.

[147] Jorio, A. *et al.*, Characterizing carbon nanotube samples with resonance Raman scattering. *New Journal of Physics* **5** (2003) 139.

[148] *Electricity at work: Safe working practices*. Health and Safety Executive, 2013.

[149] Ling-min, Y. *et al.*, Field emission property of printed CNTs-mixed ZnO nanoneedles. *Applied Surface Science* **257**(15) (2011) 6332.

[150] Cole, M.T. *et al.*, In-situ deposition of sparse vertically aligned carbon nanofibres on catalytically activated stainless steel mesh for field emission applications. *Diamond and Related Materials* **23** (2012) 66.

[151] Forbes, R.G., Extraction of emission parameters for large-area field emitters, using a technically complete Fowler-Nordheim-type equation. *Nanotechnology* **23**(9) (2012) 095706.

[152] Bocharov, G.S. and Eletskii, A.V., Theory of carbon nanotube (CNT)-based electron field emitters. *Nanomaterials* **3**(3) (2013) 393.

[153] Minoux, E. *et al.*, Achieving high-current carbon nanotube emitters. *Nano Letters* **5**(11) (2005) 2135.

[154] Ferrari, A.C. and Robertson, J., Interpretation of Raman spectra of disordered and amorphous carbon. *Physical review B* **61**(20) (2000) 14095.

[155] Tashie-Lewis, B., The fabrication of carbon nanotube-based field electron emission devices for space applications. Master's thesis, Brunel University, 2011.

[156] Qian, C. *et al.*, Fabrication of small diameter few-walled carbon nanotubes with enhanced field emission property. *Journal of Nanoscience and Nanotechnology* **6**(5) (2006) 1346.

[157] Schneider, C.A., Rasband, W.S. and Eliceiri, K.W., NIH Image to ImageJ: 25 years of image analysis. *Nature Methods* **9**(7) (2012) 671.

[158] Liu, W.H. *et al.*, On the uniformity of field emission in screen printed CNT-cathodes: The effects of the cathode roughness. *Microelectronics Journal* **37**(5) (2006) 404.

[159] Ummethala, R. *et al.*, Effect of substrate material on the growth and field emission characteristics of large-area carbon nanotube forests. *Journal of Applied Physics* **119**(4).

[160] Zhang, J. *et al.*, Interaction between carbon nanotubes and substrate and its implication on field emission mechanism. *Carbon* **44**(3) (2006) 418 .

[161] Wong, Y. *et al.*, Array geometry, size and spacing effects on field emission characteristics of aligned carbon nanotubes. *Diamond and Related Materials* **14**(11–12) (2005) 2078 .

[162] Poa, C.H.P. *et al.*, Field emission from nonaligned carbon nanotube–polymer matrix cathodes. *Journal of Vacuum Science & Technology B: Microelectronics and Nanometer Structures Processing, Measurement, and Phenomena* **21**(4) (2003) 1715.

[163] Jung, S.M., Jung, H.Y. and Suh, J.S., Horizontally aligned carbon nanotube field emitters having a long term stability. *Carbon* **45**(15) (2007) 2917 .

[164] Parmee, R.J. *et al.*, X-ray generation using carbon nanotubes. *Nano Convergence* **2**(1) (2015) 1.

[165] Li, J.T. *et al.*, Field emission characteristic of screen-printed carbon nanotube cathode. *Applied Surface Science* **220**(1-4) (2003) 96.

[166] Fardad, M.A., Catalysts and the structure of SiO2 sol-gel films. *Journal of Materials Science* **35**(7) (2000) 1835.

[167] Boughton, E., A large-area, screen-printed nanostructured carbon-based field emission cathode. In *2016 IEEE International Vacuum Electronics Conference (IVEC)*, 1–2.